UNIVERSITA' DEGLI STUDI DI PAVIA
FACOLTA' DI INGEGNERIA
DIPARTIMENTO DI MECCANICA STRUTTURALE

Arc-Length Strategies in Structural Equilibrium Path-Following

Metodi Arc-Length per la Determinazione del Percorso di Equilibrio Strutturale

Tesi di laurea specialistica in ingegneria civile di

EMANUELE CALO'

Relatore:

Chiar.mo Prof. FERDINANDO AURICCHIO

Correlatore:

Dott. Ing. ALESSANDRO REALI

Anno Accademico 2005-2006

Abstract

Questa tesi tratta il problema dell'instabilià strutturale da un punto di vista computazionale. L'elevata non linearità dei fenomeni connessi alla stabilità dei sistemi strutturali hanno reso la tecnica risolutiva denominata arc-length nei primi anni 70 (3; 4; 5; 6), lo strumento più diffuso per la rappresentazione del percorso di equilibrio strutturale. Questa tecnica numerica rappresenta il cuore del presente lavoro. L'efficacia del metodo arc-length (che significa lunghezza d'arco) è dovuta alla sua capacità di superare punti critici per il sistema preso in esame vincolando l'analisi a procedere secondo archi della superficie di equilibrio a lunghezza costante. In particolare il successo di tale metodo è qui dimostrato avvalendosi di considerazioni inerenti la caratteristiche di punti critici strutturali, quali punti limite e punti di biforcazione. La costruzione di un algoritmo robusto, che passa attraverso una completa considerazione delle possibili varianti al metodo presenti in letteratura, è l'obiettivo che ci si propone di raggiungere. Le prove numeriche presentate dimostrano le potenzialità del metodo analizzato che non manifesta problemi nemmeno in corrispondenza di punti di biforcazione.

Acknowledgements

Ringrazio in primo luogo il professore Ferdinando Auricchio e Alessandro per la disponibilità che hanno mostrato nei miei confronti. In questi mesi condivisi anche con loro ho capito come non solo la loro intelligenza e professionalità, ma soprattutto la loro profonda umanità, li ha resi e li renderà grandi.

Per il sostegno che non mi ha mai abbandonato, ringrazio la mia famiglia e Vale. A loro dedico questo lavoro.

Ricordo e ringrazio tutti gli amici (i collegiali, il rettore ed i compagni di corso) che mi hanno ascoltato (e sopportato) quando ne avevo più bisogno.

Ringrazio, infine, tutto il personale bibliotecario senza il quale tutto ciò non sarebbe stato possibile.

"[...] io vi vorrei pregare quanto posso, caro signore, di avere pazienza verso quanto non è ancora risolto nel vostro cuore, e tentare di aver *care le domande stesse* come stanze serrate e libri scritti in lingua straniera. Non cercate ora le risposte che non possono venirvi date perchè non le potreste vivere. E di questo si tratta, di vivere tutto. *Vivete* ora le domande. Forse v'insinuate così a poco a poco, senz'avvertirlo, a vivere un giorno lontano la risposta."

Rainer Maria Rilke

Contents

Introduction

Instability problems play a key role in structural engineering, and it can be argued that most structural failures contain an element of instability. In general a strong degree of nonlinearity governs the response of such problems and so a proper technique is required to follow the structural equilibrium state under variation of a number of system parameters, such as load intensity, imperfection amplitudes and design variables.

In this sense, the first steps were moved by Koiter, see for example (24), who developed in 1945 a general method for the stability analysis of elastic systems subjected to conservative loading. However the implementation of his theory within a computational framework is relatively recent, as heavy computations are required. Moreover as these methods rely on power-series expansion techniques, they yield results approximating the equilibrium surface only locally, i.e. around a pre-determined solution point of the surface at which the series are evaluated. This approach is not treated here.

While the finite element methods began to spread all over the world, the first 60's gave rise to the so called *incremental-iterative strategies* which cover the exact behaviour of structures by means of the definition of successive equilibrium configurations for certain load levels. In this work we deal with such methods, also called *continuation techniques*. As we said, they are based on an incremental method which features Newton's method and a special parameter controlling the computation progress along the equilibrium path. A special attention is here given to those approaches, initially introduced by Riks in (3; 4; 5; 6), which select a control parameter corresponding, in good approximation to the *arc-length* of the equilibrium path to be computed.

The problem of elastic stability is intimately connected with singularities that occur somewhere along the path under consideration. These singular points are better known as *critical points*. Thus, if we divide the equilibrium path into a pre-critical and a post-critical state (calling the transition state critical state), we would like to be able to predict the structural response throughout **arc-length strategy**. Here we propose to prove the effectiveness of some of the most commonly used *arc-length techniques*. Clearly, a mathematical characterization of the critical state is in order; in fact the success of traditional continuation and *arc-length* methods is determined by

their behaviour when dealing with critical conditions.

Chapter 1

The equilibrium problem

1.1 Equilibrium

We start considering an elastic system under conservative loading conditions defined by parameters $\mathbf{p}$, λ. In the following, we assume $\mathbf{p}$ to be representative of a set of nodal point displacement vectors in the displacement-based FE-formulation and to belong to $\mathbb{R}^n$; we also assume λ to be rappresentative of a single intensity load parameter introduced by external forces.

The *total potential energy* of such a system is denoted by

$$V = V(\mathbf{p}, \lambda), \tag{1.1}$$

and it is convenient to calculate it starting from the undeformed reference state

$$\mathbf{p} = \mathbf{0}, \quad \lambda = 0. \tag{1.2}$$

The equilibrium of the structure is then determined from the stationarity of function (1.1) with respect to $\mathbf{p}$, i.e. by the set of equations

$$\mathbf{r}(\mathbf{p}, \lambda) = \frac{\partial V(\mathbf{p}, \lambda)}{\partial \mathbf{p}} = \mathbf{0}, \tag{1.3}$$

where $\mathbf{r}$ is a regular function called the unbalanced or residual force vector. It is assumed that the undeformed state (1.2) is a solution of this set of equations.

Equations (1.3) represent N relations between $N+1$ degrees of freedoms; i.e. p_i for $i = 1, 2, \ldots, N$, and λ. Together they describe a number of curves in the space $\mathbb{R}^{N+1}$, the equilibrium paths of the structure, spanned by $\mathbf{p}$ and λ.

1.2 Stability and critical points

Stationarity of the total potential energy V is not sufficient to evaluate the "quality" of equilibrium configurations $(\mathbf{p}, \lambda)$. For such a reason, we need

to detect also its second variation, i.e.

$$V_2(\Delta\mathbf{p}) = \frac{1}{2}\frac{\partial^2 V(\mathbf{p},\lambda)}{\partial p_i \partial p_j}\Delta p_i \Delta p_j, \tag{1.4}$$

which can be rewritten as

$$V_2(\Delta\mathbf{p}) = \frac{1}{2}\Delta\mathbf{p}^{\mathrm{T}}\mathbf{K}_t\Delta\mathbf{p}, \tag{1.5}$$

where

$$\mathbf{K}_t = \frac{\partial^2 V(\mathbf{p},\lambda)}{\partial \mathbf{p}^2} = \frac{\partial \mathbf{r}(\mathbf{p},\lambda)}{\partial \mathbf{p}}, \tag{1.6}$$

being $\mathbf{K}_t$ the matrix of the quadratic form. In structural elastic applications, this represents the stiffness matrix of the considered structure with respect to its generalized displacements. Now, according to the theory of the stability of conservative systems, the stability of the equilibrium configurations is ensured if the quadratic form (1.4) is positive definite. Unstable configurations occur if $V_2(\Delta\mathbf{p})$ is negative, while a transition between a stable and unstable point of a path is marked by a semi-definite or indefinite $V_2(\Delta\mathbf{p})$. Such transition state is called **critical state** and is always associated to a singular matrix of the quadratic form.

The precise definition of a **critical point** is given by means of the generalized eigenvalue problem

$$[\mathbf{K}_t - \omega_k\mathbf{I}]\,\mathbf{a}_k = \mathbf{0}, \tag{1.7}$$

where $\mathbf{a}_k$ denote the characteristic vectors, ω_k the characteristic values of $\mathbf{K}_t$ at a given configuration of the equilibrium $\mathbf{r}(\mathbf{p},\lambda)$ and $\mathbf{I}$ the identity matrix. The characteristic values ω_k are supposed to be arranged according to the sequence

$$\omega_1 \leq \omega_2 \leq \omega_3 \leq \ldots \leq \omega_N. \tag{1.8}$$

The quadratic form $V_2(\Delta\mathbf{p})$ is positive definite as long as the characteristic values ω_k satisfy

$$0 < \omega_1 \leq \omega_2 \leq \omega_3 \leq \ldots \leq \omega_N. \tag{1.9}$$

The stability limit is reached when

$$0 = \omega_1 = \omega_2 = \ldots = \omega_K < \omega_{K+1} \leq \ldots \leq \omega_N. \tag{1.10}$$

thus when one or more eigenvalues ω_k in sequence (1.8) are zero.

There is another criterion which is useful in applications but which can only be appreciated as a **necessary condition**. Such a criterion is the result of the fact that a necessary but not sufficient condition for positive definiteness of the quadratic form is that

$$D > 0, \tag{1.11}$$

being D the determinant of the matrix $\mathbf{K}_t$

$$D = \det(\mathbf{K}_t). \tag{1.12}$$

As D can also be written as

$$D = \prod_{k=1}^{N} \omega_k, \tag{1.13}$$

it is clear that an even number of characteristic values $\omega_k < 0$ makes $D > 0$. Such a situation, however, does not satisfy condition (1.9) for which all the eigenvalues associated to $\mathbf{K}_t$ must be positive; it is thus proved that (1.11) can be regarded only as a necessary, but not sufficient, condition. Finally, from equation (1.10), it follows that at a critical state

$$D = 0. \tag{1.14}$$

1.3 Limit point and bifurcation point

Two fundamentally different types of loss of stability, i.e. critical points, are known in the general theory. These types of singular behaviour are related to the concept of **limit point** and **bifurcation point**. In the following we give precise definitions of these critical conditions.

1.3.1 Limit point

We now suppose that s is a suitably chosen path parameter such that the equilibrium state

$$\mathbf{p}(s), \quad \lambda(s) \tag{1.15}$$

is uniquely determined by s along the path in the range of interest. Following (1), a **limit point** is an equilibrium point if it satisfies the following conditions:

- The tangent to the equilibrium curve $\mathbf{r}(\mathbf{p}(s), \lambda(s))$ is "horizontal" in the sense that its component, following the axis λ in the space $\mathbb{R}^n \times \mathbb{R}$, is zero, i.e.
$$\frac{d\lambda}{ds} = 0. \tag{1.16}$$
- The equilibrium curve at this point is unique.

Limit points have significant physical meaning since they correspond to the extremum values of the external force introduced; moreover the elastic behaviour of a structure which is associated with loss of stability in a limit point is called *snapping*.

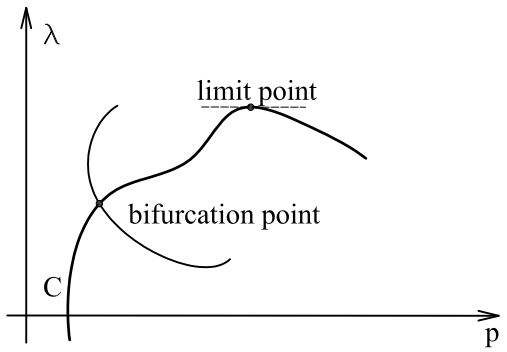

Figure 1.1: Limit point and bifurcation point.

1.3.2 Bifurcation point

Following (1), a **bifurcation point** is an equilibrium point in which multiple equilibrium curves intersect; such an equilibrium state is called *buckling*. Since two curves can intersect transversally or tangentially, there is an angular or tangent bifurcation depending on the fact that the tangent directions at the bifurcation point are different or not (figures 1.2 and 1.3).

So bifurcations can be distinguished in simple bifurcations (figure 1.2a and 1.3b), bifurcation at limit point (figure 1.2b) and limit bifurcation (figure 1.3a). The main distinction in these kinds of bifurcation is that at limit bifurcation $d\lambda(s)/ds = 0$ on every branch but not so at a bifurcation at a limit point and simple bifurcations. As limit bifurcation is quite complex to analyze, in this context we will only deal with simple bifurcations and bifurcation at a limit point.

1.3.3 Rate problem

The study of critical points is straightforward if it is possible to solve the fundamental problem of finding the equilibrium curves going through a given equilibrium point. Such a problem is however *a priori* very difficult to be solved because of the non-linearity of the equilibrium equation (1.3).

A simpler problem, denoted as the **rate problem**, may be introduced giving the tangent direction and its derivative associated with an equilibrium curve, i.e.

$$\dot{\mathbf{p}} = \frac{d\mathbf{p}}{ds} \quad , \qquad \dot{\lambda} = \frac{d\lambda}{ds} \tag{1.17}$$

$$\ddot{\mathbf{p}} = \frac{d^2\mathbf{p}}{ds^2} \quad , \qquad \ddot{\lambda} = \frac{d^2\lambda}{ds^2}; \tag{1.18}$$

the aim now is the determination of these curve tangent directions and derivatives.

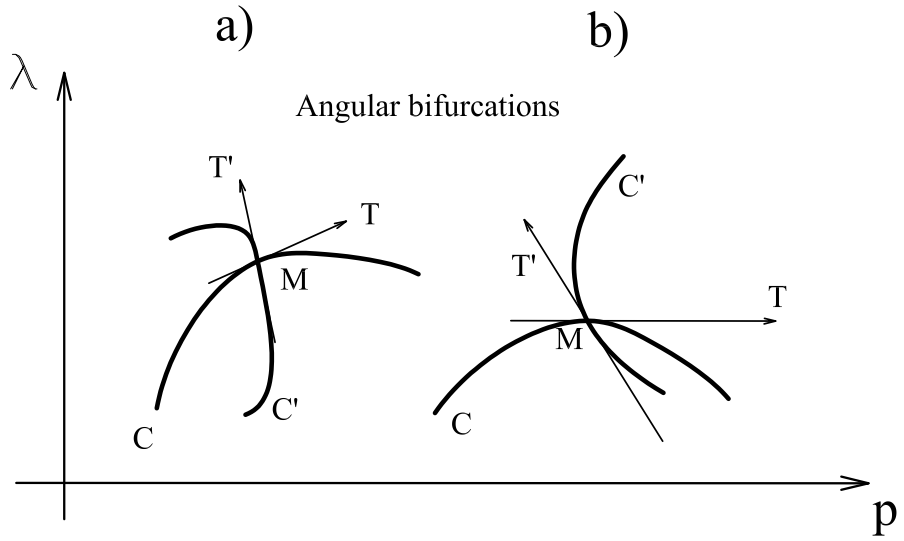

Figure 1.2: a) Simple angular bifurcation. b) Angular bifurcation at a limit point.

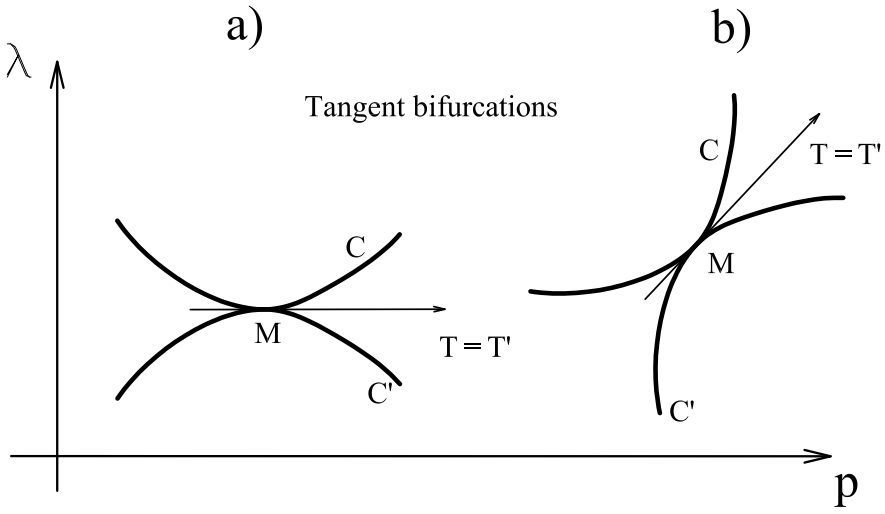

Figure 1.3: a) Tangent limit bifurcation. b) Simple tangent bifurcation.

The **rate equations** can be derived from the equilibrium equation (1.3) by differentiating twice with respect to s, yielding

$$\frac{d}{ds}[\mathbf{r}(\mathbf{p},\lambda)] = \mathbf{0} \tag{1.19}$$

$$\frac{d^2}{ds^2}[\mathbf{r}(\mathbf{p},\lambda)] = \mathbf{0} \tag{1.20}$$

and in particular

$$\mathbf{K}_t\dot{\mathbf{p}} + \mathbf{f}\dot{\lambda} = \mathbf{0} \tag{1.21}$$

$$\mathbf{K}_t\ddot{\mathbf{p}} + \mathbf{f}\ddot{\lambda} = -(\nabla_{\mathbf{p}}(\mathbf{K}_t)\dot{\mathbf{p}} + 2\nabla_\lambda(\mathbf{K}_t)\dot{\lambda} + \nabla_\lambda(\mathbf{f})\dot{\lambda}^2), \tag{1.22}$$

where $\mathbf{f} = \nabla_\lambda(\mathbf{r})$ is assumed to be constant in the following . However, at a critical point, $\mathbf{K}_t$ is singular in accordance to definition (1.14).

For the present discussion we use the symbols

$$\mathrm{r}(\cdot), \quad \mathrm{Im}(\cdot) \quad \text{and} \quad \mathrm{Ker}(\cdot)$$

to indicate respectively the rank, the range and the null space of a certain matrix.

As $\mathbf{K}_t$ is a $N \times N$ symmetric matrix, it is always possible to construct, from the generalized eigenvalue problem (1.7), a basis of eigenvectors

$$[\mathbf{a}_1, \mathbf{a}_2, \ldots, \mathbf{a}_m, \mathbf{a}_{m+1}, \ldots, \mathbf{a}_N]. \tag{1.23}$$

We indicate with $m = \dim[\mathrm{Ker}(\mathbf{K}_t)]$ the dimension of the null space of $\mathbf{K}_t$, i.e.

$$\mathbf{K}_t\mathbf{a}_k = \mathbf{0}, \quad k = 1, 2, \ldots, m. \tag{1.24}$$

In other words eigenvectors $\mathbf{a}_k$ for $k = 1, 2, \ldots, m$ satisfy the eigenvalue problem with $\omega_k = 0$ and are associated with the critical state.

The computation of the tangent at the critical point is carried out observing that a solution $\dot{\mathbf{p}}$ of (1.21) can be written as

$$\dot{\mathbf{p}} = \dot{\lambda}\mathbf{y} + \sum_{k=1}^{m} \mu_k \mathbf{a}_k. \tag{1.25}$$

i.e. as, the sum of the particular solution $\dot{\lambda}\mathbf{y}$, where $\mathbf{y}$ is such that

$$\begin{cases} \mathbf{K}_t\mathbf{y} = \mathbf{f}, \\ \mathbf{y}^{\mathrm{T}}\mathbf{a}_k = 0, \quad k = 1, 2, \ldots, m, \end{cases} \tag{1.26}$$

and an arbitrary multiple of the eigenvectors $\mathbf{a}_k$ where $k = 1, 2, \ldots, m$.

A proof for the general solution (1.25) is given in the following.

Proof 1.1. Let consider a particular solution $\mathbf{y}$ and the eigenvectors $\mathbf{a}_k$, with $k = 1, 2, \ldots, m$, defined respectively in (1.26) and in (1.24), and rewrite first **rate equation** (1.21) as

$$\mathbf{0} = \mathbf{K}_t \left(\sum_{k=1}^{m} \mu_k \mathbf{a}_k \right) = \mathbf{K}_t \dot{\mathbf{p}} - (\mathbf{K}_t \mathbf{y}) \dot{\lambda}. \tag{1.27}$$

Multiplying the above equation by $\mathbf{K}_t^{-1}$ and rearranging terms, we get equation (1.25). ■

At the present, the scalars μ_k are arbitrary. If we use solution (1.25) in the second **rate equation** (1.22) and we multiply both members by $\mathbf{a}_k$, following (20), we get

$$\sum_{k=1}^{m} \sum_{j=1}^{m} \hat{A}_{ijk} \mu_k \mu_j + \mathbf{a}_i^{\mathrm{T}} \mathbf{f} \ddot{\lambda} + 2 \sum_{j=1}^{m} \hat{B}_{ij} \mu_k \dot{\lambda} + \hat{C}_i \dot{\lambda}^2 = 0, \quad i = 1, \ldots, m. \tag{1.28}$$

Here we have introduced

$$\begin{aligned} \hat{A}_{ijk} &= \hat{A}_{ikj} = \mathbf{a}_i^{\mathrm{T}} [\nabla_{\mathbf{p}} (\mathbf{K}_t \mathbf{a}_j) \mathbf{a}_k], & (1.29) \\ \hat{B}_{ij} &= \mathbf{a}_i^{\mathrm{T}} [\nabla_{\mathbf{p}} (\mathbf{K}_t \mathbf{a}_j) \mathbf{y} + \nabla_{\lambda} (\mathbf{K}_t \mathbf{a}_j)], & (1.30) \\ \hat{C}_i &= \mathbf{a}_i^{\mathrm{T}} [\nabla_{\mathbf{p}} (\mathbf{K}_t \mathbf{y}) \mathbf{y} + \nabla_{\lambda} (\mathbf{K}_t \mathbf{y}) + \nabla_{\lambda} (\mathbf{f})]. & (1.31) \end{aligned}$$

System (1.28) can be written in the compact form

$$\hat{\mathbf{A}}(\boldsymbol{\mu}) \boldsymbol{\mu} + \mathbf{e} \ddot{\lambda} + 2 \hat{\mathbf{B}}(\boldsymbol{\mu}) \boldsymbol{\mu} \dot{\lambda} + \hat{\mathbf{C}} \dot{\lambda}^2 = \mathbf{0}, \tag{1.32}$$

where

$$\begin{aligned} &\boldsymbol{\mu} = (\mu_1, \ldots, \mu_m)^{\mathrm{T}}, \quad \hat{\mathbf{A}} = (\hat{A}_{ij}) = \left(\sum_{k=1}^{m} \hat{A}_{ijk} \mu_k \right), \\ &\hat{\mathbf{B}} = (\hat{B}_{ij}), \quad \mathbf{e} = (\mathbf{a}_i^{\mathrm{T}} \mathbf{f}, \ldots, \mathbf{a}_m^{\mathrm{T}} \mathbf{f})^{\mathrm{T}}, \\ &\hat{\mathbf{C}} = (\hat{C}_1, \ldots, \hat{C}_m)^{\mathrm{T}}. \end{aligned} \tag{1.33}$$

In the following subsection we show that the first rate equation (1.21) is useful to distinguish between limit and bifurcation point while the second rate equation (1.22), in the form of (1.32), may serve to calculate solutions as expressed in (1.25) or to make some additional considerations about critical points.

1.3.4 Limit point analysis

We start introducing matrix $\mathbf{A}$ arising from the first **rate equation** (1.21) defined as

$$\mathbf{A} = [\mathbf{K}_t \quad \mathbf{f}]. \tag{1.34}$$

A *critical point* on a solution path is said to be **limit point** if

$$\begin{cases} \mathbf{f} \in \mathrm{Ker}(\mathbf{K}_t) \\ m = 1, \end{cases} \tag{1.35}$$

or, alternatively, if

$$\begin{cases} \mathrm{r}(\mathbf{K}_t) = N - 1 \\ \mathrm{r}(\mathbf{A}) = N, \end{cases} \tag{1.36}$$

that is, $\mathbf{f}$ augments $\mathrm{r}(\mathbf{K}_t)$, rank of matrix $\mathbf{K}_t$ and only the eigenvalue ω_1 is zero. Conditions (1.35) imply that the only way to satisfy the first rate condition (1.21) is to have both the following condition

$$\begin{aligned} &\dot{\lambda} = 0, \\ &\dot{\mathbf{p}} \in \mathrm{Ker}(\mathbf{K}_t). \end{aligned} \tag{1.37}$$

A precise proof of such **limit point** conditions is given in the following. [chapter]

Proof 1.2. If we assume $\dot{\lambda} \neq 0$, we could write

$$\mathbf{f} = -\mathbf{K}_t \dot{\mathbf{p}} \frac{1}{\dot{\lambda}}, \tag{1.38}$$

which contradicts (1.35). Thus $\dot{\lambda} = 0$ and substituting this into the first rate equation we obtain $\mathbf{K}_t \dot{\mathbf{p}} = \mathbf{0}$. This coincides with the null space definition (1.24) and the entire proposition (1.37) follows. ■

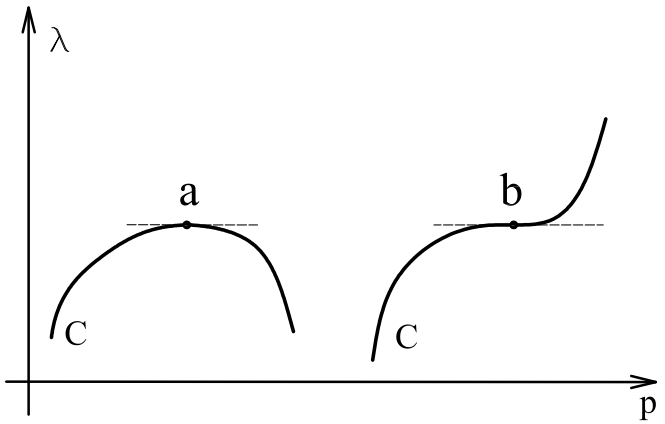

Figure 1.4: a: Non-degenerate or quadratic limit point. b: Degenerate or cubic limit point.

Many authors (see references (21) and (31)) consider further distinctions among limit points. In particular, they also consider so-called *degenerate* or *cubic* limit points, figure 1.4b, while up to now we have considered only *non-degenerate* or *quadratic* limit points, figure 1.4a. A limit point is non-degenerate if both the following conditions are satisfied

$$\begin{array}{l} \dot{\lambda} = 0, \\ \ddot{\lambda} \neq 0. \end{array} \tag{1.39}$$

If we consider second rate equation written in compact form (1.32) with $m = 1$, conditions (1.39) yield

$$\ddot{\lambda} = -\frac{\mathbf{a}_1^{\mathrm{T}} \nabla_{\mathbf{p}} (\mathbf{K}_t \mathbf{a}_1) \mathbf{a}_1}{\mu_1 \mathbf{a}_1^{\mathrm{T}} \mathbf{f}} \neq 0; \tag{1.40}$$

that is

$$\mathbf{a}_1^{\mathrm{T}} \nabla_{\mathbf{p}} (\mathbf{K}_t \mathbf{a}_1) \mathbf{a}_1 \neq 0. \tag{1.41}$$

Instead a limit point is called *degenerate* or *cubic* if both following conditions are satisfied

$$\begin{array}{l} \ddot{\lambda} = 0, \\ \dddot{\lambda} \neq 0. \end{array} \tag{1.42}$$

The analogous of condition (1.41) for *non-degenerate* limit points can be obtained by differentiating with respect to s the second rate equation and applying condition (1.42) to the result. So

$$\mathbf{a}_1^{\mathrm{T}} \{ 3 \nabla_{\mathbf{p}} (\mathbf{K}_t \mathbf{a}_1) \ddot{\mathbf{p}} + \nabla_{\mathbf{p}} [\nabla_{\mathbf{p}} (\mathbf{K}_t \mathbf{a}_1) \mathbf{a}_1] \mathbf{a}_1 \} \neq 0. \tag{1.43}$$

The existence of a unique branch of solution of the equilibrium equation in a neighborhood of a non-degenerate limit point is proved in (21) while solution (1.25) for a quadratic limit point is given by

$$(\dot{\mathbf{p}}, \dot{\lambda}) = [\mu_1 \mathbf{a}_1, 0]. \tag{1.44}$$

1.3.5 Bifurcation point analysis

A *critical point* on a solution path is said to be a **simple bifurcation point**, if

$$\begin{cases} \mathbf{f} \in \mathrm{Im}(\mathbf{K}_t) \\ m = 1, \end{cases} \tag{1.45}$$

or, alternatively, if

$$\begin{cases} \mathrm{r}(\mathbf{K}_t) = N - 1 \\ \mathrm{r}(\mathbf{A}) = N - 1, \end{cases} \tag{1.46}$$

that is, the rank of the singular matrix $\mathbf{K}_t$ is equal to the rank of the complete matrix $\mathbf{A}$. This condition implies

$$\mathbf{f}^{\mathrm{T}} \mathbf{a}_1 = 0, \tag{1.47}$$

which is an orthogonality condition between $\mathbf{f}$ and the vector $\mathbf{a}_1$ belonging to the null space of matrix $\mathbf{K}_t$.

Brezzi et al. in reference (22) proved that in a neighborhood of a bifurcation point, the solution of the equilibrium equation consists of two branches which intersect transversally at such critical point. As we have previously said the tangent directions at a bifurcation point to the primary and to the secondary paths, denoted by $(\dot{\mathbf{p}}_{\mathrm{I}}, \dot{\lambda}_{\mathrm{I}})$ and $(\dot{\mathbf{p}}_{\mathrm{II}}, \dot{\lambda}_{\mathrm{II}})$, respectively can be expressed, from (1.25), as

$$\begin{aligned} \dot{\mathbf{p}}_{\mathrm{I}} &= \dot{\lambda}_{\mathrm{I}}\mathbf{y} + \mu_{\mathrm{I}}\mathbf{a}_1 \\ \dot{\mathbf{p}}_{\mathrm{II}} &= \dot{\lambda}_{\mathrm{II}}\mathbf{y} + \mu_{\mathrm{II}}\mathbf{a}_1. \end{aligned} \tag{1.48}$$

We now rename $\dot{\lambda}_{\mathrm{I}}$ and $\dot{\lambda}_{\mathrm{II}}$ simply as $\dot{\lambda}$; μ_{I} and μ_{II} as μ. Considering (1.32), we particularize it taking into account simple bifurcation point conditions (1.45) and (1.47), i.e.

$$\hat{A}\mu^2 + 2\hat{B}\mu\dot{\lambda} + \hat{C}\dot{\lambda}^2 = 0, \tag{1.49}$$

being

$$\hat{A} = \mathbf{a}_1^{\mathrm{T}}[\nabla_{\mathbf{p}}(\mathbf{K}_t\mathbf{a}_1)\mathbf{a}_1], \tag{1.50}$$

$$\hat{B} = \mathbf{a}_1^{\mathrm{T}}[\nabla_{\mathbf{p}}(\mathbf{K}_t\mathbf{a}_1)\mathbf{y} + \nabla_{\lambda}(\mathbf{K}_t\mathbf{a}_1)], \tag{1.51}$$

$$\hat{C} = \mathbf{a}_1^{\mathrm{T}}[\nabla_{\mathbf{p}}(\mathbf{K}_t\mathbf{y})\mathbf{y} + \nabla_{\lambda}(\mathbf{K}_t\mathbf{y}) + \nabla_{\lambda}(\mathbf{f})]. \tag{1.52}$$

In addition, following (22), a **simple bifurcation point** must satisfy

$$\hat{B}^2 - \hat{A}\hat{C} > 0. \tag{1.53}$$

From condition $(1.26)_1$, vector $\mathbf{y}$ can be computed as

$$\mathbf{y} = \mathbf{K}_t^{-1}\mathbf{f}. \tag{1.54}$$

Equation (1.49), together with a proper adjoined equation will be useful to follow structural response even on secondary branches.

A special case common in engineering stability problems is the *cusp* or *symmetric bifurcation*. Analogously to *cubic* and *quadratic limit points*, it is possible to distinguish among bifurcation points (see (22)). An *asymmetric* or *fold bifurcation point*, figure 1.5a, is such that $\hat{A} \neq 0$, i.e.

$$\mathbf{a}_1^{\mathrm{T}}\nabla_{\mathbf{p}}(\mathbf{K}_t\mathbf{a}_1)\mathbf{a}_1 \neq 0. \tag{1.55}$$

while *symmetric* or *cusp bifurcation*, figure 1.5b, is such that $\hat{A} = 0$ and $\hat{B} \neq 0$.

Finally, while **bifurcation at a limit point** can be treated as a simple bifurcation point, for **limit bifurcation** we must have $m \geq 2$ (see (20)).

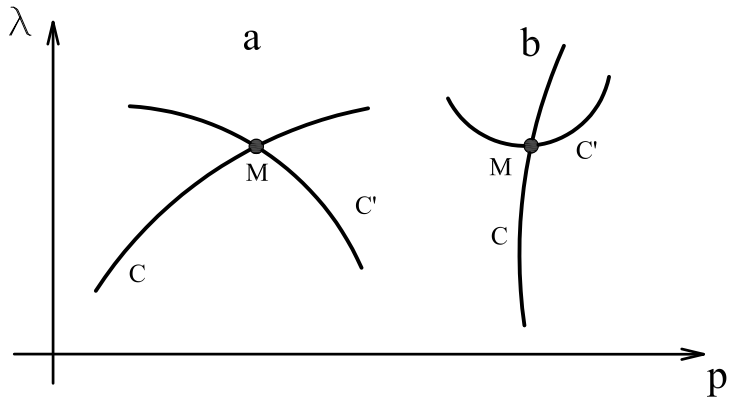

Figure 1.5: a: Asymmetric or fold bifurcation. b: Symmetric or cusp bifurcation.

1.3.6 Alternative formulation for critical points

Following (5), limit (1.37) and bifurcation (1.47) point conditions can be seen in a way such that the determinant of $\mathbf{K}_t$, D, is directly included in the formulation for critical points. This alternative conditions arise from a particular expression of $\mathbf{K}_t^{-1}$, i.e.

$$\mathbf{K}_t^{-1} = \mathbf{C}\frac{1}{D}, \tag{1.56}$$

where

$$C_{ij} = \left[\frac{\partial D}{\partial K_{tij}}\right]. \tag{1.57}$$

$\mathbf{C}$ is the cofactors' matrix of $\mathbf{K}_t$ and D can be expanded, in function of the first row of $\mathbf{C}$, as follows

$$D = K_{t11}C_{11} + K_{t12}C_{12} + \ldots + K_{t1N}C_{1N}; \tag{1.58}$$

The same expansion can be written along any row of $\mathbf{K}_t$. If we express the first rate equation (1.21) as

$$\dot{\mathbf{p}} = \mathbf{K}_t^{-1}\mathbf{f}\dot{\lambda}, \tag{1.59}$$

and we use expression (1.56), we get

$$D\dot{\mathbf{p}} = \mathbf{d}\dot{\lambda}, \tag{1.60}$$

being

$$\mathbf{d} = \mathbf{C}\mathbf{f}. \tag{1.61}$$

As we see in Section 1.2 a necessary condition for the loss of stability is $D = 0$ (1.14), thus from (1.60) we obtain

$$\mathbf{d}\dot{\lambda} = \mathbf{0}. \tag{1.62}$$

The above condition is satisfied if and only if either

$$\dot{\lambda} = 0, \tag{1.63}$$

which is the limit point condition already obtained in (1.37), or

$$\mathbf{d} = \mathbf{C}\mathbf{f} = \mathbf{0}, \tag{1.64}$$

which is an alternative bifurcation condition. A careful observation of two the limit condition (1.47) and (1.64) leads us to the conclusion that the properties of $\mathbf{K}_t$ and $\mathbf{C}$ are complementary at the critical points. In fact from condition (1.64) we get

$$\mathbf{f} \in \mathrm{Ker}(\mathbf{C}) \tag{1.65}$$

and from (1.47)

$$\mathbf{f} \in \mathrm{Im}(\mathbf{K}_t). \tag{1.66}$$

In the appendix A is given a precise proof of the following condition

$$\mathrm{Im}(\mathbf{K}_t) = \mathrm{Ker}(\mathbf{C}). \tag{1.67}$$

which is called *complementarity condition*.

1.4 Equilibrium resolution and its parametrization

In general, to specify a particular point on an equilibrium curve we must add an extra equation to equilibrium (1.3). If this equation is denoted by $G(\mathbf{p}, \lambda) = 0$ we can find specific equilibrium solutions by solving

$$\begin{cases} \mathbf{r}(\mathbf{p}, \lambda) = \mathbf{0}, & (1.68) \\ G(\mathbf{p}, \lambda) = 0. & (1.69) \end{cases}$$

From a geometrical point of view, these equations describe, in $\mathbb{R}^{n+1}$, the intersections of the equilibrium curve (1.68) with an N-dimensional surface, represented by (1.69). In particular, if we introduce an auxiliary surface

$$G(\mathbf{p}, \lambda, \tau) = g(\mathbf{p}, \lambda) - \tau = 0, \tag{1.70}$$

we can deduce that if we vary the parameter τ, this surface will travel in $\mathbb{R}^{n+1}$ and if there are intersections with the curve described by (1.68) the moving surface will generate a sequence of points along such equilibrium curve. Equation (1.70) thus defines τ as a path parameter.

Solutions

$$\mathbf{x} = \begin{bmatrix} \mathbf{p} \\ \lambda \end{bmatrix} = \begin{bmatrix} \mathbf{p}(\tau) \\ \lambda(\tau) \end{bmatrix}, \quad \mathbf{x} \in \mathbb{R}^{n+1}, \tag{1.71}$$

for some range of the parameter τ, $\tau^0 < \tau < \tau^1$, satisfy the following extended equilibrium problem

$$\mathbf{R}(\mathbf{x}, \tau) = \mathbf{0}, \tag{1.72}$$

i.e.

$$\begin{cases} \mathbf{r}(\mathbf{x}) = \mathbf{0} \\ G(\mathbf{x}, \tau) = g(\mathbf{x}) - \tau = 0. \end{cases} \tag{1.73}$$

Suppose now that we measure the length of the segment of the curve (1.71) between two points τ^0 and τ, where the first value is kept fixed. This distance, previously introduced and denoted by s, is the so-called chord- or arc-length of the segment.

For obvious reasons we would like, however, to choose τ, and as a consequence $g(\mathbf{p}, \lambda)$, in a way such that the relationship between the natural measure of progress along the path s and τ is one-to-one. This condition corresponds to the natural requirement that $ds/d\tau$ should keep its sign along the segment under consideration.

The meaning of this for the required property of $g(\mathbf{p}, \lambda)$ is easy to deduce if we differentiate (1.70) with respect to τ along the path

$$\frac{dG}{d\tau} = \frac{dg}{ds}\frac{ds}{d\tau} - 1 = \tag{1.74}$$

$$= \left[\frac{\partial g}{\partial \mathbf{p}}\frac{d\mathbf{p}}{ds} + \frac{\partial g}{\partial \lambda}\frac{d\lambda}{ds}\right]\frac{ds}{d\tau} - 1 = \tag{1.75}$$

$$= (\mathbf{m} \cdot \dot{\mathbf{x}})\frac{ds}{d\tau} - 1 = 0, \tag{1.76}$$

with

$$\dot{\mathbf{x}} = \frac{d\mathbf{x}}{ds} = \begin{bmatrix} \dot{\mathbf{p}} \\ \dot{\lambda} \end{bmatrix} = \begin{bmatrix} \dfrac{\partial \mathbf{p}}{\partial s} \\ \dfrac{\partial \lambda}{\partial s} \end{bmatrix}, \quad \mathbf{m} = \nabla_{\mathbf{x}} G = \left[\frac{\partial g}{\partial \mathbf{p}}, \frac{\partial g}{\partial \lambda}\right]. \tag{1.77}$$

According to the definition of the chord-length s, $\dot{\mathbf{x}}$ is the vector tangent to the equilibrium curve, while the vector $\mathbf{m}$ corresponds to the normal to the constraint surface (1.70). We see that, if we want $ds/d\tau$ to keep its sign along the segment of interest, the angle θ between $\mathbf{m}$ and $\dot{\mathbf{x}}$ at the points of intersection should be acute. The singular case occurs when

$$\mathbf{m} \cdot \dot{\mathbf{x}} = 0 \quad \text{or} \quad \theta = \frac{\pi}{2}. \tag{1.78}$$

An illustration of the two situations, i.e. of a regular and singular intersection, is given in figure 1.6. Note that in the singular case there is a point

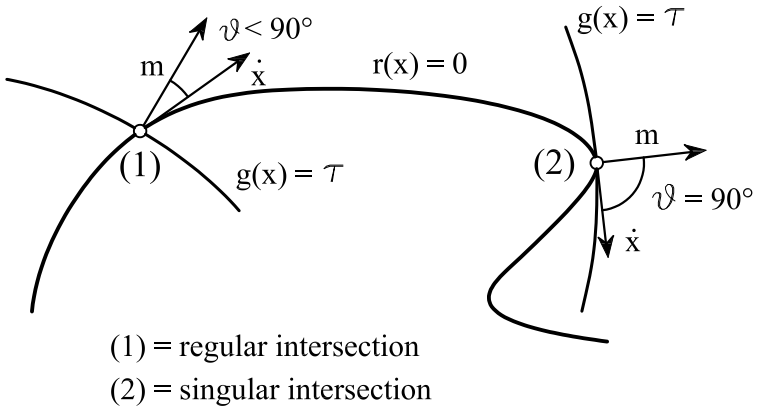

Figure 1.6: Regular intersection and turning point

at which the solution curve turns with respect to the direction in which the auxiliary surface $G = 0$ is moving. In other words, this point of the curve is a *turning point* with respect to the direction $\mathbf{m}$.

This illustrates that the parameter choice for the description of (1.70) should be guided by the way the solution develops in the space $\mathbb{R}^{N+1}$.

1.5 Efficient parametrization

In Section (1.3.3) we said that the first equation of the *rate problem* is useful to distinguish between a bifurcation point and a limit point. We now examine the first *rate problem* equation associated to the "augmented" equilibrium system, as we would like to discover the effects of limit and bifurcation point on the resolution of equation (1.72).

After that, as we said in the previous section, we would like also to understand what kind of role an **efficient parametrization** can play to obtain the correct resolution of the entire equilibrium problem.

The first equation of the *rate problem* can be derived from equation (1.72) by differentiation with respect to τ. At a given equilibrium $(\mathbf{p}, \lambda)$, we obtain

$$\frac{d\mathbf{R}}{d\tau} = (\nabla_{\mathbf{x}}\mathbf{R})\mathbf{x}' + \left.\frac{\partial \mathbf{R}}{\partial \tau}\right|_{\mathbf{x}} = \mathbf{0}; \tag{1.79}$$

thus

$$\mathbf{H}\mathbf{x}' = \boldsymbol{\delta}_{\lambda} \tag{1.80}$$

where

$$\mathbf{H} = (\nabla_{\mathbf{x}}\mathbf{R}) \tag{1.81}$$

$$\mathbf{x}' = \frac{d\mathbf{x}}{d\tau} = \begin{bmatrix} \mathbf{p}' \\ \lambda' \end{bmatrix} = \begin{bmatrix} \dfrac{\partial \mathbf{p}}{\partial \tau} \\ \dfrac{\partial \lambda}{\partial \tau} \end{bmatrix}, \tag{1.82}$$

$$\boldsymbol{\delta}_\lambda = \begin{bmatrix} \mathbf{0} \\ 1 \end{bmatrix} \in \mathbb{R}^{N+1}. \tag{1.83}$$

Equation (1.80) can be written as

$$\begin{cases} (\nabla_{\mathbf{p}}\mathbf{r})\mathbf{p}' + (\nabla_\lambda \mathbf{r})\lambda' = \mathbf{0}, \\ (\nabla_{\mathbf{p}}G)^{\mathrm{T}}\mathbf{p}' + (\nabla_\lambda G)\lambda' = 1, \end{cases}$$

or, alternatively, as

$$\begin{cases} \mathbf{K}_t\mathbf{p}' + \mathbf{f}\lambda' = \mathbf{0}, \\ \mathbf{n}^{\mathrm{T}}\mathbf{p}' + \nu\lambda' = 1 \end{cases}. \tag{1.84}$$

Note that

$$\mathbf{H} = \begin{bmatrix} \mathbf{K}_t & \mathbf{f} \\ \mathbf{n}^{\mathrm{T}} & \nu \end{bmatrix} = \begin{bmatrix} K_{t11} & K_{t12} & \cdots & K_{t1N} & f_1 \\ \vdots & \vdots & & \vdots & \vdots \\ K_{tN1} & K_{tN2} & \cdots & K_{tNN} & f_N \\ n_1 & n_2 & \cdots & n_N & \nu \end{bmatrix}. \tag{1.85}$$

Now, we would like to focus our attention on the analysis of the so-called Jacobian matrix $\mathbf{H}$. System (1.84) in fact has a unique solution $\mathbf{x}'$, if $\mathbf{H}$ is nonsingular. Then, we are interested to know how limit and bifurcation points contribute to the singularity of $\mathbf{H}$.

A characterization of these different situations can be obtained examining the determinant of the Jacobian $\mathbf{H}$. For this reason, in analogy to what we have done for limit and bifurcation point analysis [see Section 1.3.4, matrix $\mathbf{A}$ (1.34)], we introduce

$$\mathbf{A}^\alpha = \begin{bmatrix} K_{t11} & K_{t12} & \cdots & K_{t1\alpha-1} & K_{t1\alpha+1} & \cdots & K_{t1N} & f_1 \\ \vdots & & & \vdots & \vdots & & \vdots & \vdots \\ K_{t1} & K_{tN2} & \cdots & K_{tN\alpha-1} & K_{tN\alpha+1} & \cdots & K_{tNN} & f_N \end{bmatrix}, \tag{1.86}$$

by eliminating row $N+1$ and column α ($\alpha = 1, 2, \ldots, N, N+1$) from matrix $\mathbf{H}$. We also denote the determinants of the matrices $\mathbf{H}$ and $\mathbf{A}^\alpha$ by

$$F = \det(\mathbf{H}); \quad D_\alpha = \det(\mathbf{A}^\alpha), \quad \alpha = 1, 2, \ldots, N, N+1. \tag{1.87}$$

Expansion of F with respect to the last row yields

$$F = \sum_{\alpha=1}^{N} n_\alpha (-1)^{\alpha+N+1} D_\alpha + \nu D_{N+1}. \tag{1.88}$$

Introducing

$$d_\alpha = (-1)^{\alpha+N+1} D_\alpha, \tag{1.89}$$

i.e. the cofactor of $\mathbf{H}$ with respect to n_α, we can express F as

$$F = \sum_{\alpha=1}^{N} (n_\alpha \, d_\alpha) + \nu \, d_{N+1} = \mathbf{m} \cdot \mathbf{d}, \tag{1.90}$$

with

$$\mathbf{m} = [\mathbf{n}, \nu], \quad \mathbf{d} = (d_1, d_2, \ldots, d_N, d_{N+1})^{\mathrm{T}}. \tag{1.91}$$

We see immediately that $\mathbf{H}$ is singular, if either

$$\mathbf{m} \cdot \mathbf{d} = 0, \tag{1.92}$$

or

$$\mathbf{d} = \mathbf{0}. \tag{1.93}$$

Expression (1.93) is exactly the one obtained for the bifurcation point in Section 1.3.6 (equation (1.64)).

If (1.93) does not apply we can write for every index α corresponding to a nonzero d_α

$$x'_\alpha = \frac{d_\alpha}{F} \tag{1.94}$$

that is, the application of the Cramer's rule to the first N equation of system (1.84).

In view of studying F when limit points occur we would like to express two generic rate problem solutions, x'_β and x'_α for every $\beta \neq \alpha$ as

$$x'_\beta = f(D_\alpha, d_\alpha, \mathbf{x}'_\alpha).$$

Applying Cramer's rule to the first N equations of (1.84) also for x'_β and using equation (1.94), we get

$$x'_\beta = \frac{d_\beta}{F} \tag{1.95}$$

$$= \left(\frac{d_\beta}{d_\alpha}\right) x'_\alpha, \quad d_\alpha \neq 0, \quad \alpha \neq \beta, \tag{1.96}$$

where cofactors d_α and d_β are such that

$$\sum_{h=1}^{N} \frac{\partial D_\alpha}{\partial t_{h\beta}} t_{h\alpha} = (-1)^{\alpha+\beta-1} D_\beta, \quad \alpha \neq \beta. \tag{1.97}$$

In the above expression $t_{h\alpha}$ and $t_{h\beta}$ are respectively the α^{th} and β^{th} columns of $\mathbf{A}^\alpha$ and $\mathbf{A}^\beta$ matrixes being

$$\alpha = 1, 2, \ldots, N+1, \quad \beta = 1, 2, \ldots, N, \quad \alpha \neq \beta. \tag{1.98}$$

Thus, if $D_\alpha \neq 0$ for some α (or $\mathbf{d} \neq \mathbf{0}$) satisfaction of the first N equilibrium equation of the rate problem implies

$$\mathbf{d} = F\mathbf{x}' \tag{1.99}$$

$$\mathbf{d} = \left(\frac{d_\alpha}{x'_\alpha}\right)\mathbf{x}' \quad \text{for every } \alpha \quad \Longleftrightarrow \quad d_\alpha \neq 0. \tag{1.100}$$

The first equation is derived considering once more Cramer's rule for the first N equation now written in compact form, while the second comes from (1.99) simply taking F from equation (1.94). Finally, multiplying equation (1.99) by $\mathbf{m}$ and considering F given by expressions (1.90) and (1.95), we get

$$F = \left(\frac{d_\beta}{x'_\beta}\right)(\mathbf{m} \cdot \mathbf{x}'). \tag{1.101}$$

Equation (1.101) holds for every β corresponding to $d_\beta \neq 0$.

When $F \neq 0$, and thus $\mathbf{A}$ is nonsingular, the solutions of (1.84) are unique and we call regular the points of the solution curve where this hold. Of particular interest to the collapse analysis of the structure are limit points where the tangent $\mathbf{x}'$ takes the form

$$\mathbf{x}' = \begin{bmatrix} \mathbf{p}' \\ 0 \end{bmatrix}. \tag{1.102}$$

In this case, as it follows from (1.96) in which $\beta = N + 1$,

$$d_{N+1} = \det\{\mathbf{K}_t\} = 0. \tag{1.103}$$

We see, looking at (1.84), that $\mathbf{p}'$ must correspond to the null-vector of $\mathbf{K}_t$ ($\mathbf{p}' = \mu\mathbf{a}(1)$ where $\mathbf{a}(1) \in \mathrm{Ker}(\mathbf{K}_t)$, equation (1.44)). Similarly, if some component of $\mathbf{p}'$ is equal to zero, i.e. $p_K = 0$, we deal with a turning point with respect to $\boldsymbol{\delta}_K$, and we must have

$$d_K = \det\{\mathbf{A}^K\} = 0. \tag{1.104}$$

The solution of $\mathbf{x}'$ in that particular case corresponds to the null vector of $\mathbf{A}^K$.

We now inspect the situation in which the Jacobian $\mathbf{H}$ *becomes singular.* Limit points (1.92) correspond to the condition $\mathbf{m} \cdot \mathbf{x}' = 0$ (see (1.101)), where $\mathbf{x}'$ is the solution of the first N equations of (1.84). However, this inequality is in contradiction with the last equation of (1.84). In other words, equations (1.84) are *incompatibile* in this situation. We regard the point of the solution curve where this occur as a turning point with respect to the direction $\mathbf{m}$. This particular solution is thus the result of our particular choice of the constraint equation, G, and notice that, in principle, it can always be avoided if we take another G^* so that $\mathbf{m}^* \neq \mathbf{m}$, i.e. $(\mathbf{m}^* \cdot \mathbf{x}') \neq 0$

which is the result of an efficient parametrization, treated in the previous section.

Bifurcation points (1.93), as it follows from the examination of the augmented matrix $\mathbf{H}^* = (\mathbf{H}, \boldsymbol{\delta}_\lambda)$ of system (1.84), correspond to a rank deficiency of at least 1 for both $\mathbf{H}$ and $\mathbf{H}^*$. In general, this indicates the existence of multiple solutions $\mathbf{x}'$ of (1.84) and thus the presence of bifurcation of the solution curve $\mathbf{x}(\tau)$ at the point $\mathbf{x}(\tau^*)$ where (1.93) occurs.

We can now summarize the results as follows:

1. At a limit point for λ we encounter the conditions

$$F \neq 0, \quad D_M = 0, \quad \lambda' = 0,$$

and at a turning point with respect to $\boldsymbol{\delta}_K$

$$F \neq 0, \quad D_K = 0, \quad p'_K = 0.$$

2. At a bifurcation point we have:

$$F = 0, \quad D_\alpha = 0 \quad \forall \alpha. \tag{1.105}$$

3. At a regular point of the solution curve we can compute F from (1.101) with $\beta = N + 1$, thus for instance from

$$F = \left(\frac{D}{\lambda'}\right)(\mathbf{m} \cdot \mathbf{x}') \quad \text{where} \quad D = \det\{\mathbf{K}_t\}. \tag{1.106}$$

Chapter 2

Traditional continuation method

2.1 Basic algorithm

If we consider a structure, equilibrium equation (1.68) is often written as

$$\mathbf{r}(\mathbf{p}, \lambda) = \mathbf{F}_{int}(\mathbf{p}) - \mathbf{F}_{ext}(\lambda) = \mathbf{0} \tag{2.1}$$

where $\mathbf{F}_{int}$ is the internal resistance force vector, while $\mathbf{F}_{ext} = \lambda \mathbf{f}_{ext}$ is the external load, in which $\mathbf{f}_{ext}$ is fixed and the scalar λ is the load-control parameter.

As we said in Section (1.4), to follow an equilibrium path a proper parametrization is needed. Procedures to trace such equilibrium solutions of equation (2.1) are called **continuation** or **path following methods**. In general they are incremental, step-wise algorithms.

Simple **load-control** is the oldest and most traditional type of parametrization; moreover it is normally the most efficient one in the regular part of a path. The idea behind **load-control** techniques is to consider λ as a prescribed variable; this imply that we fix points of the solution curve particularizing equation (1.69) as follows

$$G = \lambda - \tau = 0, \tag{2.2}$$

where τ is the prescribed value of the load. Naturally, in this case it would not be necessary to solve the $N + 1$ equations (1.68)-(1.69) because we can reduce the augmented equilibrium problem (1.72) to the form of (1.68) by elimination of λ.

Equation (2.1) can be considered time dependent as $\mathbf{F}_{ext} = \mathbf{F}_{ext}(t)$, implying $\mathbf{p} = \mathbf{p}(t)$. In particular, simple variation rules can be given, as for instance

$$\mathbf{F}_{ext}(t) = t\mathbf{f}_{ext} \quad \text{with} \quad \mathbf{f}_{ext} = \text{const},$$

or

$$\mathbf{F}_{ext}(t) = \begin{cases} t\mathbf{f}_0 & 0 < t \leq t_1 \\ \mathbf{f}_1 + t\mathbf{f}_{ext} & t > t_1 \end{cases}$$

with $\mathbf{f}_1 = t_1\mathbf{f}_1$ and in which t is known.

Solution of the non-linear set of equations (2.1) is done in a stepwise manner by incrementing the external load vector $\mathbf{F}_{ext}$. The aim of the algorithm is to find the new $\mathbf{p}^{n+1}$, which corresponds to the prescribed load level $\mathbf{F}_{ext}^{n+1}$, starting from a given point $\mathbf{p}^n$, which corresponds to the load level $\mathbf{F}_{ext}^n$, such that

$$\mathbf{r}^n \equiv \mathbf{r}(\mathbf{p}^n) = \mathbf{0}. \tag{2.3}$$

In order to find $\mathbf{p}^{n+1}$, it is required the satisfaction of equation (2.1) written in the following discrete form

$$\mathbf{r}(\mathbf{p}^{n+1}) = \mathbf{F}_{int}(\mathbf{p}^{n+1}) - \mathbf{F}_{ext}^{n+1} = \mathbf{0}. \tag{2.4}$$

Starting from now, we use apexes to specify quantities evaluated at a certain time step, e.g.

$$\mathbf{p}^n = \mathbf{p}(t^n).$$

2.2 Incremental - iterative techniques

2.2.1 General remarks

As roots of the non-linear equation (2.1) cannot in general be expressed in closed form, some forms of successive approximation are always required. Moreover, in order to avoid "propagation errors" due to the absence of control of the generic step error (as for example in Euler's method), such methods are also iterative; that is, starting from a given $\mathbf{p}^n$, which is a converged solution at a previous load level such that $\mathbf{r}^n = \mathbf{0}$, and an initial approximation $\mathbf{p}_0^{n+1}$ (*predictor*), they produce a sequence $\mathbf{p}_1^{n+1}$, $\mathbf{p}_2^{n+1}$, $\mathbf{p}_3^{n+1}$,... which presumably converges to the desired solution. Here subscripts specify quantities evaluated within an iteration procedure which characterizes such **iterative techniques**. Then for unknown quantities there will also be a time index, e.g.

$$\mathbf{p}_{i+1}^{n+1} = \mathbf{p}_{i+1}(t^{n+1}).$$

The control of the generic step error is provided by the *corrector* phase. In fact, written the equilibrium residual at a generic iteration i

$$\mathbf{r}(\mathbf{p}_i^{n+1}) = \mathbf{F}_{int}(\mathbf{p}_i^{n+1}) - \mathbf{F}_{ext}^{n+1}, \tag{2.5}$$

the *corrector* procedure computes a new solution $\mathbf{p}_{i+1}^{n+1}$, which improves the current estimation $\mathbf{p}_i^{n+1}$ of the solution $\mathbf{p}^{n+1}$ until the residual force norm $||\mathbf{r}_{i+1}^{n+1}||$ satisfies, e.g., the follow inequality

$$||\mathbf{r}_{i+1}^{n+1}|| < \epsilon\, ||\mathbf{r}_0^{n+1}||, \tag{2.6}$$

where ϵ is a given tolerance.
The *corrector* phase has to be designed in order to produce an iterative scheme that produces a sequence $\mathbf{p}_2^{n+1}$, $\mathbf{p}_3^{n+1}$, $\mathbf{p}_4^{n+1}$, ... realizing

$$||\mathbf{r}_0^{n+1}|| > \cdots > ||\mathbf{r}_m^{n+1}|| > ||\mathbf{r}_{m+1}^{n+1}||. \tag{2.7}$$

What in general characterizes different methods is the relation

$$\mathbf{p}_{i+1}^{n+1} = \gamma(\mathbf{p}_i^{n+1}), \tag{2.8}$$

which links $\mathbf{p}_i^{n+1}$ to $\mathbf{p}_{i+1}^{n+1}$.

2.2.2 Newton - Raphson's method

The idea behind Newton-Raphson's method is to construct function $\gamma(\mathbf{p}_i^{n+1})$ imposing the linearization of discrete equilibrium equation (2.5), that is

$$\mathbf{r}(\mathbf{p}_{i+1}^{n+1}) \cong \mathbf{r}(\mathbf{p}_i^{n+1}) + \left.\frac{\partial \mathbf{r}}{\partial \mathbf{p}}\right|_i d\mathbf{p}_{i+1}^{n+1} = \mathbf{0}. \tag{2.9}$$

The jacobian matrix (or, in structural terms, the stiffness matrix) corresponding to a tangent direction is given by

$$\mathbf{K}_t = \left.\frac{\partial \mathbf{r}}{\partial \mathbf{p}}\right|_i. \tag{2.10}$$

Equation (2.9) gives immediately the iterative correction as

$$d\mathbf{p}_{i+1}^{n+1} = -\mathbf{K}_t^{-1}\mathbf{r}(\mathbf{p}_i^{n+1}). \tag{2.11}$$

A series of successive approximations gives

$$\begin{aligned} \mathbf{p}_{i+1}^{n+1} &= \mathbf{p}_i^{n+1} + d\mathbf{p}_{i+1}^{n+1} && (2.12)\\ &= \mathbf{p}^n + \Delta\mathbf{p}_{i+1}^{n+1}, && (2.13) \end{aligned}$$

where

$$\Delta\mathbf{p}_{i+1}^{n+1} = \sum_{k=1}^{i+1} d\mathbf{p}_k^{n+1}; \tag{2.14}$$

so

$$\gamma(\mathbf{p}_i^{n+1}) = \mathbf{p}_i^{n+1} - \mathbf{K}_t^{-1}\mathbf{r}(\mathbf{p}_i^{n+1}). \tag{2.15}$$

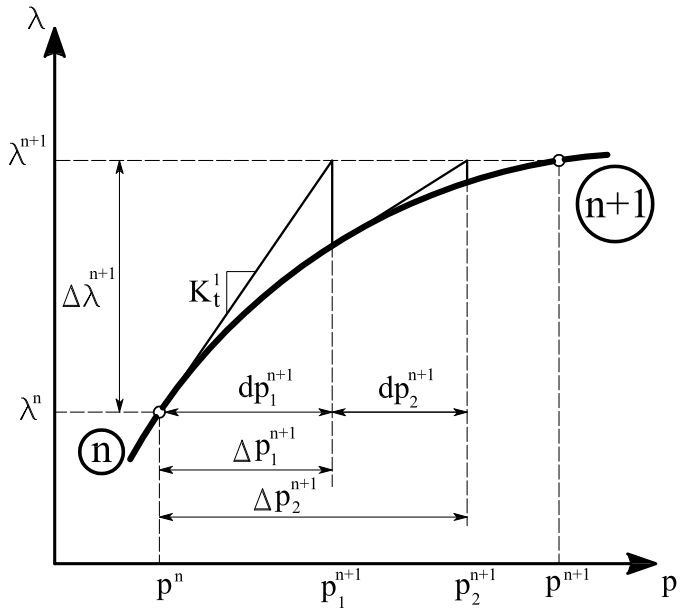

Figure 2.1: Newton-Raphson's method.

Quadratical convergence

To study convergence properties of Newton-Raphson's method we assume that $\mathbf{r}(\mathbf{p})$ has two continuous derivatives, and that the root $\boldsymbol{\alpha}$ which we are seeking is a simple root. Then we suppose $f'(\boldsymbol{\alpha}) \neq 0$ and thus $f'(\mathbf{p}) \neq 0$ for all $\mathbf{p}$ in a certain neighborhood of the root $\boldsymbol{\alpha}$. Let $\boldsymbol{\epsilon}_i$ be the error in the estimate $\mathbf{p}_i$; i.e.,

$$\boldsymbol{\epsilon}_i = \mathbf{p}_i - \boldsymbol{\alpha}. \tag{2.16}$$

Under the above assumptions, we derive now a relation between $\boldsymbol{\epsilon}_i$ and $\boldsymbol{\epsilon}_{i+1}$. Expanding $\mathbf{r}(\boldsymbol{\epsilon}_{i+1})$ in a Taylor's series about $\mathbf{p}_i$ we get

$$\mathbf{0} = \mathbf{r}(\boldsymbol{\alpha}) = \mathbf{r}(\mathbf{p}_i) + (\mathbf{p}_i - \boldsymbol{\alpha})\mathbf{r}'(\mathbf{p}_i) + \frac{1}{2}(\mathbf{p}_i - \boldsymbol{\alpha})^2\mathbf{r}''(\boldsymbol{\xi}), \quad \boldsymbol{\xi} \in \text{int}(\mathbf{p}_i, \boldsymbol{\alpha}),$$

or multiplying by $[\mathbf{r}'(\mathbf{p}_i)]^{-1} = \left(\dfrac{d\mathbf{r}(\mathbf{p}_i)}{d\mathbf{p}_i}\right)^{-1} = \mathbf{K}_t^{-1}$,

$$-\mathbf{r}(\mathbf{p}_i)\mathbf{K}_t^{-1} + \boldsymbol{\alpha} - \mathbf{p}_i = \boldsymbol{\alpha} - \mathbf{p}_{i+1} = \frac{1}{2}(\mathbf{p}_i - \boldsymbol{\alpha})^2\mathbf{r}''(\boldsymbol{\xi})\mathbf{K}_t^{-1}.$$

Thus we have

$$\boldsymbol{\epsilon}_{i+1} = -\frac{1}{2}\boldsymbol{\epsilon}_i^2\mathbf{r}''(\boldsymbol{\xi})\mathbf{K}_t^{-1}, \tag{2.17}$$

Since $\boldsymbol{\epsilon}_{i+1}$ is related to the square of $\boldsymbol{\epsilon}_i$, Newton-Raphson's method is said to be *quadratically convergent* or to be a *a second order method*. A more precise definition can be found in (2).

Sufficient conditions for convergence

A more detailed study of the convergence of the method can be obtained by observing how the secant stiffness "follows" the tangent stiffness matrix $\mathbf{K}_t$.

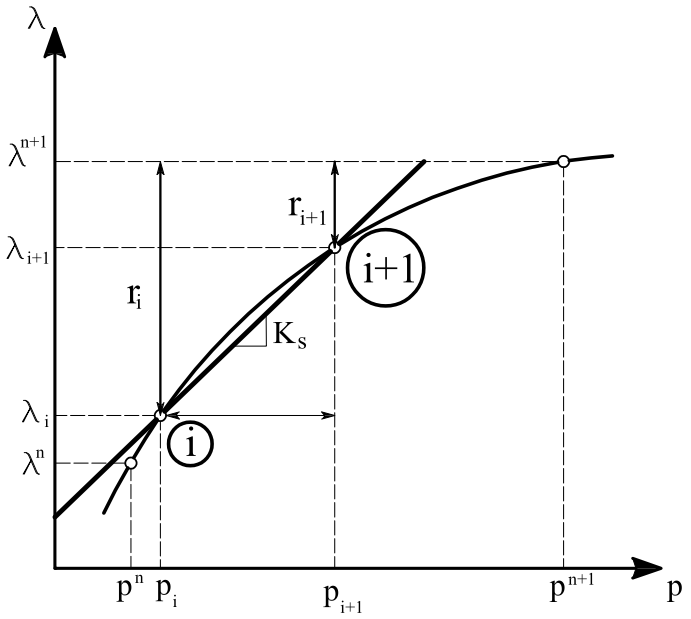

Figure 2.2: Graphic construction of residual difference between two successive iterations.

We can in general express the difference between residual vectors at two successive iterations within step $n+1$ (see figure 2.2) as

$$\mathbf{r}_{i+1} - \mathbf{r}_i = \mathbf{K}_s(\mathbf{p}_{i+1} - \mathbf{p}_i), \tag{2.18}$$

where $\mathbf{K}_s$ is the secant stiffness matrix, defined as

$$\mathbf{K}_s = \int_0^1 \mathbf{K}[\mathbf{p}_i + t(\mathbf{p}_{i+1} - \mathbf{p}_i)]\mathrm{d}t. \tag{2.19}$$

From expressions (2.11) and (2.12) we get the expression of $\mathbf{p}_{i+1}$ which inserted in (2.18) gives

$$\mathbf{r}_{i+1} = [\mathbf{I} - \mathbf{K}_s\mathbf{K}_t^{-1}]\mathbf{r}_i. \tag{2.20}$$

As we see in (2.7) we require that the iterative scheme produces

$$||\mathbf{r}_{i+1}|| < ||\mathbf{r}_i||. \tag{2.21}$$

Now, if matrix $[\mathbf{I}-\mathbf{K}_s\mathbf{K}_t^{-1}]$ has eigenvalues $\mu_1, \mu_2, \ldots, \mu_n$ and corresponding eigenvectors $\mathbf{y}_1, \mathbf{y}_2, \ldots, \mathbf{y}_n$ linearly independent, it is possible to express r_i in such a base of eigenvectors as

$$\mathbf{r}_i = \sum_j^n \alpha_j \mathbf{y}_j \quad \alpha_j \in \mathbb{R}. \tag{2.22}$$

So $\mathbf{r}_{i+1}$ takes the form of

$$\mathbf{r}_{i+1} = \sum_j^n \alpha_j \mu_j \mathbf{y}_j, \tag{2.23}$$

that is, every $\mathbf{r}_i$ component in the direction of eigenvector $\mathbf{y}_j$ is scaled by eigenvalue μ_j. From this, it follows that a sufficient condition for convergence

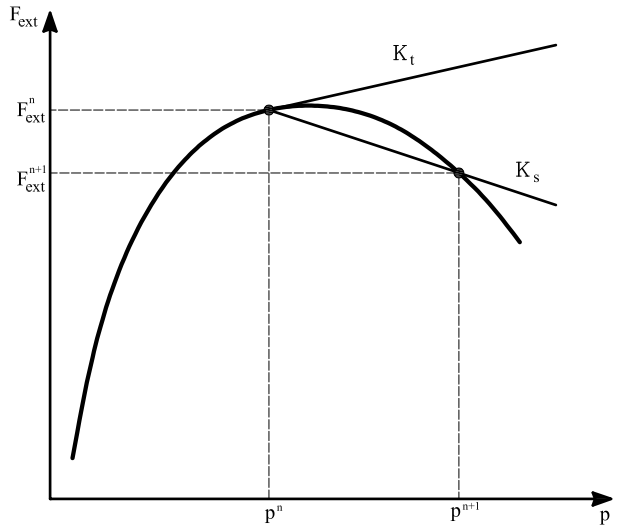

Figure 2.3: Failure in convergence of Newton-Raphson method

is that

$$|\mu_j| < 1 \quad \text{or} \quad -1 < \mu_j < 1. \tag{2.24}$$

It is easy to prove that condition (2.24) is equivalent to write

$$0 < \eta_j < 2, \quad j = 1, \ldots, n, \tag{2.25}$$

with η_j eigenvalues of the matrix $[\mathbf{K}_s\mathbf{K}_t^{-1}]$. Thus we expect difficulty in convergence either near a limit point, where $\eta_j = 0$ or, where the secant stiffness $\mathbf{K}_s$ is at least twice the tangent stiffness matrix $\mathbf{K}_t$, that is when $\eta_j \geq 2$.
In fact, from condition (2.25) we get that no convergence is reached when

$\eta_j < 0$, i.e., as shown in figure 2.3 for $j = 1$, when there is a passage through a limit point. Such a failure is strictly related to the necessity of load factor to decrease; this phenomenon is often associated with changes in the equilibrium path "slope".

2.2.3 Modified Newton - Raphson's method

This method uses essentially the same algorithm as the Newton-Raphson's technique but replaces the variable matrix $\mathbf{K}_t$ by a constant approximation

$$\mathbf{K}_t \approx \overline{\mathbf{K}}_t = \text{const.} \tag{2.26}$$

giving, in place of Equation (2.11),

$$d\mathbf{p}_{i+1}^{n+1} = -\overline{\mathbf{K}}_t^{-1}\mathbf{r}(\mathbf{p}_i^{n+1}). \tag{2.27}$$

Many possible choices exist here. For instance, $\overline{\mathbf{K}}_t$ can be chosen as the matrix corresponding to the first iteration (as shown in Figure 2.4) or may even be one corresponding to some previous time step or load increment. Alternatively, the approximation can be chosen every few iterations.

Obviously, the procedure generally will converge at a slower rate (generally the norm of the residual $\mathbf{r}$ has a linear asymptotic convergence instead of the quadratic one of the full Newton-Raphson's method) but some difficulties mentioned above for Newton process disappear.

2.2.4 Some observations about Newton - Raphson's method

Newton's method is the most rapidly convergent process for solution of problems in which only one evaluation of $\mathbf{r}$ is made in each iteration. Of course, this assumes that the initial solution (*predictor*) is within the *zone of attraction* and, thus, divergence does not occur. Figure 2.1 shows the very rapid convergence that can be achieved.

The Newton-Raphson's process, despite its rapid convergence, has some negative features:

1. its failure when matrix $\mathbf{K}_t$ becomes singular;
2. a new $\mathbf{K}_t$ matrix has to be computed at each iteration;
3. if direct solution for Equation (2.11) is used, the matrix needs to be factored at each iteration;
4. on some occasions the tangent matrix is symmetric at a solution state but unsymmetric otherwise. In these cases un unsymmetric solver is needed in general.

Some of these drawbacks are absent in alternative procedures, although generally then a quadratic asymptotic rate of convergence is lost.

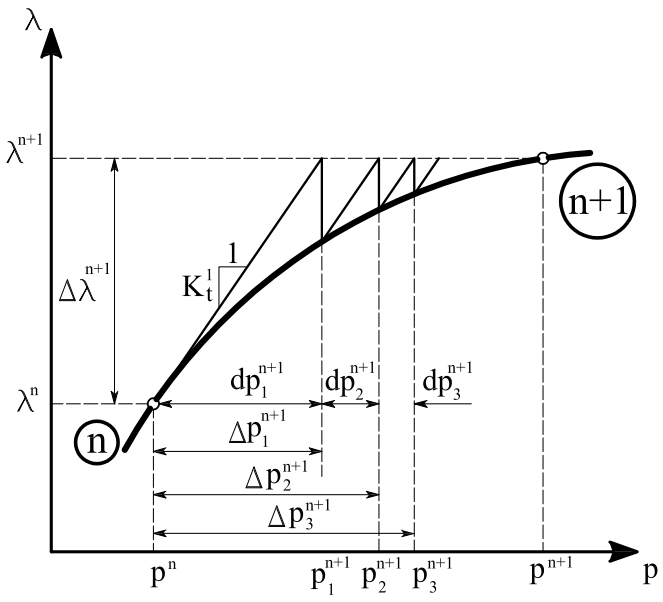

Figure 2.4: Modified Newton-Raphson's method.

Chapter 3

Arc-Length methods

3.1 Basic algorithm

Although the *load-control method* is the most efficient in following equilibrium path in its regular parts, it breaks down near the so called limit points, where the structure loses its load carrying capacity (at least locally). At limit points in fact the stiffness matrix $\mathbf{K}_t$ is singular and the load parameter start to decrease. In other words, for such a method it is always possible to define a turning point so that no solution can be obtained, as shown in figure 3.1.

In fact, as we discussed in Section 1.4, the aim is to choose τ, thus $g(\mathbf{p}, \lambda)$, maintaining a one-to-one correspondence between the natural measure along the path, s, and τ itself. So the load parameter λ is an unknown, differently from the *load-control method*.

Remembering equation (1.72), we have in this case

$$\mathbf{R}(\mathbf{x}, \tau) = \left\{ \begin{array}{l} \mathbf{r}(\mathbf{x}, \tau) = \mathbf{F}_{int}[\mathbf{p}(\tau)] - \lambda(\tau)\mathbf{f}_{ext} \\ G(\mathbf{x}, \tau) = g(\mathbf{x}) - \tau \end{array} \right\} = \mathbf{0}, \quad \mathbf{R} \in \mathbb{R}^{n+1}. \tag{3.1}$$

The question is now how to define a suitable parametrization τ.

It is clear that in general it will not be possible to find a fixed equation G that gives τ the desired properties. Consequently, the definition of τ must be variable and take into account the nature of the curves to be computed; this results in a particular *adaptive parametrization* since the surface orientation, described by its normal, changes with time. In Section 1.4, see (1.101), we proved that turning points do not occur as long as we keep acute angle θ at the intersection point between the normal $\mathbf{m}$ to the surface G and the tangent to the path $\dot{\mathbf{x}}(s)$. The best choice in this sense would then be $\theta = 0$, which we achieve if we take $\mathbf{m} = \dot{\mathbf{x}}(s)$. In figure 3.1 it is possible to observe that the *load-control method* fails in giving back an efficient intersection between equilibrium curve and constraint surface when limit point is approached; in fact in such a case $\mathbf{m}$ is orthogonal to $\dot{\mathbf{x}}$.

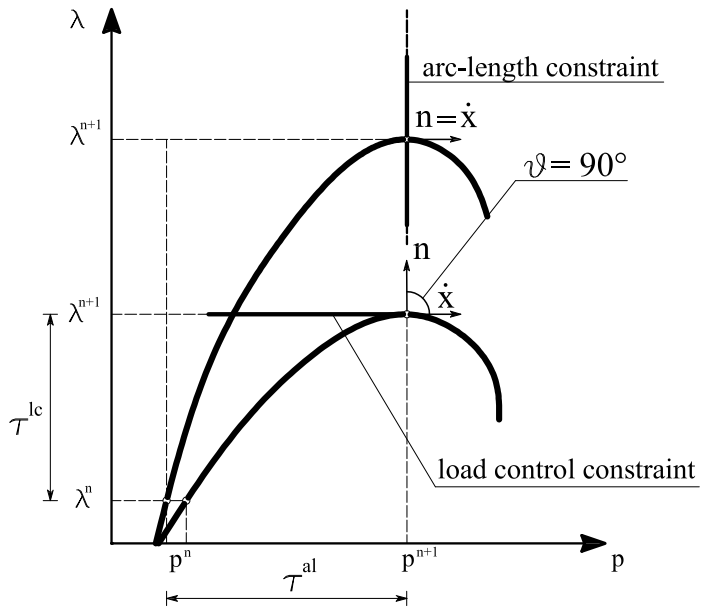

Figure 3.1: Arc-length success and load-control failure.

3.2 Incremental - iterative techniques

Equation (3.1) represents a nonlinear system of N+1 unknowns which may be solved iteratively, e.g. using the standard Newton-Raphson scheme, for a sequence of successive increments of τ starting from the known point ($\mathbf{p} = \mathbf{0}$, λ=0). In particular there are two ways of resolution

1. Linearize both the equilibrium equation and constraint surface G, obtaining the so called *linearized arc-length methods*;

2. Linearize the equilibrium equation and satisfy the constraint G identically (8).

3.2.1 Newton - Raphson's method

Once the first step has been established (*predictor step*), we proceed with the second of the approaches introduced above, initially writing (3.1) in discrete form

$$\mathbf{R}(\mathbf{x}^{n+1}, \tau) = \left\{ \begin{array}{c} \mathbf{r}(\mathbf{x}^{n+1}) \\ g(\mathbf{x}^{n+1}) - \tau \end{array} \right\} = \mathbf{0}. \tag{3.2}$$

In the following, for the sake of simplicity, for unknown quantities we indicate only the iteration subscript, e.g.

$$\mathbf{x}_{i+1} = \mathbf{x}_{i+1}^{n+1} = \mathbf{x}_{i+1}(t_{n+1}).$$

Now we linearize the equilibrium equation

$$\begin{aligned}\mathbf{r}_{i+1} = \mathbf{r}(\mathbf{x}_{i+1}) &= \mathbf{r}_i + (\nabla_{\mathbf{x}_i}\mathbf{r})d\mathbf{x}_{i+1} = \\ &= \mathbf{r}_i + \left.\frac{\partial \mathbf{r}}{\partial \mathbf{p}}\right|_{\mathbf{x}=\mathbf{x}_i} d\mathbf{p}_{i+1} + \left.\frac{\partial \mathbf{r}}{\partial \lambda}\right|_{\mathbf{x}=\mathbf{x}_i} d\lambda_{i+1} = \mathbf{0}, \quad (3.3)\end{aligned}$$

and remembering (2.10), Newton's resolution of equation (3.2) at iteration $i+1$ becomes

$$\begin{cases}\mathbf{K}_t d\mathbf{p}_{i+1} - d\lambda_{i+1}\mathbf{f}_{ext} = -\mathbf{r}_i \\ g(\mathbf{x}_i + d\mathbf{x}_{i+1}) - \tau = 0\end{cases} \quad d\mathbf{x}_{i+1} = \begin{bmatrix} d\mathbf{p}_{i+1} \\ d\lambda_{i+1}\end{bmatrix} = \begin{bmatrix} \mathbf{p}_{i+1} - \mathbf{p}_i \\ \lambda_{i+1} - \lambda_i\end{bmatrix}. \quad (3.4)$$

The first approach is instead obtained extending Newton-Raphson's formulation also to the constraint equation G of *corrector* (3.2). So the constraint becomes

$$\begin{aligned}[g(\mathbf{x}_{i+1}) - \tau] = g(\mathbf{x}_i) - \tau^{n+1} + (\nabla_{\mathbf{x}_i} g)d\mathbf{x}_{i+1} = 0 \\ \Longrightarrow \quad (\nabla_{\mathbf{x}_i} g)d\mathbf{x}_{i+1} = \tau - g(\mathbf{x}_i). \quad (3.5)\end{aligned}$$

Hence, the iterative scheme associated to the *linearized arc-length method* is given by

$$\mathbf{H}d\mathbf{x}_{i+1} = -\mathbf{R}_i \quad d\mathbf{x}_{i+1} := \begin{bmatrix} \mathbf{p}_{i+1} - \mathbf{p}_i \\ \lambda_{i+1} - \lambda_i \end{bmatrix} \quad \mathbf{R}_i := \begin{bmatrix} \mathbf{r}_i \\ g(\mathbf{x}_i) - \tau \end{bmatrix}, \quad (3.6)$$

being $\mathbf{H}$ the Jacobian matrix of equation (3.1), i.e.

$$\mathbf{H} := \begin{bmatrix} \mathbf{K}_t & -\mathbf{f}_{ext} \\ \nabla_{\mathbf{p}} g & \nabla_\lambda g \end{bmatrix}, \quad (3.7)$$

with

$$\nabla_{\mathbf{p}} g = \left.\frac{\partial g}{\partial \mathbf{p}}\right|_{\mathbf{x}=\mathbf{x}_i}, \quad \nabla_\lambda g = \left.\frac{\partial g}{\partial \lambda}\right|_{\mathbf{x}=\mathbf{x}_i}. \quad (3.8)$$

3.2.2 Partitioned solution

System (3.7) is solved in a partitioned form in order to exploit structure of the stiffness matrix. Two possible approaches can be used.

1. Solve first the equilibrium equation and insert the result into the constraint equation, i.e.

$$\begin{cases} d\lambda_{i+1} = \dfrac{\mathbf{d}_i^{\mathrm{T}}\mathbf{r}_i + \tau - g(\mathbf{x}_i)}{\nabla_\lambda g + \mathbf{d}_i^{\mathrm{T}}\mathbf{f}_{ext}} & (3.9) \\ d\mathbf{p}_{i+1} = \mathbf{K}_t^{-1}[\lambda_i \mathbf{f}_{ext} - \mathbf{r}_i], & (3.10) \end{cases}$$

where

$$\mathbf{d}_i = \mathbf{K}_t^{-1}(\nabla_{\mathbf{p}} g). \quad (3.11)$$

2. Solve first the constraint equation and insert the result into the equilibrium equation, i.e.

$$\begin{cases} d\lambda_{i+1} = \dfrac{\mathbf{r}_i + \mathbf{K}_t \, d\mathbf{p}_i}{\mathbf{f}_{ext}} & (3.12) \\ d\mathbf{p}_{i+1} = \left[\mathbf{K}_t + \dfrac{\mathbf{f}_{ext} \, (\nabla_{\mathbf{p}} g)^{\mathrm{T}}}{\nabla_\lambda g}\right]^{-1} \left\{ \dfrac{[\tau - g(\mathbf{x}_i)] \, \mathbf{f}_{ext}}{\nabla_\lambda g} - \mathbf{r}_i \right\}. & (3.13) \end{cases}$$

Note that $\left[\mathbf{K}_t + \dfrac{\mathbf{f}_{ext} \, (\nabla_{\mathbf{p}} g)^{\mathrm{T}}}{\nabla_\lambda g}\right]$ is a rank 1 modification of $\mathbf{K}_t$ (11).

Matrix $\mathbf{K}_t$ can be updated at each iteration loop (*Newton-Raphson's* scheme) or it can be evaluated only once at the beginning of the incremental step (*Modified Newton-Raphson's* scheme).
Iterative corrections have the form

$$\begin{cases} \mathbf{p}_{i+1} = \mathbf{p}_i + d\mathbf{p}_{i+1} & (3.14) \\ \lambda_{i+1} = \lambda_i + d\lambda_{i+1}, & (3.15) \end{cases}$$

or

$$\begin{cases} \mathbf{p}_{i+1} = \mathbf{p}^n + \Delta\mathbf{p}_{i+1} & (3.16) \\ \lambda_{i+1} = \lambda^n + \Delta\lambda_{i+1}, & (3.17) \end{cases}$$

where $\Delta\mathbf{p}_{i+1}$ (2.14) and $\Delta\lambda_{i+1}$ are

$$\begin{aligned} \Delta\mathbf{p}_{i+1} &= \mathbf{p}_{i+1} - \mathbf{p}^n = \Delta\mathbf{p}_i + d\mathbf{p}_{i+1} & (3.18) \\ \Delta\lambda_{i+1} &= \lambda_{i+1} - \lambda^n = \Delta\lambda_i + d\lambda_{i+1}, & (3.19) \end{aligned}$$

with

$$\begin{aligned} \Delta\mathbf{p}_i &= \sum_{k=1}^{i} d\mathbf{p}_k, \\ \Delta\lambda_i &= \sum_{k=1}^{i} d\lambda_k. & (3.20) \end{aligned}$$

3.3 Different constraint equations

Till now we have spoken about constraint surface in general terms, i.e. as

$$G(\mathbf{x}, \tau) = g(\mathbf{x}) - \tau = 0. \tag{3.21}$$

Now, we would like to determine a form for such a surface so that the intersection between the equilibrium curve and G does not degenerate. We have said also that a measure of the quality of the intersection is given by θ, the angle between the tangent of the equilibrium curve, $\dot{\mathbf{x}}$, and the normal

to the intersecting surface at the point of intersection, $\mathbf{m}$; such intersection is considered "good" if θ is close to zero and "bad" if it is close to $\pi/2$. In this sense, it would be ideal selecting a family of surfaces G which intersects the equilibrium curve everywhere according to condition $\theta = 0$ as shown in figure 3.1. However, it is not necessary to have exactly $\theta = 0$ at any point to be computed, but also a small value $\theta < \pi/2$ is sufficient to protect the procedure against failure. The relaxation of the condition $\theta = 0$ to $\theta < \pi/2$ opens a whole world of possible formulation of equation (3.21).

In the mid 1970s, Riks (3) initially proposed a certain parametrization such that the control parameter τ is used as a good approximation of the arc-length s, i.e.

$$\dot{\lambda}^2 + \dot{\mathbf{p}}^{\mathrm{T}}\dot{\mathbf{p}} = 1. \tag{3.22}$$

We recall that $(\dot{\ }) = d/ds(\ ) = d/d\tau(\ )$, as introduced in Section 1.4. For this reason this kind of approaches are called **arc-length methods**.

Let $\mathbf{x}^* = (\mathbf{p}^*, \lambda^*)$ denote a point of the path and let τ^* denote the value of the control parameter τ at this point. A large class of constraint equations, which approximate $s = \tau$ in the sense of (3.22), can be written in the form

$$G = \mathbf{m}^{\mathrm{T}}(\mathbf{x} - \mathbf{x}^*) - (\tau - \tau^*) = 0, \tag{3.23}$$

that is, a surface such as its projection with respect to normal $\mathbf{m} = (\mathbf{n}, \nu)$ has a fixed distance $(\tau - \tau^*)$ from origin $\mathbf{x}^*$, kept fixed; moreover, it can be noticed that there will be intersections with a small angle θ if the distance $(\tau - \tau^*)$ is kept small.

The scalar product expressed in equation (3.23) must be suitable for homogenizing variables of different nature. For this reason it is necessary to define a weighting matrix $\mathbf{M}$ partitioned as

$$\mathbf{M} = \begin{bmatrix} \mathbf{N} & 0 \\ \mathbf{0} & \mu \end{bmatrix}, \tag{3.24}$$

and such that

$$\begin{cases} \mathbf{M}^{\mathrm{T}} = \mathbf{M} \\ \mathbf{x}^{\mathrm{T}}\,\mathbf{M}\,\mathbf{x} > 0 \quad \text{if} \quad \mathbf{x} \neq \mathbf{0}, \end{cases} \tag{3.25}$$

i.e., $\mathbf{M}$ is symmetric and positive definite. Constraint equation is then expressed as

$$\boxed{G = \mathbf{m}^{\mathrm{T}}\mathbf{M}(\mathbf{x} - \mathbf{x}^*) - (\tau - \tau^*) = 0.} \tag{3.26}$$

3.3.1 Linearized arc-length methods

We refer now to those kinds of methods which utilize as resolution technique the linearization of both the equilibrium and the constraint equation (3.26) (first approach).

Within an iterative procedure the fixed point $\mathbf{x}^*$, used as reference for the constraint surface, is taken equal to $\mathbf{x}^n$ previously computed. Thus considering equation (3.26) and indicating $\tau^{n+1} - \tau^n$ with $\Delta\tau$, we get the entire expression of the constraint equation, written in discrete form at iteration $i+1$, as

$$\mathbf{m}^{\mathrm{T}}\,\mathbf{M}\,(\mathbf{x}_{i+1} - \mathbf{x}^n) - \Delta\tau = 0. \tag{3.27}$$

Linearization of the above equation leads to

$$\mathbf{m}^{\mathrm{T}}\,\mathbf{M}\,d\mathbf{x}_{i+1} = \Delta\tau - \mathbf{m}^{\mathrm{T}}\,\mathbf{M}\,(\mathbf{x}_i - \mathbf{x}^n), \tag{3.28}$$

and requiring, as in (4), that $\Delta\tau - \mathbf{m}^{\mathrm{T}}\,\mathbf{M}\,(\mathbf{x}_i - \mathbf{x}^n) = 0$, we get

$$\mathbf{m}^{\mathrm{T}}\,\mathbf{M}\,d\mathbf{x}_{i+1} = 0. \tag{3.29}$$

The original method proposed by Riks in (4) considered

$$\mathbf{m} = \begin{bmatrix} \mathbf{p}_0 - \mathbf{p}^n \\ \lambda_0 - \lambda^n \end{bmatrix}. \tag{3.30}$$

Such a method is called **Normal Plane** and ensures that increment $d\mathbf{x}_{i+1} = (d\mathbf{p}_{i+1}, d\lambda_{i+1})$ is orthogonal to the *tangent prediction* increment $\mathbf{m} = \Delta\mathbf{x}_0 = (\Delta\mathbf{p}_0, \Delta\lambda_0)$. In figure 3.2 it is possible to observe Normal Plane rate of convergence with a Modified Newton-Raphson's iterative scheme.

An analogous procedure is the **Updated Normal Plane** proposed by Ramm in reference (9) which ensures that the iterative increment $d\mathbf{x}_{i+1} = (d\mathbf{p}_{i+1}, d\lambda_{i+1})$ is orthogonal to the previous "secant increment" $\mathbf{m} = \Delta\mathbf{x}_i = (\Delta\mathbf{p}_i, \Delta\lambda_i)$. Thus

$$\mathbf{m} = \begin{bmatrix} \mathbf{p}_i - \mathbf{p}^n \\ \lambda_i - \lambda^n \end{bmatrix}, \tag{3.31}$$

which means that the normal $\mathbf{m}$ is variable within each iteration. Figure 3.3 shows the quick convergence of the Updated Normal Plane method with a Modified Newton-Raphson's iterative scheme.

Another method, the so called **Orthogonal Trajectory Method**, was proposed by Fried in (10). It consist of an orthogonal trajectory approach to the equilibrium curve without the need for an explicit constraint, and without the involvement of an equilibrium point $\mathbf{x}^*$. The orthogonality condition to be imposed is

$$\nabla_{\mathbf{x}}[\mathbf{r}(\mathbf{x})]\mathbf{m} = \mathbf{0}. \tag{3.32}$$

If we require a linear constraint relating $d\mathbf{p}_{i+1}$ and $d\lambda_{i+1}$, orthogonal accession (3.32) is satisfied if we take $\mathbf{m}$ of the form

$$\mathbf{m} = \begin{bmatrix} \hat{\mathbf{p}} \\ 1 \end{bmatrix}, \tag{3.33}$$

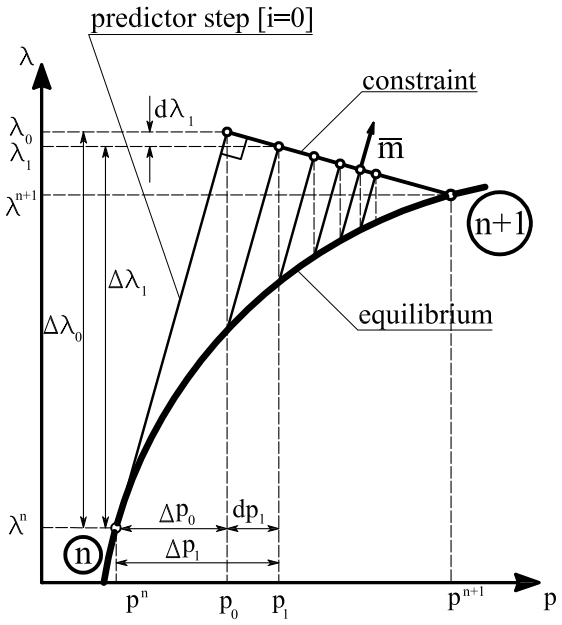

Figure 3.2: **Normal Plane** method with Modified Newton as iterative scheme

where $\hat{\mathbf{p}}$ is

$$\hat{\mathbf{p}} = \mathbf{K}_t^{-1}\mathbf{f}_{ext}. \tag{3.34}$$

Orthogonality is in fact proved by the following simple calculation

$$\begin{aligned} \nabla_{\mathbf{x}}[\mathbf{r}(\mathbf{x})]\mathbf{m} &= [\mathbf{K}_t, -\mathbf{f}_{ext}][\mathbf{n}, \mu]^{\mathrm{T}} \\ &= [\mathbf{K}_t, -\mathbf{f}_{ext}][\hat{\mathbf{p}}, 1]^{\mathrm{T}} \\ &= [\mathbf{K}_t, -\mathbf{f}_{ext}][\mathbf{K}_t^{-1}\mathbf{f}_{ext}, 1]^{\mathrm{T}} \\ &= \mathbf{0} \end{aligned}$$

Comparing this with (3.30) for Riks' method, we can see that the orthogonal constraint is here updated every iteration, as in Ramm's technique (3.31).

Remembering equations (3.1), (3.6) and the structure of matrix $\mathbf{M}$ (3.24), the jacobian matrix $\mathbf{H}$ and the residual force vector $\mathbf{R}_i$ for this approach become

$$\mathbf{H} := \begin{bmatrix} \mathbf{K}_t & -\mathbf{f}_{ext} \\ \mathbf{n}^{\mathrm{T}}\mathbf{N} & \nu\mu \end{bmatrix}, \quad \mathbf{R}_i := \begin{bmatrix} \mathbf{r}_i \\ 0 \end{bmatrix}. \tag{3.35}$$

Thus the two partitioned solutions take the following forms.

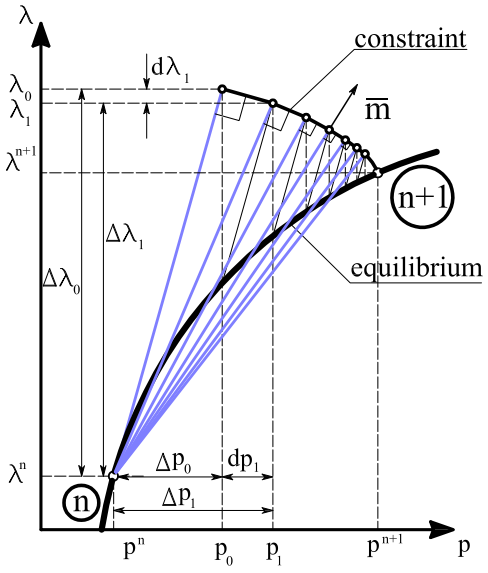

Figure 3.3: **Updated Normal Plane** method with Modified Newton as iterative scheme

1. Equations (3.9) and (3.10) become

$$\begin{cases} d\lambda_{i+1} = \dfrac{\mathbf{d}_i^{\mathrm{T}}\mathbf{r}_i}{\mu\nu + \mathbf{d}_i^{\mathrm{T}}\mathbf{f}_{ext}} & (3.36) \\ d\mathbf{p}_{i+1} = \mathbf{K}_t^{-1}[d\lambda_i\mathbf{f}_{ext} - \mathbf{r}_i] = -\mathbf{K}_t^{-1}\left[\mathbf{I} - \dfrac{\mathbf{f}_{ext}\mathbf{d}_i^{\mathrm{T}}}{\mu\nu + \mathbf{f}_{ext}^{\mathrm{T}}\mathbf{d}_i}\right]\mathbf{r}_i, & (3.37) \end{cases}$$

   with

$$\mathbf{d}_i = \mathbf{K}_t^{-1}\mathbf{N}\mathbf{n}; \tag{3.38}$$

2. Equations (3.12) and (3.13) become

$$\begin{cases} d\lambda_{i+1} = -\dfrac{\mathbf{n}^{\mathrm{T}}\mathbf{N}\, d\mathbf{p}_i}{\mu\nu} = \mathbf{n}^{\mathrm{T}}\mathbf{N}\left[\mathbf{K}_t + \dfrac{\mathbf{f}_{ext}\mathbf{n}^{\mathrm{T}}\mathbf{N}}{\mu\nu}\right]^{-1}\dfrac{\mathbf{r}_i}{\mu\nu} & (3.39) \\ d\mathbf{p}_{i+1} = -\left[\mathbf{K}_t + \dfrac{\mathbf{f}_{ext}\mathbf{n}^{\mathrm{T}}\mathbf{N}}{\mu\nu}\right]^{-1}\mathbf{r}_i. & (3.40) \end{cases}$$

3.3.2 Second approach in Newton's resolution and spherical arc-length method

We refer now to those kinds of methods which utilize as resolution technique the linearization of only the equilibrium equation, while the constraint equation (3.26) is identically satisfied (second approach).

Historically this resolution technique was proposed by Crisfield in reference (8) who also used a quadratic constraint with $\mathbf{m} = \mathbf{x} - \mathbf{x}^*$ in equation (3.26), i.e.

$$(\mathbf{x} - \mathbf{x}^*)^{\mathrm{T}} \mathbf{M} (\mathbf{x} - \mathbf{x}^*) - (\tau - \tau^*) = 0. \tag{3.41}$$

Crisfield explicitly forces the cylindrical constraint at every iteration, and this results in a quadratic scalar equation for the solution of the load parameter increment, in contrast to the linearized procedure of the methods previously described. The surface which defines the so called **spherical arc-length method** is an hypersphere in $\mathbb{R}^{n+1}$ and is given in its discrete form at iteration $i+1$ by

$$(\mathbf{x}_{i+1} - \mathbf{x}^n)^{\mathrm{T}} \mathbf{M} (\mathbf{x}_{i+1} - \mathbf{x}^n) - \Delta\tau = 0, \tag{3.42}$$

that is

$$\Delta\mathbf{x}_{i+1}^{\mathrm{T}} \mathbf{M} \Delta\mathbf{x}_{i+1} - \Delta\tau^2 = 0, \tag{3.43}$$

being

$$\Delta\mathbf{x}_{i+1} = \mathbf{x}_{i+1} - \mathbf{x}^n, \qquad \mathbf{M} = \begin{bmatrix} \mathbf{I} & 0 \\ \mathbf{0} & \psi^2 \mathbf{f}_{ext}^{\mathrm{T}} \mathbf{f}_{ext} \end{bmatrix}. \tag{3.44}$$

In the above equation, ψ is the scaling parameter required because the load contribution depends on the adopted scaling between the load and the displacement terms. This means that, depending on the value of the scaling factor ψ, the iterations are constrained to the surface of an ellipsoid ($\psi \neq 0$) or a cylinder ($\psi = 0$).

Considering the linearized equilibrium equation (3.3) and the discrete spherical constraint (3.43), the second approach in Newton-Raphson's resolution particularizes as

$$\begin{cases} \mathbf{K}_t d\mathbf{p}_{i+1} - d\lambda_{i+1} \mathbf{f}_{ext} = -\mathbf{r}_i & (3.45) \\ \Delta\mathbf{p}_{i+1}^{\mathrm{T}} \Delta\mathbf{p}_{i+1} + \Delta\lambda_{i+1}^2 \psi^2 \mathbf{f}_{ext}^{\mathrm{T}} \mathbf{f}_{ext} - \Delta\tau^2 = 0. & (3.46) \end{cases}$$

The problem is solved in a partitioned form by inserting the linearized equilibrium equation (3.45) within the constraint equation (3.46) which is identically satisfied for every iteration steps. From equation (3.45)

$$\begin{aligned} d\mathbf{p}_{i+1} &= -\mathbf{K}_t^{-1} \mathbf{r}_i + \mathbf{K}_t^{-1} \mathbf{f}_{ext} d\lambda_{i+1} \\ &= d\bar{\mathbf{p}} + \hat{\mathbf{p}}\, d\lambda_{i+1} \end{aligned} \tag{3.47}$$

where $d\bar{\mathbf{p}} = -\mathbf{K}_t^{-1}\mathbf{r}$ and $\hat{\mathbf{p}} = \mathbf{K}_t^{-1}\mathbf{f}_{ext}$ (see figure 3.4), so the problem becomes

$$\begin{cases} d\mathbf{p}_{i+1} = d\bar{\mathbf{p}} + \hat{\mathbf{p}} d\lambda_{i+1} & (3.48) \\ \Delta\mathbf{p}_{i+1}^{\mathrm{T}} \Delta\mathbf{p}_{i+1} + \Delta\lambda_{i+1}^2 \psi^2 \mathbf{f}_{ext}^{\mathrm{T}} \mathbf{f}_{ext} = \Delta\tau^2, & (3.49) \end{cases}$$

where the new incremental displacements and load parameters are

$$\Delta\mathbf{p}_{i+1} = \mathbf{p}_i - \mathbf{p}^n = \Delta\mathbf{p}_i + d\mathbf{p}_{i+1} \tag{3.50}$$

$$\Delta\lambda_{i+1} = \lambda_i - \lambda^n = \Delta\lambda_i + d\lambda_{i+1}, \tag{3.51}$$

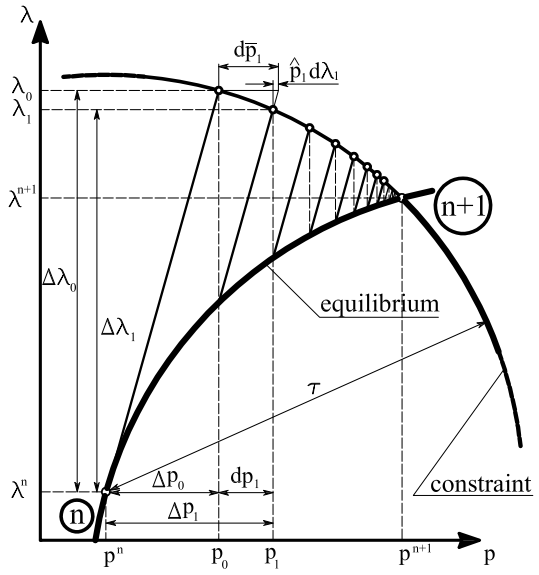

Figure 3.4: **Spherical arc-length** method with Modified Newton as iterative scheme

with $\Delta\mathbf{p}_i = \mathbf{p}_i - \mathbf{p}^n$ and $\Delta\lambda_i = \lambda_i - \lambda^n$.
Substitution of the expression for $d\mathbf{p}_{i+1}$ (3.48) within the constraint (3.49) leads to the scalar quadratic equation

$$a_1 d\lambda_{i+1}^2 + a_2 d\lambda_{i+1} + a_3 = 0, \tag{3.52}$$

where

$$\begin{aligned} a_1 &= \hat{\mathbf{p}}^{\mathrm{T}}\hat{\mathbf{p}} + \psi^2 \mathbf{f}_{ext}^{\mathrm{T}}\mathbf{f}_{ext} \\ a_2 &= 2\hat{\mathbf{p}}(\Delta\mathbf{p}_i + d\bar{\mathbf{p}}) + 2\Delta\lambda_i\psi^2\mathbf{f}_{ext}^{\mathrm{T}}\mathbf{f}_{ext} \\ a_3 &= (\Delta\mathbf{p}_i + d\bar{\mathbf{p}})^{\mathrm{T}}(\Delta\mathbf{p}_i + d\bar{\mathbf{p}}) - \Delta\tau^2 + \Delta\lambda_i^2\psi^2\mathbf{f}_{ext}^{\mathrm{T}}\mathbf{f}_{ext}. \end{aligned}$$

Equation (3.52) can be solved for $d\lambda_{i+1}$ so that, from (3.50) and (3.51), the desired increments can be computed. The method, however, suffers from the limitation that, precisely at the limit point, $\mathbf{K}_t$ is singular and the equations cannot be solved. Anyway, we must first address the issue of finding an appropriate root to (3.52). The idea is to compute both $d\lambda_{i+1,1}$ and $d\lambda_{i+1,2}$ and hence to have two sets of increments

$$\begin{aligned} \Delta\mathbf{p}_{i+1,1} &= \Delta\mathbf{p}_i + d\bar{\mathbf{p}} + \hat{\mathbf{p}}d\lambda_{i+1,1} \quad \text{e} \quad \Delta\lambda_{i+1,1} = \Delta\lambda_i + d\lambda_{i+1,1} \\ \Delta\mathbf{p}_{i+1,2} &= \Delta\mathbf{p}_i + d\bar{\mathbf{p}} + \hat{\mathbf{p}}d\lambda_{i+1,2} \quad \text{e} \quad \Delta\lambda_{i+1,2} = \Delta\lambda_i + d\lambda_{i+1,2}. \end{aligned}$$

We finally have to find which of $\Delta\mathbf{p}_{i+1,1}$ e $\Delta\mathbf{p}_{i+1,2}$ lies closest to the old incremental direction $\Delta\mathbf{p}_i$. This should prevent the solution from "doubling

back on its tracks". This procedure can be implemented by finding the solution with the minimum angle θ between $\Delta\mathbf{p}_{i+1}$ and $\Delta\mathbf{p}_i$ and, hence, the maximum cosine of θ, using

$$\begin{aligned} cos\theta &= \frac{\Delta\mathbf{p}_i^{\mathrm{T}}\Delta\mathbf{p}_{i+1} + \Delta\lambda_i\Delta\lambda_{i+1}\psi^2\mathbf{f}_{ext}^{\mathrm{T}}\mathbf{f}_{ext}}{\Delta\tau^2} \\ &= \frac{\Delta\mathbf{p}_i^{\mathrm{T}}(\Delta\mathbf{p}_i^{\mathrm{T}} + d\bar{\mathbf{p}}) + \Delta\lambda_i^2\psi^2\mathbf{f}_{ext}^{\mathrm{T}}\mathbf{f}_{ext}}{\Delta\tau^2} + d\lambda_{i+1}\frac{\Delta\mathbf{p}_i^{\mathrm{T}}\hat{\mathbf{p}} + \Delta\lambda_i\psi^2\mathbf{f}_{ext}^{\mathrm{T}}\mathbf{f}_{ext}}{\Delta\tau^2} \\ &= \frac{a_4 + a_5 d\lambda_{i+1}}{\Delta\tau^2}, \end{aligned}$$

where:
$a_4 = \Delta\mathbf{p}_i^{\mathrm{T}}\Delta\mathbf{p}_i + \Delta\mathbf{p}_i^{\mathrm{T}}d\bar{\mathbf{p}} + \Delta\lambda_i^2\psi^2\mathbf{f}_{ext}^{\mathrm{T}}\mathbf{f}_{ext}$
$a_5 = \Delta\mathbf{p}_i^{\mathrm{T}}\hat{\mathbf{p}} + \Delta\lambda_i\psi^2\mathbf{f}_{ext}^{\mathrm{T}}\mathbf{f}_{ext}$.

Some observations

It is interesting to linearize also Crisfield's constraint (3.46), as we have done for *linearized arc-length methods*. Thus, if we rewrite Crisfield's hypersphere as

$$G = \Delta\mathbf{p}_{i+1}^{\mathrm{T}}\Delta\mathbf{p}_{i+1} + \Delta\lambda_{i+1}^2\psi^2\mathbf{f}_{ext}^{\mathrm{T}}\mathbf{f}_{ext} - \Delta\tau^2 = 0, \tag{3.53}$$

throughout Newton-Raphson's resolution technique, we get

$$G(\mathbf{x}_{i+1}) = G(\mathbf{x}_i) + 2\Delta\mathbf{p}_{i+1}^{\mathrm{T}}d\mathbf{p}_{i+1} + 2\Delta\lambda_{i+1}d\lambda_{i+1}\ \psi^2\mathbf{f}_{ext}^{\mathrm{T}}\mathbf{f}_{ext} = 0. \tag{3.54}$$

System (3.6), imposing $G(\mathbf{x}_i) = 0$, becomes

$$\mathbf{H}d\mathbf{x}_{i+1} = -\mathbf{R}_i \qquad d\mathbf{x}_{i+1} := \begin{bmatrix} \mathbf{p}_{i+1} - \mathbf{p}_i \\ \lambda_{i+1} - \lambda_i \end{bmatrix} \qquad \mathbf{R}_i := \begin{bmatrix} \mathbf{r}_i \\ 0 \end{bmatrix}, \tag{3.55}$$

where the Jacobian (3.35), considering also the linearized equilibrium equation (3.45), particularizes as

$$\mathbf{H} := \begin{bmatrix} \mathbf{K}_t & -\mathbf{f}_{ext} \\ 2\Delta\mathbf{p}_{i+1}^{\mathrm{T}} & 2\Delta\lambda_{i+1}\psi^2\mathbf{f}_{ext}^{\mathrm{T}}\mathbf{f}_{ext} \end{bmatrix}. \tag{3.56}$$

It is possible noe to express quantities $\mathbf{M}$ and $\mathbf{m}$ as

$$\mathbf{M} := 2\begin{bmatrix} \mathbf{I} & \mathbf{0} \\ 0 & \psi^2\mathbf{f}_{ext}^{\mathrm{T}}\mathbf{f}_{ext} \end{bmatrix} \qquad \mathbf{m} := (\Delta\mathbf{p}_{i+1}, \Delta\lambda_{i+1}) \tag{3.57}$$

where $\Delta\mathbf{p}_{i+1} = \mathbf{p}_{i+1} - \mathbf{p}_0$ e $\Delta\lambda_{i+1} = \lambda_{i+1} - \lambda_0$.

Successive incremental calculations by means of orthogonality with a certain secant increment is a common procedure of this method and of the **Updated Normal Plane**. As shown in figure 3.5 in order to get increments at step 2 for the **Updated Normal Plane** the previous secant increment is required, while for Crisfield's method is required the orthogonality of the

plane tangent to the sphere at the same step (2), i.e. the secant increment referred to the current step. This is the direct consequence of the linearization of Crisfield's constraint imposed in this approach. However, such a constraint plane is not easy to implement within a finite element code because normal vector to the plane is unknown. In fact, while *linearized arc-length methods* lead to linearized constraints which vary linearly with the incremental quantities, this does not happen for this last approach.

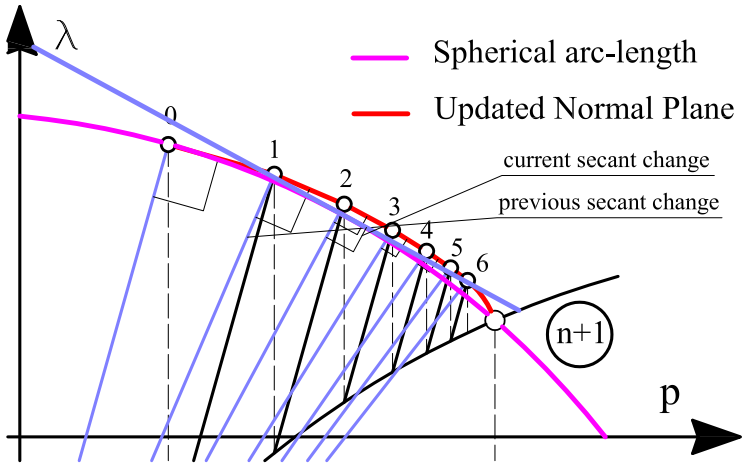

Figure 3.5: **Spherical arc-length** versus **Updated Normal Plane**.

3.4 Convergence of the algorithm

In analogy of what we have done in Section 2.2.2, we are interested in finding even a sufficient condition of convergence for **linearized arc-length method**. Following Casciaro et al. in (7) we considering the full expression of the residual vector written in (3.2); thus residual difference at two successive iterations (2.18) in this case particularizes as

$$\mathbf{R}_{i+1} - \mathbf{R}_i = \mathbf{H}_s(\mathbf{x}_{i+1} - \mathbf{x}_i), \tag{3.58}$$

where $\mathbf{H}_s$ is the secant Jacobian matrix defined as

$$\mathbf{H}_s := \int_0^1 \mathbf{H}[\mathbf{x}_i + t(\mathbf{x}_{i+1} - \mathbf{x}_i)]dt = \begin{bmatrix} \mathbf{K}_s & -\mathbf{f}_{ext} \\ \mathbf{n}^{\mathrm{T}}\mathbf{N} & \nu\mu \end{bmatrix}, \tag{3.59}$$

with $\mathbf{K}_s$ the secant stiffness matrix defined in (2.19). Substitution of equation (3.58) into the iterative scheme (3.6) leads to

$$\mathbf{R}_{i+1} = [\mathbf{I} - \mathbf{H}_s\mathbf{H}^{-1}]\mathbf{R}_i, \tag{3.60}$$

which represents the evolution law for the residual $\mathbf{R}_i$ at iteration loop $i+1$. Then, if we want to obtain an iteration scheme such as

$$||\mathbf{R}_{i+1}|| < ||\mathbf{R}_i||, \tag{3.61}$$

it is necessary to impose the sequent sufficient convergence condition

$$\rho(\mathbf{I} - \mathbf{H}_s\mathbf{H}^{-1}) < 1, \tag{3.62}$$

being $\rho(\cdot)$ the spectral radius of a matrix.
By introducing the following quantities:

$$\mathbf{B}_i = \frac{\mathbf{f}_{ext}\mathbf{d}_i^{\mathrm{T}}}{\mathbf{f}_{ext}^{\mathrm{T}}\mathbf{d}_i} \qquad c = \mu\nu + \mathbf{f}_{ext}^{\mathrm{T}}\mathbf{d}_i \qquad \omega_i = \frac{\mathbf{f}_{ext}^{\mathrm{T}}\mathbf{d}_i}{c} \tag{3.63}$$

and

$$\mathbf{d}_i = \mathbf{K}_t^{-1}\mathbf{N}\mathbf{n},$$

the inverse of $\mathbf{H}$ becomes

$$\mathbf{H}^{-1} = \begin{bmatrix} \mathbf{K}_t^{-1}[\mathbf{I} - \omega_i\mathbf{B}_i] & \dfrac{\mathbf{K}_t^{-1}\mathbf{f}_{ext}}{c} \\ -\dfrac{\mathbf{d}_i}{c} & 1/c \end{bmatrix}. \tag{3.64}$$

Thus the iteration matrix is

$$[\mathbf{H}_s\mathbf{H}^{-1}] = \begin{bmatrix} \mathbf{K}_s\mathbf{K}_t^{-1} + (\mathbf{I} - \mathbf{K}_s\mathbf{K}_t^{-1})\omega_i\mathbf{B}_i & (\mathbf{K}_s\mathbf{K}_t^{-1} - I)\mathbf{f}_{ext}/c \\ \mathbf{0} & 1 \end{bmatrix}; \tag{3.65}$$

and so matrix $[\mathbf{I} - \mathbf{H}_s\mathbf{H}^{-1}]$ takes the form of

$$\begin{bmatrix} \mathbf{I} - \mathbf{K}_s\mathbf{K}_t^{-1} - (\mathbf{I} - \mathbf{K}_s\mathbf{K}_t^{-1})\omega_i\mathbf{B}_i & (\mathbf{K}_s\mathbf{K}_t^{-1} - I)\mathbf{f}_{ext}/c \\ \mathbf{0} & 0 \end{bmatrix}. \tag{3.66}$$

Condition (3.62) can be easily studied throughout the first $n \times n$ minor of matrix $[\mathbf{I} - \mathbf{H}_s\mathbf{H}^{-1}]$ (3.66), i.e.

$$\rho([\mathbf{I} - \mathbf{K}_s\mathbf{K}_t^{-1}][\mathbf{I} - \omega_i\mathbf{B}_i]) < 1. \tag{3.67}$$

If we consider that, as for instance in the Updated Normal Plane, $\mathbf{n} = \hat{\mathbf{p}} = \mathbf{K}_t^{-1}\mathbf{f}_{ext}$, we have

$$\mathbf{f}_{ext}^{\mathrm{T}}\mathbf{d}_i = \hat{\mathbf{p}}^{\mathrm{T}}\mathbf{N}\hat{\mathbf{p}} > 0. \tag{3.68}$$

Due to (3.63), the above equation implies

$$0 < \omega_i \leq 1. \tag{3.69}$$

We have already said that near a limit point matrix $[\mathbf{K}_s\mathbf{K}_t^{-1}]$ has at least one eigenvalue η_j which becomes negative. For a *load-control method* for which convergence condition can be deduced from the assumption that $\omega_i = 0$, because in such a case $\mathbf{d}_i = \mathbf{0}$ as $\mathbf{n} = \mathbf{0}$, i.e.

$$\rho([\mathbf{I} - \mathbf{K}_s\mathbf{K}_t^{-1}] < 1,$$

convergence cannot be reached near limit points. However for **the arc-length methods**, as we can see in equation (3.67), matrix $[\mathbf{I} - \omega_i\mathbf{B}_i]$ represents a filter in the direction $\hat{\mathbf{p}}$ which tends to be complete if $(\omega_i \to 1)$, i.e. near a limit point $\Delta\lambda_i \approx 0$. In other words for this kind of methods $\mathbf{K}_t$ is free to follow $\mathbf{K}_s$ without taking the spectral radius of the iteration matrix to an undesirable value.

3.4.1 Alternative approach for convergence analysis

In the previous analysis no consideration can be done about how the choice of a proper constraint surface improves the convergence of Newton-Raphson's scheme. Instead, looking at that we expect to find a proper condition which in a certain sense inform us about the quality of the intersection between the equilibrium curve and the constraint equation. The better the intersection is defined, the quicker the convergence is reached.

Loss of convergence of the numerical procedure can be associated with the vanishing of the Jacobian $\mathbf{H}$ (see Riks in (6)). In other words, convergence conditions can be studied by detecting a proper normalization of the determinant of matrix $\mathbf{H}$, $F = \det(\mathbf{H})$, e.g. $\parallel F \parallel$ is given in (6) by

$$\parallel F \parallel = \frac{\mid F \mid}{\mid \mathbf{f}_1 \mid\mid \mathbf{f}_2 \mid\mid \mathbf{f}_3 \mid \ldots \mid \mathbf{f}_{N+1} \mid} = \frac{\mid F \mid}{\prod_{i=1}^{N+1} \mid \mathbf{f}_i \mid}, \tag{3.70}$$

with

$$\mid \mathbf{f}_i \mid = (\mathbf{j}_i\mathbf{j}_i^{\mathrm{T}})^{1/2} \tag{3.71}$$

where $\mathbf{j}_i$ are the $N+1$ rows of matrix $\mathbf{H}$. It is noted that according to definitions, (3.70) and (3.71), $\parallel F \parallel$ can never exceed unity, which is the consequence of Hadamard's inequality for determinants. In general, a small value of $\parallel F \parallel$ in comparison with unity can be associated with a nearly singular, i.e., an ill-conditioned, matrix $\mathbf{H}$. Since ill-conditioned matrix must be avoided, the choice of the constraint surface G (3.26) should be guided by the wish to keep $\parallel F \parallel$ as large as possible. In order to understand how the choice of constraint G affect the condition of matrix $\mathbf{H}$ we firstly express

F with respect to the last row of matrix $\mathbf{H}$, considering for simplicity $\mathbf{M}$ equal to the identity matrix $\mathbf{I}$. So we obtain

$$F = \mathbf{d} \cdot \mathbf{m}, \tag{3.72}$$

being $\mathbf{d}$ the cofactor vector referred the last row $\mathbf{m}$. Thus $\| F \|$ is written in the form

$$\begin{aligned} \| F \| &= \frac{| \mathbf{m}\mathbf{d}^{\mathrm{T}} |}{| \mathbf{f}_0 || \mathbf{d} |} \frac{| \mathbf{d} |}{\prod_{i=1}^{N} | \mathbf{f}_i |} \\ &= \left| \frac{\mathbf{m}\mathbf{d}^{\mathrm{T}}}{| \mathbf{m} || \mathbf{d} |} \right| \frac{| \mathbf{d} |}{\prod_{i=1}^{N} | f_i |} \qquad (3.73) \\ &= \| F_0 \| \| F^* \|, \qquad (3.74) \end{aligned}$$

where

$$| \mathbf{d} | = (\mathbf{d}\mathbf{d}^{\mathrm{T}})^{1/2}. \tag{3.75}$$

The norm $\| F \|$ thus results to be the product of two functionals $\| F_0 \|$ and $\| F^* \|$, of which only the first depends on $\mathbf{m}$. For simplicity, we assume that, in the following, the given equilibrium equations are always properly defined in the range of interest. This means that the norm $\| F^* \|$ is always supposed to be sufficiently large.

After the introduction of the vectors

$$\bar{\mathbf{d}} = \frac{\mathbf{d}}{| \mathbf{d} |}, \quad \bar{\mathbf{m}} = \frac{\mathbf{m}}{| \mathbf{m} |}, \tag{3.76}$$

$\| F_0 \|$ is reduced to

$$\| F_0 \| = | \bar{\mathbf{d}} \cdot \bar{\mathbf{m}} | . \tag{3.77}$$

If we consider the alternative critical formulation treated in Section 1.3.6, we can rewrite expression (1.60) as

$$D\dot{\mathbf{p}} = \mathbf{d}\dot{\lambda}, \tag{3.78}$$

where $D = \det(\mathbf{K}_t)$. A proper normalization of equation (3.78) shows that $\bar{\mathbf{d}}$ represents the unit tangent to the equilibrium path ($\bar{\mathbf{d}} \rightsquigarrow \dot{\mathbf{p}}$) while $\bar{\mathbf{m}}$ represents the unit normal to the surface G at the point of intersection. The value of $\| F \|$ is thus as large as possible if the inner product (3.77) is equal to the unity, which corresponds to an orthogonal intersection of the surface G with the equilibrium path. Condition (3.77) is what we would like to obtain in order to describe Newton-Raphson's convergence. Surely we can observe that standard load-control procedure leads necessarily to an ill-conditioned iteration matrix $\mathbf{H}$ as in this case $\| F_0 \| = 0$.

3.5 Continuation beyond the critical points

It is often desirable to extend the computation of the basic, or primary, equilibrium path beyond the critical state (post-buckling analysis). This task can be carried out with the arc-length procedure described in this chapter. As previously said the basic incremental method used here is only sensitive to the bifurcation point because there matrix the $\mathbf{H}$ becomes singular. Passing a limit or a turning point with respect to any other direction does therefore not pose a problem. Passing a bifurcation point is not a problem too as long as the use of equation (3.7) can be avoided close to (or at) this particular point . In fact, when the stepsize $\Delta\tau$ is chosen arbitrarily there is only a little chance that this can occur. Consequently, continuation of the computation beyond limit and bifurcation points, can be often carried out without special expedients in the implementation of the procedure.

3.6 Some computational aspects

A good implementation of the **arc-length** technique needs a careful attention to those aspects which give efficiency and robustness to the procedure. A *path following* algorithm must first of all produce a sequence of $(\mathbf{p}_i,\ \lambda_i)$ that converges to the correct value of the equilibrium curve and that minimizes the complessive computational effort. An algorithm is said robust when, starting from an assigned input proceeds, it towards the equilibrium solution without the need of any interference by the analyst. The quantities needed to start the procedure are

1. a starting length increment $\Delta\tau$;
2. a desired number of iteration for Newton-Raphson's convergence I_d [see (3.89) in Section 3.6.2];
3. a tolerance ϵ for the convergence criterion (2.6);
4. a "false step" criterion for handling failures in convergence during iteration (either divergence or failure in finding real roots in *spherical arc-length*), see Section 3.6.3.

There are (at least) three possibilities to choose an appropriate magnitude for a starting length increment. The first is to apply preliminary load-controlled steps and, with the knowledge of the initial equilibrium nonlinearity, a proper length can be chosen. Alternatively, the user may start by specifying a load increment $\Delta\lambda$. The displacement vector $\Delta\mathbf{p}$ and the starting length increment $\Delta\tau$ can be determined from the *predictor step* that will be explained in detail in Section 4.4.1. A third, very useful, strategy is to apply standard load- (or displacement-) control for the early increments

and switch to the arc-length control only once a limit point is approached. A procedure for automatically introducing such a switch is given in Section 3.6.4.

3.6.1 Predictor solution

Predictor solution is usually required at first iteration ($i = 0$) because, as

$$\mathbf{x}_1 = \mathbf{x}_0 + d\mathbf{x}_1 \quad \text{where} \quad d\mathbf{x}_1 = \mathrm{f}(\mathbf{r}_0) \tag{3.79}$$

incremental unknowns at such iteration require information about the starting residual $\mathbf{r}_0$ which is unknown. Equations (3.36), (3.37), (3.39), (3.40) and (3.52) follow scheme (3.79). The idea behind *predictor* procedure is to find an incremental vector $d\mathbf{x}_0 = \Delta\mathbf{x}_0$ with techniques, such as for instance Euler's methods, that do not require residual computation. Once $d\mathbf{x}_0$ and $d\lambda_0$ are known, initial residual $\mathbf{r}_0$ can be calculated from

$$\mathbf{r}_0 = \mathbf{F}_{int}(\mathbf{p}_0) - (\lambda^n + d\lambda_0), \tag{3.80}$$

where $\mathbf{p}_0 = \mathbf{p}^n + d\mathbf{p}_0$ and $d\mathbf{x}_0 = (d\mathbf{p}_0, d\lambda_0)$. Now, known $\mathbf{r}_0$, $d\mathbf{x}_1$ can be calculated from arc-length procedures.
Such a phase is not required in a load-control procedure as $d\lambda^n$ is constant and given within each time steps and so load parameter can be incremented. Hence residual can be found as

$$\mathbf{r}_0 = \mathbf{F}^n_{int} - \mathbf{f}_{ext}(\lambda^n + d\lambda^n). \tag{3.81}$$

and incremental displacement can be found from (2.11).

Now we focus on identifying a good arc-length predictor. We know that the predictor step proceeds from a known equilibrium configuration, i.e. a point of the equilibrium path, towards the next point of the path (see figure 3.6). Assuming the adoption of a forward-Euler, the tangential predictor takes the form

$$\Delta\mathbf{p}_0 = \mathbf{K}_t^{-1}\Delta\mathbf{F}_{ext} = \Delta\lambda_0\mathbf{K}_t^{-1}\mathbf{f}_{ext} = \Delta\lambda_0\hat{\mathbf{p}}, \tag{3.82}$$

where $\hat{\mathbf{p}}$ has already been defined in (5.18).
If we put (3.82) into the hypersphere (3.43) and hyperplane (3.42) constraints, we get for Crisfield's approach

$$\Delta\lambda_0 = \frac{\pm\Delta\tau}{\sqrt{\hat{\mathbf{p}}^T\hat{\mathbf{p}} + \psi^2\mathbf{f}_{ext}^T\mathbf{f}_{ext}}}, \tag{3.83}$$

while for the *linearized arc-length methods* we have

$$\Delta\lambda_0 = \frac{\pm\Delta\tau}{\sqrt{\hat{\mathbf{p}}^T\,\mathbf{M}\,\hat{\mathbf{p}} + \mu}}. \tag{3.84}$$

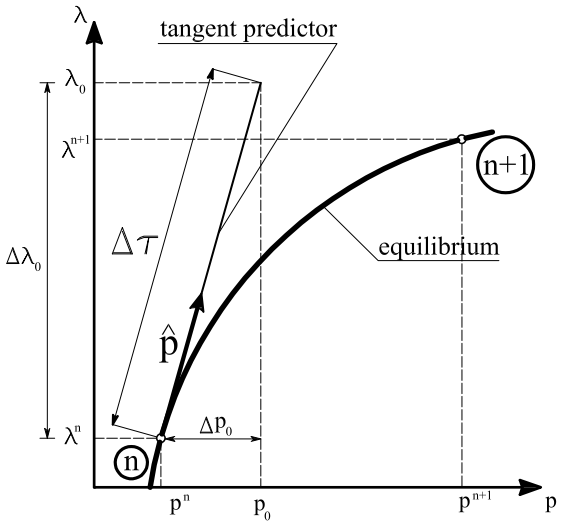

Figure 3.6: Tangent predictor solution

The proper sign selection of $\Delta\lambda_0$ is essential for determining the load direction. Here, sign selection is based on modifications of the two general stiffness parameters presented in (13). The first general stiffness parameter G^{sp1} detects the appearance of a limit point by defining the normalized tangential predictor

$$\mathbf{t}_p^{n-1} = \frac{\hat{\mathbf{p}}^{n-1}}{\|\hat{\mathbf{p}}^{n-1}\|}, \tag{3.85}$$

and comparing the angle between successive tangential predictors, $\mathbf{t}_p^{n-1}$ and $\bar{\mathbf{t}}_p^n$, evaluated at the first iteration. Referring to figure 3.7, an acute angle is formed between the vectors $\mathbf{t}_p^{n-1}$ and $\bar{\mathbf{t}}_p^n$ on the curve O-A, where no limit point is present. On the contrary an obtuse angle is formed when the limit point B1 of the curve O-B is passed. Based on these criteria, the first general stiffness parameter is given by

$$G^{sp1} = \mathbf{t}_p^T \, \bar{\mathbf{t}}_p. \tag{3.86}$$

If $G^{sp1} \geq 0$, then a limit point has not been passed, and the sign of $\Delta\lambda_0$ is not altered. Instead, if $G^{sp1} < 0$, then a limit point has been passed, and the sign is switched.

The first general stiffness parameter G^{sp1} accurately detects the presence of limit points when the curve turns "slowly", i.e. relatively small changes in the path curvature, as in the curve O-A of figure 3.8. Unfortunately, this parameter will not detect limit points if the path curvature is large, e.g. for path O-B. If $|G^{sp1}| \approx 1$, then we assume that the changes in path curvature

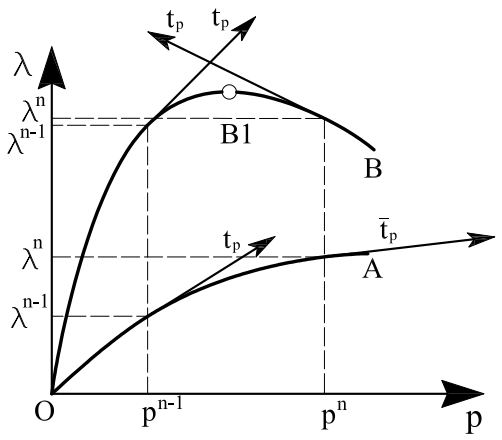

Figure 3.7: Tangent predictor vectors $\mathbf{t}_p$ and $\bar{\mathbf{t}}_p$ at two consecutive steps.

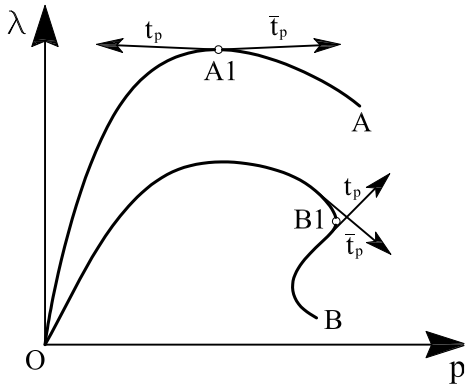

Figure 3.8: Limit point detection for small curvature trajectory O-A and large curvature trajectory O-B.

are small. Therefore, we base the sign $\Delta\lambda_0$ on G^{sp1} provided that

$$1 - |G^{sp1}| \leq \varepsilon^{sp1},$$

where $\varepsilon^{sp1} \ll 1$, e.g. $\varepsilon^{sp1} = 0.1$.
If the curvature is large, i.e. $1 - |G^{sp1}| \geq \varepsilon^{sp1}$, then we have to base the sign of $\Delta\lambda_0$ on a second general stiffness parameter G^{sp2}. Referring to figure 3.9, this parameter detects the appearance of a limit point by comparing the projections $\mathbf{n}$ and $\bar{\mathbf{n}}$ of the tangential predictors $\mathbf{t}_p^{n-1}$ and $\bar{\mathbf{t}}_p^{n}$ onto the hyperplane defined by the normalized secant $\mathbf{e}$, i.e.

$$\mathbf{e} = \frac{\mathbf{p}^n - \mathbf{p}^{n-1}}{\|\mathbf{p}^n - \mathbf{p}^{n-1}\|}. \tag{3.87}$$

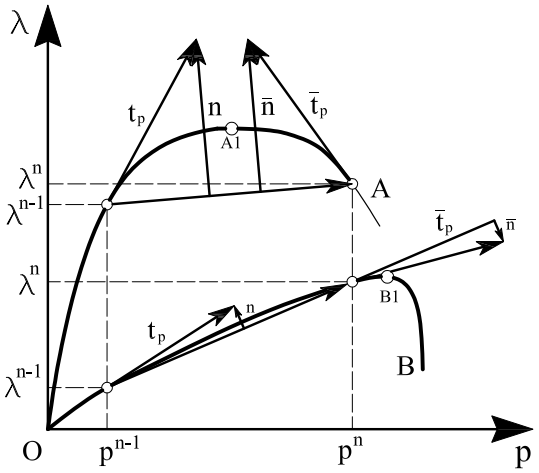

Figure 3.9: Limit point detection by projection $\mathbf{n}$ and $\bar{\mathbf{n}}$ for sharp trajectory turns.

The second stiffness parameter is expressed as

$$G^{sp2} = \mathbf{n}^T \, \bar{\mathbf{n}}, \tag{3.88}$$

where

$$\mathbf{n} = \mathbf{t}_p - (\mathbf{t}_p^T \mathbf{e})\mathbf{e}.$$

If $1 - |G^{sp1}| \geq \varepsilon^{sp1}$ and $G^{sp2} \geq 0$, then the projections are directed along the same direction, i.e. a limit point has been passed and the sign of $\Delta\lambda_0$ is switched. Otherwise, the sign is not altered.

3.6.2 Step length adaptation

Step length selection is one of the most crucial parts of continuation in view of efficiency. Several methods exist but the most popular is the one proposed by Ramm (9). Here the new step size is scaled by relating the number of iterations used in the previous step I_n to a desired value I_d

$$\Delta\tau^{n+1} = \left(\frac{I_d}{I_n}\right)^p \Delta\tau^n, \tag{3.89}$$

where a scaling exponent $p = 0.5$ is usually adopted. If the desired number of corrector iterations is properly chosen this simple arc-length control will result in a rather robust procedure. However, it can produce too small step-size which are kept unchanged for unnecessarily long times. Hence, some safeguard limit values for step-length changes should also pe used together with (3.89).

3.6.3 Automatic increment cutting

If convergence of structural equilibrium iterations is not achieved within the specific number of iterations, a simple strategy is to cut the increment size, as suggested in (8). Thus, within the "false step" criterion, together with displacement and load factor increments set to zero, the following choice could be used

$$\frac{\Delta\tau^{n+1}}{\Delta\tau^{n}} = \frac{\beta_d}{\beta^n} \tag{3.90}$$

where $\beta^n = \mathbf{r}^n$ is the convergence factor and β_d is the input desired convergence factor. Automatic increment cutting can be adopted in other situations such as the failure of the *arc-length method*.

3.6.4 Current stiffness parameter

The current stiffness parameter is a "path-measuring parameter" and so it is a very useful index to give some scalar measure of the degree of non-linearity of the equilibrium curve. In its unscaled form, it effectively measures the stiffness of the system as related to the tangential predictor, i.e. formally "$k'' = \Delta\mathbf{F}_{ext}/\Delta\mathbf{p}_0$ where $\Delta\mathbf{F}_{ext}$ is the incremental load vector and $\Delta\mathbf{p}_0$ the resulting tangential displacements. However, because $\Delta\mathbf{F}_{ext}$ and $\Delta\mathbf{p}_0$ are vectors, we have to multiply numerator and denominator by $\Delta\mathbf{p}_0$ so that

$$\text{“}k'' = C_s = \frac{\Delta\mathbf{F}_{ext}^{\mathrm{T}}\,\Delta\mathbf{p}_0}{\Delta\mathbf{p}_0^{\mathrm{T}}\,\Delta\mathbf{p}_0} = \frac{\mathbf{f}_{ext}^{\mathrm{T}}\,\hat{\mathbf{p}}}{\hat{\mathbf{p}}^{\mathrm{T}}\,\hat{\mathbf{p}}}, \tag{3.91}$$

where we have used $\Delta\mathbf{F}_{ext} = \Delta\lambda\mathbf{f}_{ext}$, (3.82) and (5.18).

Many structures exhibit a response in which the structure softens as the load is applied. In such situations, it is very useful to force the solution procedure to automatically switch from load-(or displacement-) control as the limit point is reached (C_s will be zero at the limit point). This can be achieved by introducing a value of current stiffness parameter (say $\overline{C}_s$) below which this switch is automatically introduced.

3.6.5 Non-proportional loading

The solution of the *arc-length* problem has been studied with a fixed load vector $\mathbf{f}_{ext}$ proportionally scaled via λ. For many practical structural problems, this loading regime is too restrictive. For example, we often wish to apply the dead load or self-weight and then monotonically increase the live load. In other instances, a whole range of loading stages may be required. Fortunately, many loading regimes can be applied by means of a series of loading sequences involving two loading vectors, in analogy of what we said in Section 2.1, one that will be scaled (the previous $\mathbf{f}_{ext}$) and one that will

be fixed ($\mathbf{f}_1 = \lambda_1 \mathbf{f}_1$). Thus a possible rule of variation can be

$$\mathbf{F}_{ext}(\lambda) = \begin{cases} \lambda \mathbf{f}_0 & 0 < \lambda \leq \lambda_1 \\ \mathbf{f}_1 + \lambda \mathbf{f}_{ext} & \lambda > \lambda_1, \end{cases}$$

with $\mathbf{f}_1 = \lambda_1 \mathbf{f}_1$ given. The out-of-balance force vector, in case of non-proportional loading, becomes

$$\mathbf{r} = \mathbf{F}_{int} - \mathbf{f}_1 - \lambda \mathbf{f}_{ext}. \tag{3.92}$$

As the extra term $\mathbf{f}_1$ is constant, so equal to zero when linearized, there will not be variations in the incremental update of ($\mathbf{x}_i$, λ_i). However, equation (3.92) will be used in place of $\mathbf{r}_i$ in equation (3.4).

Chapter 4

Computational aspects in critical analysis

4.1 Introduction

In the first chapter we have analyzed bifurcation conditions and we have said that only two branches can arise after the so-called *simple bifurcation point*. As the investigation of the nonlinear response of structures cannot be done without a precise knowledge of the stability behaviour, limit and simple bifurcation points have to be found and examined in detail; then decisions have be taken about which branch follow. Moreover, as loss of stability is always associated with stiffness matrix singularities, we expect to encounter difficulties in performing such an analysis.

In a numerical context, the detection of simple bifurcation and limit points have to be performed by an accurate path-following technique, in the present context an arc-length method, which allows us to trace stable equilibrium paths as well as unstable ones. Therefore, in this chapter we present some ways of detecting and calculating limit and bifurcation points.

For a simple bifurcation point, it is crucial that the secondary branch is examined in order to determine how the structure is sensitive to imperfections. To analyze the response close to a simple bifurcation point, different strategies exist. A first approach relies on a perturbation technique through which the structure is forced to follow particular (stable) branch. A different strategy is to use an asymptotic expansion, as done by Koiter (24), of the nonlinear system of equations, and use a Lyapunov-Schmidt decomposition on the solution space to obtain the reduced equilibrium equations (see (25; 26; 5; 12)). Here an approach similar to asymptotic expansion will be examined, i.e. the solution is obtained through the resolution of the *algebraic bifurcation equation* from (20). Such a result will be useful to develop an *ad-hoc* procedure to follow secondary branches, referred to as *branch-switching*.

4.2 Monitoring stability

Singular points on the equilibrium path require a careful "monitoring". This can be done by observing the evolution of certain singularity indicators or *test functions* during the incremental procedure. There are some convenient measures for this purpose, the most common ones being the following

1. **Determinant** of the tangent stiffness matrix at an equibrium point could be an interesting indicator of when we are approaching critical points. In fact, as limit or bifurcation points are always associated with a rank-deficiency of at least one of matrix $\mathbf{K}_t$, we expect that $d = \det(\mathbf{K}_t)$ changes sign at $t = t^*$. Hence, as in (32), in order to detect the singularity we can monitor the sign of d during the analysis. Considering $t_1 < t^* < t_2$ as the time-step where the sign change of d has been detected, it is possible to reduce the arc-length $\Delta\tau$ in order to compute further points in the primary curve for t values inside the interval. Once this leads to numerical difficulties or an arc-length sufficienty small, we can choose t_0 as the endpoint of the interval where $|d|$ is minimal. We can consider such a result as a good approximation of the critical point. Kouhia in (12) proposes a proper scaling of the determinant d, i.e.

$$\mathrm{sdet}(\mathbf{K}_t) = \prod_i^N |d_{ii}|^{1/N^\gamma} \tag{4.1}$$

   where d_{ii} are the non-zeros terms of the diagonal matrix $\mathbf{D}$ of the Cholesky decomposition $\mathbf{K}_t = \mathbf{L}\mathbf{D}\mathbf{L}^{\mathrm{T}}$, $\gamma \in (0, 1)$ is a parameter, which should reflect the proportion of the average rate of the change in the eigenvalues. The value $\gamma = 0$ is tha most used in the technical literature. Another relative quantity called *determinant-based singularity test function* (dbstf) is also introduced in (12); its definition is

$$\mathrm{dbstf} = \mathrm{sign}(\mathbf{K}_t)\frac{\mathrm{sdet}(\mathbf{K}_t)_n}{\mathrm{sdet}(\mathbf{K}_t)_1}, \tag{4.2}$$

   where the subscript refers to its position within iterative procedure.

2. **Current stiffness parameter** (CSP) has been already analized in subsection 3.6.4. It can only be used with limit point singularities in fact when the tangent to the equilibrium path is parallel to the displacement axis the CSP becomes zero. For this reason it can be consider only as a measure of the degree of nonlinearity of the structural response.

3. **Smallest eigenvalue** (in absolute value) is perhaps the most reliable singularity test function. It detects the possibility of a passage through a zero condition of the determinant d. If monitored simultaneosly,

eigenvalues can also be useful to separate stable and unstable solution paths. Such information cannot be provided by the determinant of the stiffness matrix if the change in the number of negative eigenvalues is an even number. The smallest eigenvalue, together with the evaluation of its corresponding eigenvector, can be another good measure for the critical state. In fact, following Seydel in (30) it is possible to define

$$\rho = \mathbf{e}_j^{\mathrm{T}} \mathbf{K}_t \mathbf{a} \tag{4.3}$$

where $\mathbf{e}_j$ is a fixed coordinate unit vector in $\mathbb{R}^N$ and $\mathbf{a}$ is the corresponding eigenvector. Index j is the equation number associated with the smallest eigenvalue of matrix $\mathbf{K}_t$. If we are approaching limit point $(\mathbf{p}^*, \lambda^*)$ we get

$$\rho \to 0 \quad \text{for} \quad (\mathbf{p}, \lambda) \to (\mathbf{p}^*, \lambda^*). \tag{4.4}$$

By remembering limit and bifurcation point properties and having in hand the eigenvector associated with the minimum eigenvalue, an efficient distinction between the two critical states is given as follows.

$$\begin{aligned} \mathbf{a}^{\mathrm{T}} \mathbf{f}_{ext} \neq 0 &\Longrightarrow \text{limit point}, \\ \mathbf{a}^{\mathrm{T}} \mathbf{f}_{ext} = 0 &\Longrightarrow \text{bifurcation point}. \end{aligned} \tag{4.5}$$

In most cases a compared observation of some of these test functions can be used to detect stability points successfully with a reduced computational effort. Wagner and Wriggers in (27) consider CSP and $\det(\mathbf{K}_t)$ and so no onerous eigenvalue extraction is required; thus

$$\begin{aligned} \det(\mathbf{K}_t) = 0; \quad \mathrm{CSP} = 0 &\Longrightarrow \text{limit point}, \\ \det(\mathbf{K}_t) = 0; \quad \mathrm{CSP} \neq 0 &\Longrightarrow \text{bifurcation point}. \end{aligned} \tag{4.6}$$

4.3 Estimation of critical point

4.3.1 Extended system

Here is presented a direct method for the computation of stability point. Such a formulation and numerical implementation was proposed first by Wriggers et al. in reference (28) and then improved by Wriggers and Simo in (29). The idea underlying such a method is essentially to augment the nonlinear equilibrium system by appending a constraint equation that characterizes the presence of a turning or bifurcation point in order to obtain a so-called **extended system**. As critical points are such that the following conditions hold

$$\begin{aligned} &\mathbf{K}_t \mathbf{a} = \mathbf{0} \\ &\det \mathbf{K}_t = 0, \end{aligned} \tag{4.7}$$

being $\mathbf{a}$ the eigenvector associated with the null eigenvalue, the following two possibilities for the formulation of the extended system have been proposed

1. The nonlinear equilibrium system is augmented by appending the constraint $\det \mathbf{K}_t = 0$, leading to the following extended system

$$\overline{\mathbf{R}}(\mathbf{p}, \lambda) = \left\{ \begin{array}{c} \mathbf{r}(\mathbf{p}, \lambda) \\ \det \mathbf{K}_t \end{array} \right\} = \mathbf{0}. \tag{4.8}$$

   Solving the above nonlinear system by means of a Newton-Raphson's iteration scheme, a difficult implementation could arise. This is given by the linearization of the constraint equation, i.e.

$$\frac{\mathrm{d}}{\mathrm{d}\epsilon}[\det \mathbf{K}_t(\mathbf{p} + \epsilon \Delta \mathbf{p})]\bigg|_{\epsilon=0} = \det(\mathbf{K}_t)\mathrm{tr}[\mathbf{K}_t^{-1}\nabla_{\mathbf{p}}(\mathbf{K}_t)\Delta \mathbf{p}], \tag{4.9}$$

   which contains the inverse $\mathbf{K}_t$, not definibile near critical points, inside the trace operation of two matrix seldom implemented in an element-by-element fashion.

2. An alternative approach computationally more appealing uses the condition $\mathbf{K}_t\mathbf{a} = \mathbf{0}$, so, in place of (4.8), we consider the following augmented set of equations

$$\overline{\mathbf{R}}(\mathbf{p}, \lambda) = \left\{ \begin{array}{c} \mathbf{r}(\mathbf{p}, \lambda) \\ \mathbf{K}_t\mathbf{a} \\ l(\mathbf{a}) \end{array} \right\} = \mathbf{0}. \tag{4.10}$$

   In the framework of numerical analysis, the above extended system was firstly studied by Seydel (30), Werner and Spence (31). In equation (4.10) $l(\mathbf{a})$ denotes some normalizing functional which restricts the magnitude of the eigenvector $\mathbf{a}$ of $\mathbf{K}_t$ at the limit point or bifurcation point. In (29) $l(\mathbf{a})$ is given by

$$l(\mathbf{a}) = \mathbf{e}_j^{\mathrm{T}}\mathbf{a} - a_0 = a_j - a_0 = 0, \quad \mathbf{a} \in \mathbb{R} \tag{4.11}$$

   where $\mathbf{e}_j$ is a fixed coordinate unit vector in $\mathbb{R}^N$. Index j is the equation number associated with the smallest eigenvalue of matrix $\mathbf{K}_t$. A simple estimate of the scaling factor a_0 is given by the expression

$$a_0 = \frac{a_{0j}}{||\mathbf{a}_0||} \tag{4.12}$$

   where $\mathbf{a}_0$ is the initial approximation to the eigenvector.

   It should be noted that the extended system (4.10) involves $2N + 1$ unknowns. Thus, it would appear that the computational effort involved in the solution of these systems increases considerably depending on the extended system of form (4.8), which involved only $N + 1$ unknowns. We show below that the actual situation is exactly the opposite that in this conjecture. In fact, in contrast with (4.8), the

solution of (4.10) can be conveniently obtained by means of a partitioning method as for the arc-length problem. This technique exploits the special structure of system (4.10), and leads to a linearized system with a remarkably simple form. However, the Newton-type iteration scheme for the present system exhibits a characteristic ill-conditioning near the stability points. In the next subsection we examine a penalty method which improves the conditioning of the iterative technique.

4.3.2 Penalty method for the extended system

The method described below and introduced by (29) improves the condition number while preserving the symmetry of $\mathbf{K}_t$. The construction of such a **penalty method** proceeds considering the penalty functional $V_p(\mathbf{p}, \lambda, \mu)$ obtained from $V(\mathbf{p}, \lambda)$, i.e. the total potential energy functional introduced in Chapter 1, by appending the constraint $(\mathbf{e}_j^{\mathrm{T}}\mathbf{p} - \mu)$; i.e.

$$V_p(\mathbf{p}, \lambda, \mu) = V(\mathbf{p}, \lambda) + \frac{\gamma}{2}(\mathbf{e}_j^{\mathrm{T}}\mathbf{p} - \mu)^2, \quad \gamma > 0. \tag{4.13}$$

The penalty equilibrium equation is now given by

$$\mathbf{r}_p(\mathbf{p}, \lambda, \mu) = \frac{\partial V_p(\mathbf{p}, \lambda, \mu)}{\partial \mathbf{p}} = \mathbf{0}, \tag{4.14}$$

that is

$$\mathbf{r}_p(\mathbf{p}, \lambda, \mu) = \mathbf{r}(\mathbf{p}, \lambda) + \gamma(\mathbf{e}_j^{\mathrm{T}}\mathbf{p} - \mu)\mathbf{e}_j = \mathbf{0}. \tag{4.15}$$

remembering $\mathbf{r}(\mathbf{p}, \lambda) = \dfrac{\partial V(\mathbf{p}, \lambda)}{\partial \mathbf{p}}$.

Equilibrium equation is obtained from (4.15) by

$$\bar{\mathbf{r}}(\mathbf{p}, \lambda, \mu) = \left\{ \begin{array}{c} \mathbf{r}(\mathbf{p}, \lambda) + \gamma(\mathbf{e}_j^{\mathrm{T}}\mathbf{p} - \mu)\mathbf{e}_j \\ \mathbf{e}_j^{\mathrm{T}}\mathbf{p} - \mu \end{array} \right\} = \mathbf{0}. \tag{4.16}$$

We also append normalizing condition (4.11) to the critical constraint equation; i.e.

$$\bar{\mathbf{c}}(\mathbf{p}, \lambda, \mathbf{a}) = \left\{ \begin{array}{c} \mathbf{K}_t\mathbf{a} + \gamma(\mathbf{e}_j^{\mathrm{T}}\mathbf{a} - a_0)\mathbf{e}_j \\ \mathbf{e}_j^{\mathrm{T}}\mathbf{a} - a_0 \end{array} \right\} = \mathbf{0}. \tag{4.17}$$

The resulting extended system, written in compact form, has the form

$$\overline{\mathbf{R}}(\mathbf{p}, \lambda, \mathbf{a}, \mu) = \left\{ \begin{array}{c} \bar{\mathbf{r}}(\mathbf{p}, \lambda, \mu) \\ \bar{\mathbf{c}}(\mathbf{p}, \lambda, \mathbf{a}) \end{array} \right\} = \mathbf{0}. \tag{4.18}$$

Reordering the terms of the above system we obtain

$$\overline{\mathbf{R}}(\mathbf{p}, \mathbf{a}, \lambda, \mu) = \left\{ \begin{array}{c} \mathbf{r}(\mathbf{p}, \lambda) + \gamma(\mathbf{e}_j^{\mathrm{T}}\mathbf{p} - \mu)\mathbf{e}_j \\ \mathbf{K}_t\mathbf{a} + \gamma(\mathbf{e}_j^{\mathrm{T}}\mathbf{a} - a_0)\mathbf{e}_j \\ \mathbf{e}_j^{\mathrm{T}}\mathbf{a} - a_0 \\ \mathbf{e}_j^{\mathrm{T}}\mathbf{p} - \mu \end{array} \right\} = \mathbf{0}. \tag{4.19}$$

Upon defining a rank-one updated tangent stiffness matrix by the expression

$$\mathbf{K}_{t_\gamma} = \mathbf{K}_t + \gamma \mathbf{e}_j \mathbf{e}_j^{\mathrm{T}} \tag{4.20}$$

linearization of (4.19) at the $(i+1)^{th}$ iteration can be written in the following form

$$\begin{bmatrix} \mathbf{K}_{t_\gamma} & \mathbf{0} & -\mathbf{f}_{ext} & -\gamma\mathbf{e}_j \\ \nabla_{\mathbf{p}}(\mathbf{K}_t\mathbf{a}) & \mathbf{K}_{t_\gamma} & \nabla_\lambda(\mathbf{K}_t\mathbf{a}) & \mathbf{0} \\ \mathbf{0}^{\mathrm{T}} & \mathbf{e}_j^{\mathrm{T}} & 0 & 0 \\ \mathbf{e}_j^{\mathrm{T}} & \mathbf{0}^{\mathrm{T}} & 0 & -1 \end{bmatrix} \begin{Bmatrix} d\mathbf{p} \\ d\mathbf{a} \\ d\lambda \\ d\mu \end{Bmatrix} = -\overline{\mathbf{R}}_i(\mathbf{p}_i, \mathbf{a}_i, \lambda_i, \mu_i), \tag{4.21}$$

considering $d(\cdot) = d(\cdot)_{i+1}$ and

$$\overline{\mathbf{R}}_i(\mathbf{p}_i, \mathbf{a}_i, \lambda_i, \mu_i) = \begin{Bmatrix} \mathbf{r}_i(\mathbf{p}_i, \lambda_i) + \gamma(\mathbf{e}_j^{\mathrm{T}}\mathbf{p}_i - \mu_i)\mathbf{e}_j \\ \mathbf{K}_t\mathbf{a}_i + \gamma(\mathbf{e}_j^{\mathrm{T}}\mathbf{a}_i - a_0)\mathbf{e}_j \\ \mathbf{e}_j^{\mathrm{T}}\mathbf{a}_i - a_0 \\ \mathbf{e}_j^{\mathrm{T}}\mathbf{p}_i - \mu_i \end{Bmatrix}, \tag{4.22}$$

i.e. the residual for system (4.19). With this constraint choice, an efficient solution for the matrix equation (4.21) can be obtained. Before presenting the resolution steps, however, we have to define

- the incremental displacements $d\mathbf{p}_1$, $d\mathbf{p}_2$ and $d\mathbf{p}_3$,

$$\begin{cases} d\mathbf{p}_1 = \mathbf{K}_{t_\gamma}^{-1}\mathbf{f}_{ext} \\ d\mathbf{p}_2 = -\mathbf{K}_{t_\gamma}^{-1}\mathbf{r}_i(\mathbf{p}_i, \lambda_i) \\ d\mathbf{p}_3 = \mathbf{K}_{t_\gamma}^{-1}\mathbf{e}_j \end{cases} \tag{4.23}$$

- the vectors $\mathbf{v}_i$ (with $i = 1, \ldots, 4$)

$$\begin{cases} \mathbf{v}_1 = \mathbf{K}_{t_\gamma}\mathbf{h}_1 \\ \mathbf{v}_2 = \mathbf{K}_{t_\gamma}\mathbf{h}_2 \\ \mathbf{v}_3 = \mathbf{K}_{t_\gamma}\mathbf{h}_3 \\ \mathbf{v}_4 = \mathbf{K}_{t_\gamma}\mathbf{h}_4 \end{cases} \tag{4.24}$$

  where

$$\begin{cases} \mathbf{h}_1 = -\nabla_{\mathbf{p}}(\mathbf{K}_t\mathbf{a})d\mathbf{p}_1 \\ \mathbf{h}_2 = -\nabla_{\mathbf{p}}(\mathbf{K}_t\mathbf{a})d\mathbf{p}_2 \\ \mathbf{h}_3 = -\nabla_{\mathbf{p}}(\mathbf{K}_t\mathbf{a})d\mathbf{p}_3 \\ \mathbf{h}_4 = -\nabla_\lambda(\mathbf{K}_t\mathbf{a}) \end{cases} \tag{4.25}$$

We are now ready to present the resolution steps for the equation (4.21).

1. *Solve the first equation in (4.21) for* $d\mathbf{p}$

$$\boxed{d\mathbf{p} = d\lambda d\mathbf{p}_1 + d\mathbf{p}_2 + \gamma(\mu_i + d\mu - \mathbf{e}_j^{\mathrm{T}}\mathbf{p}_i)d\mathbf{p}_3.} \tag{4.26}$$

2. *Solve the second equation in (4.21) for* $d\mathbf{a}$

$$d\mathbf{a} = -\mathbf{a}_i - \mathbf{K}_{t_\gamma}^{-1}[\nabla_{\mathbf{p}}(\mathbf{K}_t\mathbf{a})d\mathbf{p} + \nabla_\lambda(\mathbf{K}_t\mathbf{a})d\lambda - \gamma a_0\mathbf{e}_j], \tag{4.27}$$

that can be rewritten as

$$d\mathbf{a} = -\mathbf{a}_i + d\lambda(\mathbf{v}_1 + \mathbf{v}_4) + \mathbf{v}_2 + \gamma[(\mu_i + d\mu - \mathbf{e}_i^{\mathrm{T}}\mathbf{p}_i)\mathbf{v}_3 + a_0 d\mathbf{p}_3]. \tag{4.28}$$

3. *Compute load increments* $d\lambda$, $d\mu$.

From the last two equation of (4.21), considering (4.26) and (4.28), we get the new increments $d\lambda$ and $d\mu$. This is equivalent to solve to following non-symmetric two-by-two system of equations

$$\boxed{\begin{bmatrix} \mathbf{e}_j^{\mathrm{T}}(\mathbf{v}_1 + \mathbf{v}_4) & \gamma\mathbf{e}_j^{\mathrm{T}}\mathbf{v}_3 \\ \mathbf{e}_j^{\mathrm{T}}d\mathbf{p}_1 & (\gamma d\mathbf{p}_3 - 1) \end{bmatrix} \begin{Bmatrix} d\lambda \\ d\mu \end{Bmatrix} = \begin{Bmatrix} g_1 \\ g_2 \end{Bmatrix},} \tag{4.29}$$

with

$$g_1 = a_0 - \mathbf{e}_j^{\mathrm{T}}[\mathbf{v}_2 + \gamma(a_0 d\mathbf{p}_3 + \{\mu_i - \mathbf{e}_j\mathbf{p}_i\})\mathbf{v}_3],$$
$$g_2 = \mu_i - \mathbf{e}_j^{\mathrm{T}}[\mathbf{p}_i + d\mathbf{p}_2 + \gamma\{\mu_i - \mathbf{e}_j^{\mathrm{T}}\mathbf{p}_i\}d\mathbf{p}_3].$$

With $d\lambda$, $d\mu$ in hand, then, the other incremental unknowns can be computed from (4.26) and (4.28).

Finally, the updated quantities are given by

$$\begin{cases} \mathbf{p}_{i+1} = \mathbf{p}_i + d\mathbf{p} \\ \mathbf{a}_{i+1} = \mathbf{a}_i + d\mathbf{a} \\ \lambda_{i+1} = \lambda_i + d\lambda \\ \mu_{i+1} = \mu_i + d\mu. \end{cases} \tag{4.30}$$

4.3.3 Approximate directional derivative of the tangent matrix $\mathbf{K}_t$

In order to solve the extended system in a partitioned fashion, we need to calculate $\nabla_{\mathbf{p}}(\mathbf{K}_t\mathbf{a})d\mathbf{p}$. Closed-form expression can be calculated for certain kinds of finite element formulations, as done by Wriggers et al. in (28) for a Saint Venant-Kirchhoff model, but for others it might be very complicated. The idea (see (29)) is to consider the vector $\mathbf{K}_t\mathbf{a}$ as the directional derivative of the residual $\mathbf{r}$ in the direction of $\mathbf{a}$, i.e.

$$\mathbf{K}_t\mathbf{a} = \nabla_{\mathbf{p}}\mathbf{r}(\mathbf{p}, \lambda)\mathbf{a} = \left.\frac{\mathrm{d}}{\mathrm{d}\epsilon}\mathbf{r}(\mathbf{p} + \epsilon\mathbf{a}, \lambda)\right|_{\epsilon=0}. \tag{4.31}$$

Then exploiting the symmetry of the second derivative of $\mathbf{r}$, we can express the directional derivative of $\mathbf{K}_t\mathbf{a}$ in the direction of $d\mathbf{p}$ in the following equivalent form

$$\begin{aligned} \nabla_{\mathbf{p}}(\mathbf{K}_t\mathbf{a})d\mathbf{p} &= \nabla_{\mathbf{p}}[\nabla_{\mathbf{p}}\mathbf{r}(\mathbf{p},\lambda)\mathbf{a}]d\mathbf{p} \\ &= \nabla_{\mathbf{p}}[\nabla_{\mathbf{p}}\mathbf{r}(\mathbf{p},\lambda)d\mathbf{p}]\mathbf{a}. \end{aligned} \tag{4.32}$$

Instead of considering $\nabla_{\mathbf{p}}(\mathbf{K}_t\mathbf{a})d\mathbf{p}$ by means of its definition, i.e.

$$\nabla_{\mathbf{p}}(\mathbf{K}_t\mathbf{a})d\mathbf{p} = \frac{\mathrm{d}}{\mathrm{d}\epsilon}[\mathbf{K}_t(\mathbf{p}+\epsilon d\mathbf{p})]\mathbf{a}\Big|_{\epsilon=0} \tag{4.33}$$

thanks to (4.32), we can use

$$\nabla_{\mathbf{p}}(\mathbf{K}_t\mathbf{a})d\mathbf{p} = \frac{\mathrm{d}}{\mathrm{d}\epsilon}[\mathbf{K}_t(\mathbf{p}+\epsilon\mathbf{a})]d\mathbf{p}\Big|_{\epsilon=0}. \tag{4.34}$$

We now write an analogous definition of the directional derivative which is suitable for a numerical approximation, i.e.

$$\nabla_{\mathbf{p}}(\mathbf{K}_t\mathbf{a})d\mathbf{p} = \lim_{\epsilon=0}\frac{1}{\epsilon}[\mathbf{K}_t(\mathbf{p}+\epsilon\mathbf{a})d\mathbf{p} - \mathbf{K}_t(\mathbf{p})d\mathbf{p}]. \tag{4.35}$$

Selecting a parameter ϵ sufficiently small, we can use the approximation

$$\nabla_{\mathbf{p}}(\mathbf{K}_t\mathbf{a})d\mathbf{p} \approx \frac{1}{\epsilon}[\mathbf{K}_t(\mathbf{p}+\epsilon\mathbf{a})d\mathbf{p} - \mathbf{K}_t(\mathbf{p})d\mathbf{p}]. \tag{4.36}$$

The application of (4.36) to the algorithm described in the previous subsection leads to practical expressions for vectors $\mathbf{h}_1$, $\mathbf{h}_2$ and $\mathbf{h}_3$. Taking for instance $\mathbf{h}_1$ we have

$$\begin{aligned} \mathbf{h}_1 &\approx \frac{1}{\epsilon}[\mathbf{K}_t(\mathbf{p}+\epsilon\mathbf{a})d\mathbf{p}_1 - \mathbf{K}_t(\mathbf{p})d\mathbf{p}_1] \\ &\approx \frac{1}{\epsilon}[\mathbf{K}_t(\mathbf{p}+\epsilon\mathbf{a})d\mathbf{p}_1 + (\gamma\mathbf{e}_j\mathbf{e}_j^{\mathrm{T}} - \mathbf{K}_{t_\gamma}(\mathbf{p}))d\mathbf{p}_1] \\ &\approx \frac{1}{\epsilon}[(\mathbf{K}_t(\mathbf{p}+\epsilon\mathbf{a}) + \gamma\mathbf{e}_j\mathbf{e}_j^{\mathrm{T}})d\mathbf{p}_1 - \mathbf{f}_{ext}]. \end{aligned} \tag{4.37}$$

Similarly vectors $\mathbf{h}_2$ and $\mathbf{h}_3$ can be computed as

$$\mathbf{h}_2 \approx \frac{1}{\epsilon}[(\mathbf{K}_t(\mathbf{p}+\epsilon\mathbf{a}) + \gamma\mathbf{e}_j\mathbf{e}_j^{\mathrm{T}})d\mathbf{p}_2 - \mathbf{r}_i(\mathbf{p}_i,\lambda_i)] \tag{4.38}$$

$$\mathbf{h}_2 \approx \frac{1}{\epsilon}[(\mathbf{K}_t(\mathbf{p}+\epsilon\mathbf{a}) + \gamma\mathbf{e}_j\mathbf{e}_j^{\mathrm{T}})d\mathbf{p}_3 - \mathbf{e}_i]. \tag{4.39}$$

To obtain the expression above, we have used equations (4.36), (4.23) and (4.20).

A suitable selection of the parameter ϵ in equations (4.37), (4.38) and (4.39) is crucial for the success of the method. An extimate for ϵ is given in (29) and leads to the following formula

$$\epsilon = \max_{1<k<N} p_k \, \eta_{\mathrm{TOL}}. \tag{4.40}$$

Here p_k denotes the k^{th} component of $\mathbf{p} \in \mathbb{R}^N$, and $\eta_{\mathrm{TOL}} = 10^{-\mathrm{DIGITS}}$ is a machine precision constant, being "DIGITS" the number of computed significative digits.

4.3.4 Some remarks

a) The procedure just described with the improvement of the penalty formulation results in a quadratically convergent Newton-type iteration scheme for the calculation of limit or bifurcation points. However only one buckling mode is considered within the iteration scheme. In fact there is no proved experience which shows that it is possible to determine multiple bifurcation points.

b) The extended system approach is also referred to as *local pinpointing procedure*. The reason for such a name is illustrated in figure 4.1.

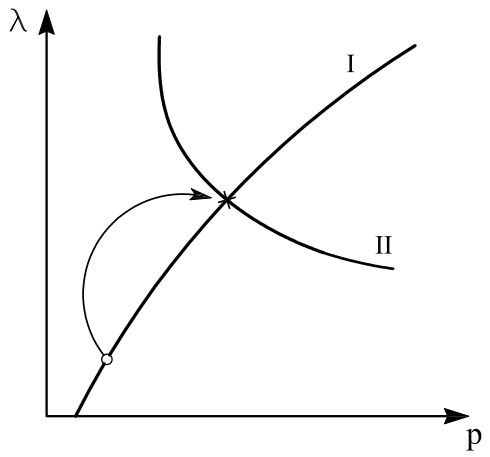

Figure 4.1: Local pinpointing procedure

c) As the convergence of the method is strictly related to the choice of the starting vector $\mathbf{a}$, one possibility is to take $\mathbf{a}$ equal to the eigenvector of $\mathbf{K}_t$ associated with the minimum eigenvalue at the actual state, i.e. the state at which we switch to the extended system.

d) In our problems we always consider that load is independent of the deformation, i.e. the term $\nabla_\lambda(\mathbf{K}_t\mathbf{a})$ is equal to zero.

4.4 Branch switching

Once a critical point has been located and identified as a bifurcation point, it may be desiderable to compute the secondary branch that crosses the branch we have followed. At the moment two possibilities exist to perfom such a switch, i.e.

1. **Branching predictor** consists of providing a set of initial data that forces the arc-length algorithm to change direction at the bifurcation point so that it will move along secondary path instead of the primary one. Clearly, a suitable set of initial data would consist of the bifurcation point itself, known from the extended system solution, and the tangent to the secondary branch obtained at this point by means of the solution of a proper set of equation;

2. **Perturbed branching**, initially presented by Huitfeldt in (33), consists of considering an auxiliary equation which defines with the perturbed equilibrium equation a closed one-dimensional curve in $(N+2)$-dimensional space. This curve passes exactly through one point on each branch determined by the unperturbed equation that we have always considered with this method. The explicit calculation of bifurcation point is not required.

In the following subsection we give further information about these two branching techniques.

4.4.1 Branching predictor

As previuosly said, such a technique requires the tangent to the secondary branch, in order to construct the prediction for the first step onto the intersecting branch as shown in figure 4.2, i.e.

$$\begin{cases} \mathbf{p}_0 = \mathbf{p}^* + \Delta\tau\dot{\mathbf{p}}_{\mathrm{II}} \\ \lambda_0 = \lambda^* + \Delta\tau\dot{\lambda}_{\mathrm{II}}. \end{cases} \tag{4.41}$$

In order to obtain the tangent direction to the intersecting path $\dot{\mathbf{x}}_{\mathrm{II}} = (\dot{\mathbf{p}}_{\mathrm{II}}, \dot{\lambda}_{\mathrm{II}})$ we briefly recall what we discussed in detail in chapter 1. Tangent solutions to primary and secondary branches are solutions of the first equation of the rate problem (1.21) and they are expressed as

$$\begin{aligned} \dot{\mathbf{p}}_{\mathrm{I}} &= \dot{\lambda}_{\mathrm{I}}\mathbf{y} + \mu_{\mathrm{I}}\mathbf{a}_1 \\ \dot{\mathbf{p}}_{\mathrm{II}} &= \dot{\lambda}_{\mathrm{II}}\mathbf{y} + \mu_{\mathrm{II}}\mathbf{a}_1. \end{aligned} \tag{4.42}$$

In the above expression we consider that $\mathbf{y} = \mathbf{K}_t^{-1}\mathbf{f}_{ext}$ belongs to the range of $\mathbf{K}_t$ by definition, $\mathbf{a}_1$ is the eigenvector associated with the critical state, known from the extended system, and μ is a proper amplification factor

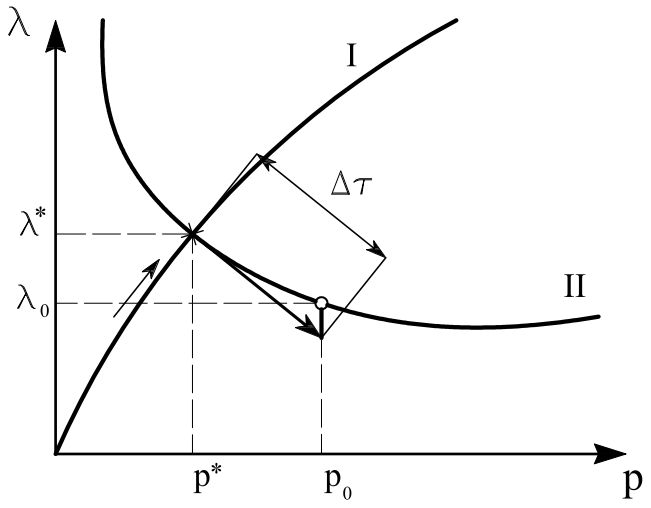

Figure 4.2: **Branching predictor**

which is crucial for the predictor definition. Thus if we rename $\dot{\lambda}_{\mathrm{I}}$ and $\dot{\lambda}_{\mathrm{II}}$ simply as $\dot{\lambda}$, then μ_{I} and μ_{II} as μ, we can get the necessary unknown informations from the *algebraic bifurcation equation* (ABE) and an adjoint normalization equation (see (20))

$$\begin{cases} \hat{A}\mu^2 + 2\hat{B}\mu\dot{\lambda} + \hat{C}\dot{\lambda}^2 = 0 \\ \mu^2 + \dot{\lambda}^2 = 1 \end{cases} \tag{4.43}$$

being

$$\hat{A} = \mathbf{a}_1^{\mathrm{T}}[\nabla_{\mathbf{p}}(\mathbf{K}_t\mathbf{a}_1)\mathbf{a}_1], \tag{4.44}$$

$$\hat{B} = \mathbf{a}_1^{\mathrm{T}}[\nabla_{\mathbf{p}}(\mathbf{K}_t\mathbf{a}_1)\mathbf{y}], \tag{4.45}$$

$$\hat{C} = \mathbf{a}_1^{\mathrm{T}}[\nabla_{\mathbf{p}}(\mathbf{K}_t\mathbf{y})\mathbf{y}], \tag{4.46}$$

with

$$\nabla_\lambda(\mathbf{K}_t\mathbf{a}_1) = \nabla_\lambda(\mathbf{K}_t\mathbf{y}) = \nabla_\lambda(\mathbf{f}) = \mathbf{0}, \tag{4.47}$$

as load is independent on deformation. An approximation of the directional derivative $\nabla_{\mathbf{p}}(\cdot)$ has been discussed in subsection 4.3.3; besides, in the implementation, we do not have to compute again its value, as at this level we have already computed it for the resolution of the extended system.

We are interested now in analyzing ABE solution in the case of symmetric bifurcation. As we have seen in chapter 1, symmetric or cusp bifurcation is such that $[\mathbf{a}_1^{\mathrm{T}}\nabla_{\mathbf{p}}(\mathbf{K}_t\mathbf{a}_1)\mathbf{a}_1 = 0]$, that is

$$\hat{A} = 0. \tag{4.48}$$

Thus branching equation (4.43) particularizes as

$$\begin{cases} \dot{\lambda}(2\hat{B}\mu + \hat{C}\dot{\lambda}) = 0 \\ \mu^2 + \dot{\lambda}^2 = 1 \end{cases} \tag{4.49}$$

i.e. the tangent to the secondary path has the form

$$\begin{cases} \dot{\lambda}_{\text{II}} = 0 \\ \mu_{\text{II}} = \pm 1. \end{cases} \tag{4.50}$$

This means that transition to the secondary path is accomplished simply by adding the buckling mode to the displacement field at the bifurcation point. In such a case the predictor solution is given by

$$\begin{cases} \mathbf{p}_0 = \mathbf{p}^* \pm \mathbf{a}_1 \Delta\tau \\ \lambda_0 = \lambda^*. \end{cases} \tag{4.51}$$

4.4.2 Perturbed branching

By remembering the equilibrium problem $\mathbf{r}(\mathbf{p}, \lambda) = \mathbf{0}$, we construct now its perturbed form, i.e.

$$\mathbf{r}(\mathbf{p}, \lambda) + \eta\mathbf{q} = \mathbf{0}, \tag{4.52}$$

or in compact form

$$\mathbf{r}_p(\mathbf{p}, \lambda, \eta) = \mathbf{0}, \tag{4.53}$$

where η and $\mathbf{q}$ are respectively a disturbing load parameter and its associated load vector. Equation (4.53) defines a $(N + 2)$-dimensional surface which intersects the unperturbed equilibrium equation every time that $\eta = 0$. Thus a possible way of switching onto a secondary branch is, starting from at unperturbed equilibrium point $\eta = 0$, to find all those points that lie on the two curves $\mathbf{r} = \mathbf{0}$ and $\mathbf{r}_p = \mathbf{0}$ and thus such that $\eta = 0$; once characterized, the analysis can restart beginning from these points $(\mathbf{p}_0, \lambda_0)$, as shown in figure 4.3.

One of the advantages of this perturbated approach is that equation (4.53) can be solved by continuation strategies. Here we apply the arc-length method to the augmented perturbated problem, the so called *Branch Connection Equation* (33), i.e.

$$\mathbf{R}_p(\mathbf{x}, \eta) = \mathbf{0}, \tag{4.54}$$

or, alternatively,

$$\begin{cases} \mathbf{r}_p(\mathbf{x}, \eta) = \mathbf{0} \\ G_p(\mathbf{x}, \eta) = g_p(\mathbf{x}, \eta) - \tau = 0 \end{cases} \tag{4.55}$$

where $\mathbf{x} = (\mathbf{p}, \lambda)$.

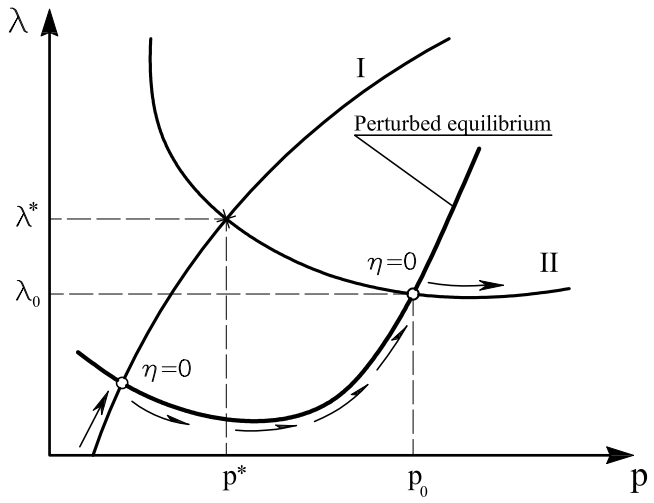

Figure 4.3: **Perturbed predictor**

System (4.55) written at iteration $i+1$ leads to

$$\begin{cases} \mathbf{r}_p(\mathbf{x}_{i+1}, \eta_{i+1}) = \mathbf{r}_{p(i+1)} = \mathbf{0} \\ G_p(\mathbf{x}_{i+1}, \eta_{i+1}) = G_{p(i+1)} = 0, \end{cases} \tag{4.56}$$

while its linearization has the form of

$$\begin{cases} \mathbf{K}_t d\mathbf{p}_{i+1} - \mathbf{f}_{ext} d\lambda_{i+1} + \mathbf{q} d\eta_{i+1} = -\mathbf{r}_{p(i)} \\ (\nabla_{\mathbf{p}} g_p)^{\mathrm{T}} d\mathbf{p}_{i+1} + (\nabla_\lambda g_p) d\lambda_{i+1} + (\nabla_\eta g_p) d\eta_{i+1} = 0, \end{cases} \tag{4.57}$$

with

$$\nabla_{\mathbf{p}} g_p = \left.\frac{\partial g_p}{\partial \mathbf{p}}\right|_{(\mathbf{x},\eta)=(\mathbf{x}_i,\eta_i)} \qquad \nabla_\lambda g_p = \left.\frac{\partial g_p}{\partial \lambda}\right|_{(\mathbf{x},\eta)=(\mathbf{x}_i,\eta_i)} \qquad \nabla_\eta g_p = \left.\frac{\partial g_p}{\partial \eta}\right|_{(\mathbf{x},\eta)=(\mathbf{x}_i,\eta_i)}.$$

In the above equations we have supposed that $g_{p(i)} = 0$.

Following (12), the linearized system (4.57) is solved by means of the block factorization method, where the iterative displacement vector is decomposed as

$$\boxed{d\mathbf{p}_{i+1} = d\mathbf{p}_\lambda d\lambda_{i+1} + d\mathbf{p}_\eta d\eta_{i+1} + d\mathbf{p}_r} \tag{4.58}$$

with

$$\begin{cases} d\mathbf{p}_\lambda = \mathbf{K}_t^{-1} \mathbf{f}_{ext} \\ d\mathbf{p}_\eta = -\mathbf{K}_t^{-1} \mathbf{q} \\ d\mathbf{p}_r = -\mathbf{K}_t^{-1} \mathbf{r}_{p(i)}. \end{cases} \tag{4.59}$$

The solution of system (4.57) is then obtained through the following steps.

1. Take $d\eta_{i+1}$ from the second equation of the linearized BCE (4.57) and insert in the result the displacement decomposition (4.59), obtaining

$$\boxed{d\eta_{i+1} = k_0 + k_1 d\lambda_{i+1},} \tag{4.60}$$

where

$$\begin{cases} k_0 = -\dfrac{(\nabla_{\mathbf{p}} g_p)^{\mathrm{T}} d\mathbf{p}_r}{(\nabla_\eta g_p) + (\nabla_{\mathbf{p}} g_p)^{\mathrm{T}} d\mathbf{p}_\eta} \\ k_1 = -\dfrac{(\nabla_\lambda g_p) + (\nabla_{\mathbf{p}} g_p)^{\mathrm{T}} d\mathbf{p}_\lambda}{(\nabla_\eta g_p) + (\nabla_{\mathbf{p}} g_p)^{\mathrm{T}} d\mathbf{p}_\eta}. \end{cases} \tag{4.61}$$

2. Take $d\lambda_{i+1}$ from the second equation of the linearized BCE (4.57) and insert in the result the displacement decomposition (4.59) and the expression for $d\eta_{i+1}$ from (4.60), obtaining

$$\boxed{d\lambda_{i+1} = -\frac{(\nabla_\eta g_p) k_0 + (\nabla_{\mathbf{p}} g_p)^{\mathrm{T}} (d\mathbf{p}_\eta k_0 + d\mathbf{p}_r)}{(\nabla_\lambda g_p) + (\nabla_\eta g_p) k_1 + (\nabla_{\mathbf{p}} g_p)^{\mathrm{T}} (d\mathbf{p}_\eta k_0 + d\mathbf{p}_\lambda)}.} \tag{4.62}$$

3. With $d\lambda_{i+1}$ in hand, get $d\eta_{i+1}$ from (4.60) and $d\mathbf{p}_{i+1}$ from (4.58).

Finally, the updated quantities are given by

$$\begin{cases} \mathbf{p}_{i+1} = \mathbf{p}_i + d\mathbf{p}_{i+1} \\ \lambda_{i+1} = \lambda_i + d\lambda_{i+1} \\ \eta_{i+1} = \eta_i + d\eta_{i+1}. \end{cases} \tag{4.63}$$

A careful definition of the constraint surface must be here considered. Here we use a plane constraint in order to avoid the presence of inconvenient roots, as for example with spherical surfaces. Besides, we would like a continuous requirement of orthogonality while we are following the perturbed equilibrium path. In this sense the Orthogonal Trajectory Method satisfies our requirement and written at $(i+1)^{th}$ iteration has the form of

$$\mathbf{m}^{\mathrm{T}}\, \mathbf{M}\, (\mathbf{x}_{i+1} - \mathbf{x}^n) + c(\eta_{i+1} - \eta^n) + \Delta\tau = 0, \tag{4.64}$$

where $\mathbf{m}$ and c should satisfy the orthogonality condition

$$\nabla_{\mathbf{x}}[\mathbf{r}_p(\mathbf{x}, \eta)]\mathbf{m} + \nabla_\eta[\mathbf{r}_p(\mathbf{x}, \eta)]c = \mathbf{0}. \tag{4.65}$$

In order to satisfy condition (4.65) $\mathbf{m}$ and c are selected as

$$\mathbf{m} = [\mathbf{n}, \nu] = [\mathbf{K}_t^{-1}(\mathbf{f}_{ext} - \mathbf{q}), 1], \quad c = 1; \tag{4.66}$$

in fact with this choice we have

$$\begin{aligned} \nabla_{\mathbf{x}}[\mathbf{r}_p(\mathbf{x}, \eta)]\mathbf{m} + \nabla_\eta[\mathbf{r}_p(\mathbf{x}, \eta)]c &= [\mathbf{K}_t, -\mathbf{f}_{ext}][\mathbf{K}_t^{-1}(\mathbf{f}_{ext} - \mathbf{q}), 1]^{\mathrm{T}} + \mathbf{q} \\ &= \mathbf{0}. \end{aligned}$$

Linearization of constraint equation (4.65) leads to

$$\mathbf{m}^{\mathrm{T}}\,\mathbf{M}\,d\mathbf{x}_{i+1} + cd\eta_{i+1} = \Delta\tau - \mathbf{m}^{\mathrm{T}}\,\mathbf{M}\,(\mathbf{x}_i - \mathbf{x}^n) - c(\eta_i - \eta^n), \tag{4.67}$$

and requiring $[\Delta\tau - \mathbf{m}^{\mathrm{T}}\,\mathbf{M}\,(\mathbf{x}_i - \mathbf{x}^n) - c(\eta_i - \eta^n) = 0]$, we get

$$\mathbf{m}^{\mathrm{T}}\,\mathbf{M}\,d\mathbf{x}_{i+1} + cd\eta_{i+1} = 0. \tag{4.68}$$

Using the form (3.24) of matrix $\mathbf{M}$, we obtain

$$\begin{cases} \nabla_{\mathbf{p}} g_p = \mathbf{K}_t^{-1}(\mathbf{f}_{ext} - \mathbf{q})\mathbf{N} \\ \nabla_{\lambda} g_p = \mu \\ \nabla_{\eta} g_p = 1 \end{cases} \tag{4.69}$$

from which the incremental unknowns (4.59), (4.62) and (4.60) follow.

4.5 Overall algorithm for path-following

In the following box we finally present the overall algorithm for global path-following of nonlinear stability problems.

a. Calculation of equilibrium branch with arc-length method. GO TO b.

b. Observation of some test-functions (Section 4.2) while proceeding

  b1. IF the limit point is passed: GO TO a.

  b2. ELSEIF the bifurcation point is passed: GO TO c.

  b3. ELSEIF the required number of load steps is reached: GO TO g.

  b4. ELSE: GO TO a.

c. Choose the branch you would like to follow:

  c1. IF primary path: GO TO a.

  c2. ELSE: GO TO d.

d. With a *false step* criterion return to the point previously calculated. GO TO e.

e. Pinpoint bifurcation point via extended system (subsection 4.3.2) and save information to restart the problem. GO TO f.

f. Perform *branch-switching*:

  f1. IF *branching predictor* (subsection 4.4.1) is used:

    f1.1. solve ABE system (4.43);

    f1.2. store tangent directions;

    f1.3. perfom a *predictor step* onto secondary branch, once chosen, and GO TO a.

  f2. ELSE *perturbed branching* (subsection 4.4.2) is used:

    f2.1. solve BCE (4.57) with block factorization method;

    f2.2. store points where $\eta = 0$ and stop continuation when a stationary number of branching points is found;

    f3.3. beginning from the BCE point already found, once chosen, GO TO a.

g. Test number of other branching points:

  g1. IF other branches have to be inspected: restart from stored points during *branch-switching* procedure and GO TO a.

  g2. ELSE terminate the analysis.

Chapter 5

Numerical examples

5.1 Introduction

The numerical results shown in the following cover different types of nonlinear structural behaviours such as costitutive (perfect plasticity) and geometrical (*snapping* modes and bifurcation phenomena) nonlinearities; in particular, we consider here some examples for which it is possible to find an analytical solution.

Usually for these problems characterized by the presence of critical points, the traditional load control method fails in following equilibrium solutions because the stiffness matrix $\mathbf{K}_t$ becomes singular at such points; in this chapter we show how the proposed arc-length strategy gives good results also in these situations. Such numerical examples are also useful for a better understanding of critical conditions, and in particular of bifurcations, as a precise monitoring of the stiffness matrix eigenvalues is performed. We moreover highlight that we have implemented the arc-length strategy proposed in section 3.3.1 within the finite element formulation described in appendix B. For the implementation the MATLAB® environment has been selected.

As the choice of the constraint condition does not affect the performance of the finite element formulation except when locking phenomena appear (see (7)), an *Orthogonal Trajectory Method* which constantly imposes an orthogonality condition has been used. This arc-length strategy has been combined with the *Newton Raphson*'s iterative scheme for which the stiffness matrix is assembled at each iteration. In reference (7) this scheme is proved to be robust and efficient, in terms of performed loops, in particular as compared with its *Modified* variant. The value of the tolerance for convergence has been set equal to 10^{-7} for all tests.

We finally remark that for all length measures we use [m] while for force measures we use [KN]; thus material properties such as the Young's modulus E and the shear modulus G are expressed in terms of [KN/m^2].

5.2 Elasto-perfectly plastic hinged beam

We consider now an hinged beam, presented in figure 5.1, with a rectangular cross section b × h and ideally supposed elasto-perfectly-plastic, for which we neglect shear deformation effect. The aim is firstly to solve this structure analytically and then to compare the results with our finite element solutions.

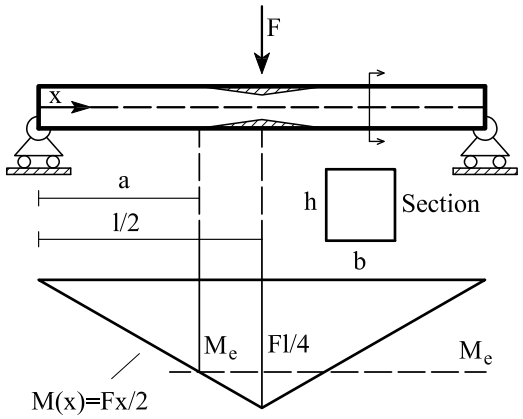

Figure 5.1: Elasto-perfectly plastic hinged beam. Problem definition.

The elastic moment-curvature relation for a beam is

$$M = EJ\chi, \quad \text{for} \quad \chi < \chi_e, \tag{5.1}$$

where E is the Young's modulus, J is the moment of inertia of the rectangular cross section and χ_e is the curvature at the elastic limit. When the plastic phase is entered the moment-curvature relation becomes

$$M = M_e\left[\frac{3}{2} - \frac{1}{2}\left(\frac{\chi_e}{\chi}\right)^2\right], \quad \text{for} \quad \chi \geq \chi_e. \tag{5.2}$$

The elastic phase ends when the extreme fibre stress reaches its elastic limit, thus when

$$M_e = \frac{1}{6}bh^2\sigma_y, \quad \chi_e = \frac{M_e}{EJ} = \frac{2}{h}\frac{\sigma_y}{E}, \tag{5.3}$$

being σ_y the stress yield limit. In figure 5.1 we can see the elastic beam bending moment diagram with its maximum value $Fl/4$ in the central section. If such a moment exceeds its elastic limit M_e there will be a plastic region that spreading from the central section (cfr. figure 5.1).

We would like now to study the beam plasticity evolution. In term of forces, the beam starts showing a plastic behaviour when F exceeds F_e,

defined as

$$F_e = \frac{4M_e}{l}. \tag{5.4}$$

The parts of the beam remaining elastic have length a, with a such that

$$M_e = \frac{F}{2}a \tag{5.5}$$

hence, using (5.4), we obtain

$$a = \frac{l}{2}\frac{F_e}{F}. \tag{5.6}$$

Then, being $M(x) = Fx/2$, from (5.5) we obtain

$$\frac{M(x)}{M_e} = \frac{x}{a}. \tag{5.7}$$

Taking advantage of the symmetry of the problem we analyze only half of the beam. Considering moments in the elastic (5.1) and plastic (5.2) parts of the beam, it is now possible to express the curvature as

$$\chi(x) = \begin{cases} \dfrac{M(x)}{EJ} = \dfrac{M_e}{EJ}\dfrac{x}{a} = \dfrac{\chi_e}{a}x, & 0 \le x \le a \\ \dfrac{\chi_e}{[3-2(M(x)/M_e)]^{1/2}} = \dfrac{\chi_e}{[3-2(x/a)]^{1/2}}, & a \le x \le l/2. \end{cases} \tag{5.8}$$

Moreover, the curvature is such that

$$\chi = -\frac{\mathrm{d}\varphi}{\mathrm{d}x}; \tag{5.9}$$

thus from the above expression, section rotations are given by

$$\varphi(x) = \varphi(0) - \int_0^x \chi \mathrm{d}x. \tag{5.10}$$

Problem symmetry requires

$$\varphi(l/2) = \varphi(0) - \int_0^{l/2} \chi \mathrm{d}x = 0. \tag{5.11}$$

Taking $\varphi(0)$ from (5.11), equation (5.10) becomes

$$\begin{aligned} \varphi(x) &= \int_x^{l/2} \chi \mathrm{d}x = \\ &= \begin{cases} \chi_e \left\{ \displaystyle\int_x^a (x/a)\mathrm{d}x + \int_a^{l/2} [3-2(x/a)]^{-1/2}\mathrm{d}x \right\}, & 0 \le x \le a \\ \chi_e \displaystyle\int_x^{l/2} [3-2(x/a)]^{-1/2}\mathrm{d}x, & a \le x \le l/2; \end{cases} \end{aligned}$$

that is

$$\varphi(x) = \begin{cases} \chi_e a\left\{\dfrac{3}{2} - [3-(l/a)]^{1/2} - \dfrac{1}{2}(x^2/a^2)\right\}, \; 0 \le x \le a \\ \chi_e a\{[3-2(x/a)]^{-1/2} - [3-(l/a)]^{1/2}\}, \quad a \le x \le l/2. \end{cases} \tag{5.12}$$

As we do not consider shear deformations, rotations are such that

$$\varphi = \frac{\mathrm{d}v}{\mathrm{d}x}. \tag{5.13}$$

Vertical displacement is then obtained integrating (5.13) and considering compatibility conditions at the hinged ends $v(0) = 0$. Thus for vertical displacement we get

$$v(x) = \int_0^x \varphi \mathrm{d}x. \tag{5.14}$$

We are now interested in the displacement f at bea central section. We can it, from (5.14) and considering (5.12), as

$$\begin{aligned} f &= \int_0^{l/2} \varphi \mathrm{d}x = \chi_e a\left\{ \int_0^a \left(\frac{3}{2} - \left[3-\frac{l}{a}\right]^{1/2} - \frac{1}{2}\frac{x^2}{a^2}\right)\mathrm{d}x + \right. \\ &+ \left. \int_a^{l/2} \left(\left[3-2\frac{x}{a}\right]^{1/2} - \left[3-\frac{l}{a}\right]^{1/2}\right)\mathrm{d}x \right\} = \\ &= \frac{1}{3}\chi_e a^2\left\{5 - \left(3+\frac{1}{2}\frac{l}{a}\right)\left[3-\frac{l}{a}\right]^{1/2}\right\}. \end{aligned} \tag{5.15}$$

For $a = l/2$, from (5.15) we get the central displacement at the elastic limit, i.e.

$$f_e = \frac{1}{12}\chi_e l^2. \tag{5.16}$$

Remembering (5.6) we can express equation (5.15) in a dimensionless form as

$$\boxed{\frac{f}{f_e} = \left(\frac{F_e}{F}\right)^2\left\{5 - \left(3+\frac{F}{F_e}\right)\left[3-2\frac{F}{F_e}\right]^{1/2}\right\}.} \tag{5.17}$$

So, if we consider the beam properties as follows

l	E	b	h	σ_y
10	1000	1	1	600

we get

M_e	F_e	F_{pl}	f_e	f_{pl}
100	40	60	10	22.2

A finite element solution is obtained using 10 two-node elements within the Eulero-Bernoulli theory, i.e no shear included, and considering a 1D elasto-perfectly plastic costitutive relation which is integrated along cross direction; thus the element results in a "fibre" beam element. We choose to plot dimensionless central beam displacement f/f_e versus dimensionless point load F/F_e in order to compare our results with the analytical solution (5.17). Figure 5.2 shows the good agreement of numerical and analytical results. We would like now to show the good performance of our **arc-length**

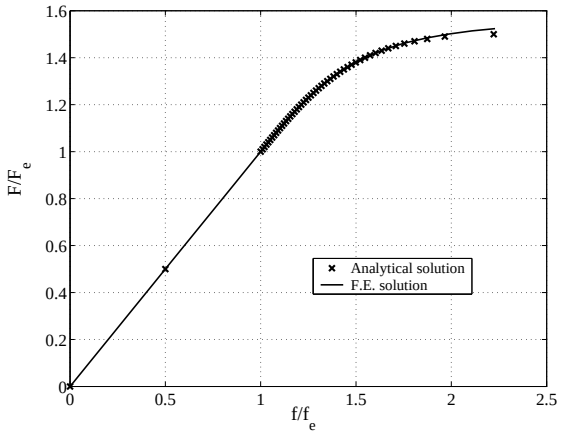

Figure 5.2: Elasto-perfectly plastic hinged beam. Analytic solution versus finite element solution.

method even well beyond the elastic limit. Recalling that for an arc-length strategy

$$\mathbf{F} = \mathbf{F}_{ext} = \lambda \mathbf{f}_{ext},$$

where $\mathbf{f}_{ext}$ is kept fixed, for next plots we have $F/F_e = \lambda/\lambda_e$.

In the plastic zones of the equilibrium path we have to consider that

1. $\Delta\lambda = 0$, i.e. no possibilities to increment load factor λ;
2. the matrix $\mathbf{K}_t$ is singular.

For these reasons we use:

1. An *Elastic Plane* constraint, i.e. $\mathbf{m} = (\hat{\mathbf{p}}, 1)$, being $\hat{\mathbf{p}}$ the displacement derivative with respect to λ, evaluated in elastic step:

$$\hat{\mathbf{p}} := \left.\frac{d\mathbf{p}}{d\lambda}\right|_{elastic} = \mathbf{K}_{elas}^{-1}\mathbf{f}_{ext} \tag{5.18}$$

2. a Modified Newton-Raphson's scheme, employing the elastic stiffness matrix $\mathbf{K}_{elas}$ instead of the tangent $\mathbf{K}_t$ in both *predictor* and *corrector phases*.

The obtained good performance in following the beam plastic evolution is shown in figure 5.3. The arc-length method has also been tested on a suc-

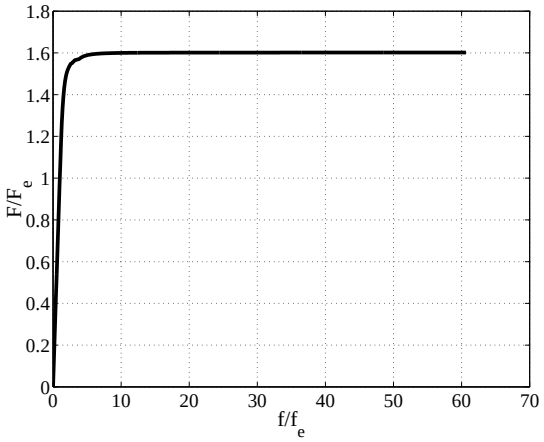

Figure 5.3: Elasto-perfectly plastic hinged beam. Arc-length performance in following the plastic evolution of the beam.

cession of loading and unloading cycles, figures (5.4); we can observe a good capability of unloading even at hight level of fibre plasticization.

5.3 Arches

Elastic structures, such as arches, can exhibit a non-linear geometric response immediately after the application of load conditions. This is due to the important effect that even small displacements have to the equilibrium configuration of such structures. Thus the hypothesis of small-displacements has to be removed in order to catch important features of the structural behaviour. Moreover, as arches work mainly carrying large axial forces rather than large bending moments, the classical first-order theory of structures that neglects interaction between axial forces and bending moments is unable to give a true picture of the behaviour of an arch.

In general, nonlinear geometric behaviour is not necessarily a source of instability. While cables, for instance, show a stiffened behaviour when loaded in a certain direction, i.e. deformed conditions can improve their stiffening, arches can lose their load-bearing capacity because of the progressive increase of the degree of nonlinearity. In other words for this kind of structures there exists a limit point after that they are not able to achieve equilibrium configurations. In such situations, a critical event is always associated with loss of stiffening towards fundamental modes or, when bifurcation occurs, secondary modes.

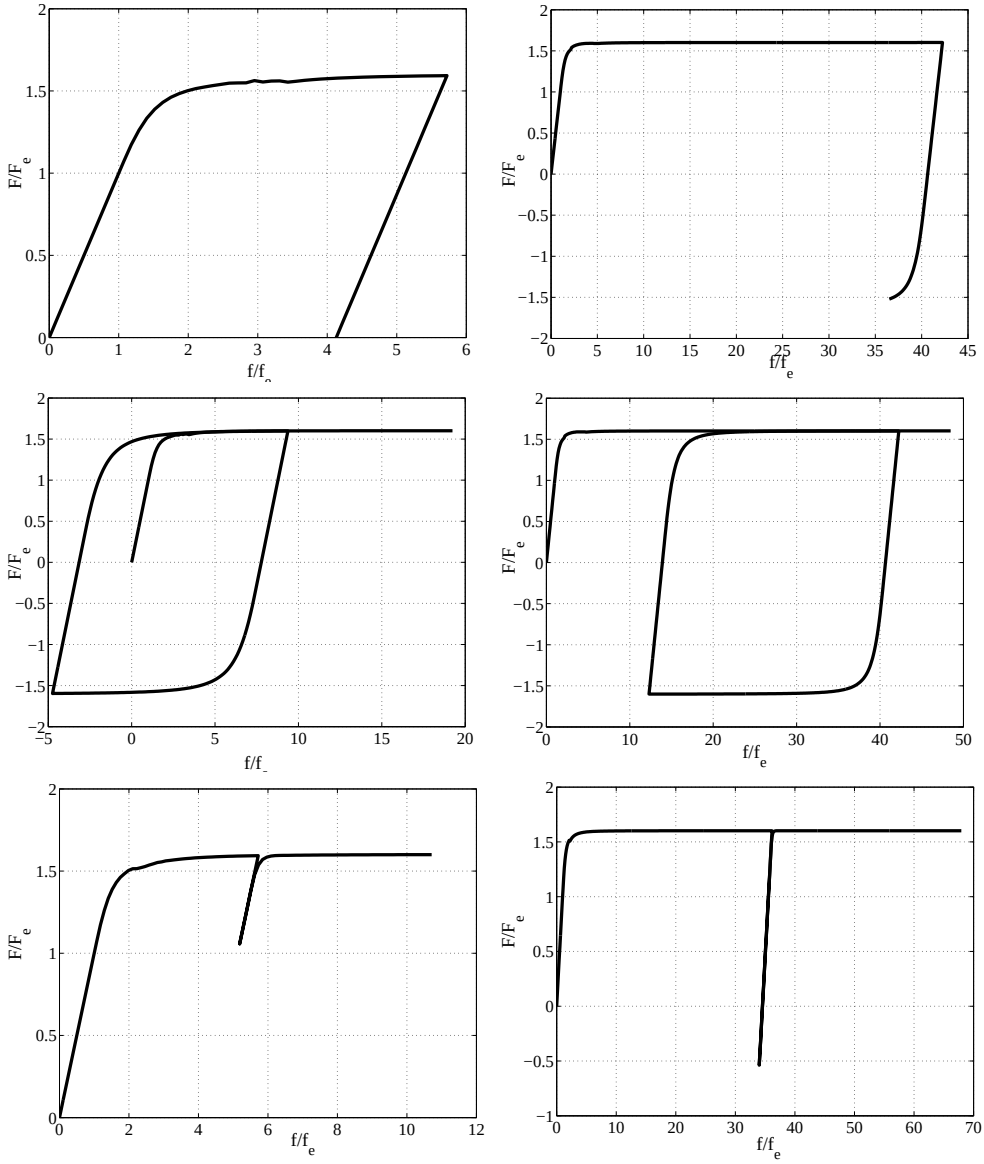

Figure 5.4: Elasto-perfectly plastic hinged beam. Loading and unloading cycles.

5.3.1 A non-shallow clamped-hinged arch

In this test, we consider a circular arch with one end clamped, the other hinged and loaded by a single point load, as shown in figure 5.5 where we also report geometrical and material parameter values. This example has been already examined by Da Deppo and Schmidt in (16), where the result were obtained by means of the nonlinear equations and the solution method described in (18). In (16), the authors present critical values for load and displacement parameters, as well as a complete series of graphs of the dimensionless load $\alpha = PR^2/EJ$ versus dimensionless displacements, i.e. u_x/R, u_y/R and versus the amplified rotation, 10β.

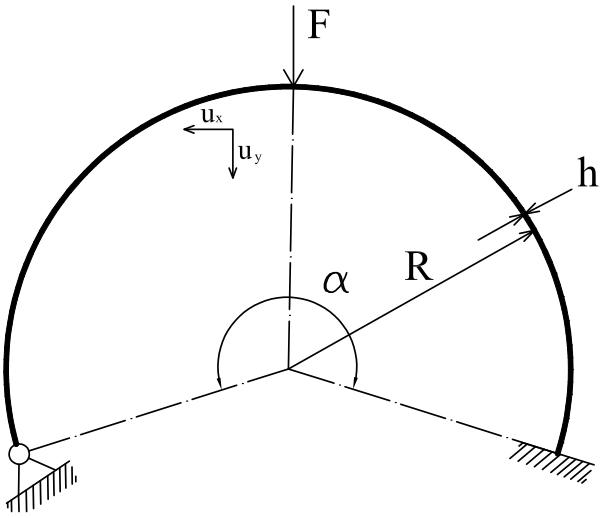

R	α	EJ	ν	A	h
100	215°	10^6	0.5	1	1

Figure 5.5: A clamped-hinged arch. Problem definition.

All the solutions are obtained using 40 two-node elements within the two-dimensional large-displacement large-strain theory described in (15) (called *geometrically exact* since no small-angle approximations are involved) and the two-dimensional large-displacement small-strain theory developed in appendix B.

Figures 5.6-5.11, show that:

a. good agreement exists between the large-displacement small-strain theory described in appendix B and Da Deppo's analitical solution (figures 5.6, 5.7 and 5.8);

b. the large-strain versus small-strain (figure 5.11);

c. the large-displacement small-strain formulation and the small-displacement one (Timoshenko beam) (figure 5.11).

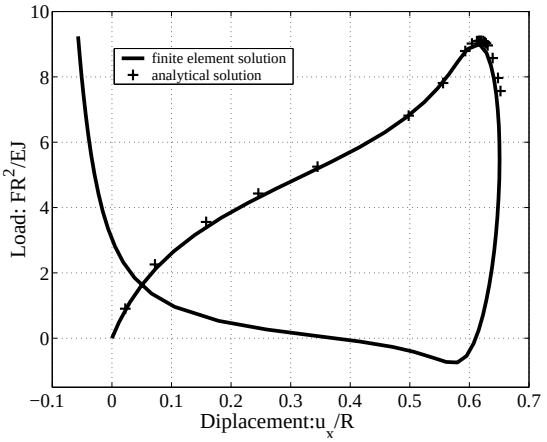

Figure 5.6: A clamped-hinged arch. Dimensionless load, $\alpha = PR^2/EJ$, versus dimensionless horizontal displacement, u_x/R. Notice the good agreement between the large-displacement beam element (15) and the analytical solution (16).

Examining such load displacement curves, we note that, after a very large pre-buckling deflection, when the crown and, therefore, the load application point are approaching the level of the support (see figure 5.9), the arch configuration is such not to permit a further increase in the vertical displacement at arch crown. In a certain sense, the structure reacts to the loss of stiffness with a sudden stiffened position towards vertical displacements; rotations and horizontal displacements (see figures 5.6-5.7) begin to change their incremental direction and, slowly, a new equilibrium configuration is established. It is not a surprise that, after limit point is reached, only "asymmetrical" quantities such as rotations and horizontal displacements contribute to the new equilibrium stabilization. This is in fact typical for non-shallow or high arches for which the centre-line may be considered incompressible. Thus, negligible center-line shortening makes the asymmetry of bending the paramount feature. Such real incompressibility is confirmed by the good agreement between the finite element solution, taking in account axial deformations, and the analytical solution obtained by Da Deppo and Schmidt in (16) under the assumption of axial inextensibility.

Such kind of asymmetrical mode, which is associated neither to a bifurcation phenomenon nor to a symmetric mode (snap-through), is called *snap-back*.

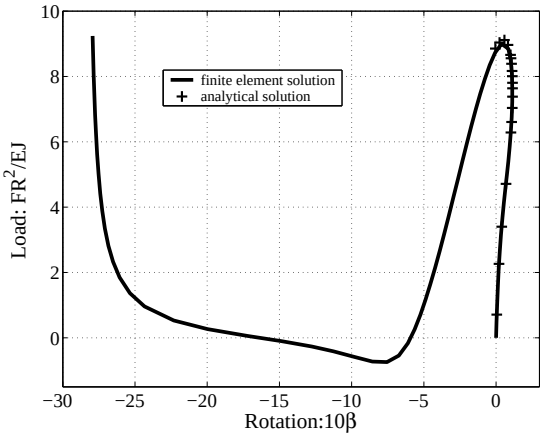

Figure 5.7: A clamped-hinged arch. Dimensionless load, $\alpha = PR^2/EJ$, versus amplified rotation, 10β. Notice the good agreement between the large-displacement beam element (15) and the analytical solution (16).

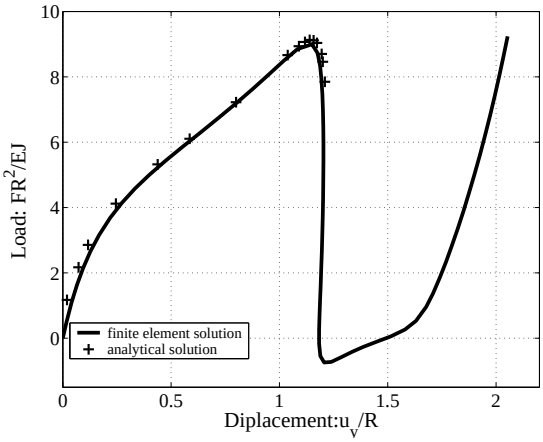

Figure 5.8: A clamped-hinged arch. Dimensionless load, $\alpha = PR^2/EJ$, versus respectively dimensionless vertical displacement, u_y/R. Notice the good agreement between the large-displacement beam element (15) and the analytical solution from (16).

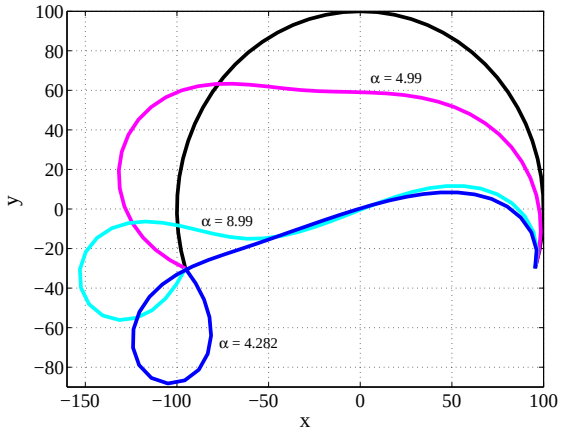

Figure 5.9: A clamped-hinged arch. Deformed configuration for different load values $\alpha = PR^2/EJ$ with $0 < u_y/R < 1.2$.

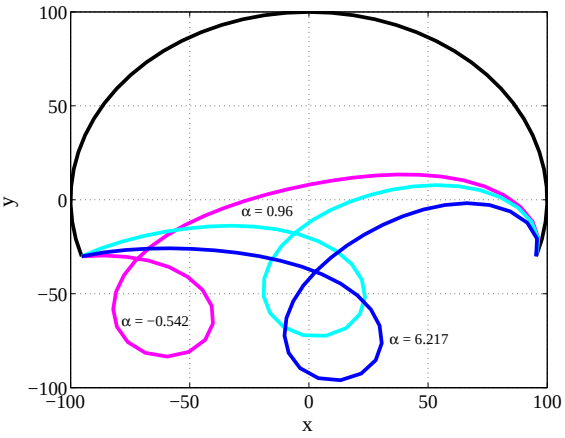

Figure 5.10: A clamped-hinged arch. Deformed configuration for different load values $\alpha = PR^2/EJ$ with $1.2 < u_y/R < 1.8$.

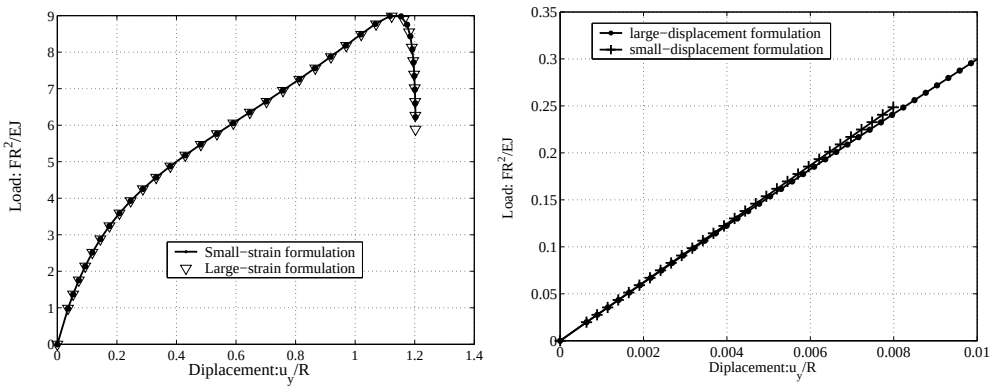

Figure 5.11: A clamped-hinged arch. Left: large-strain (15) and small-strain theory from appendix B, clash for the present problem. Right: the large-displacement small-strain and the small-displacement theory (Timoshenko beam) have the same initial curve.

5.3.2 A shallow two-hinged arch

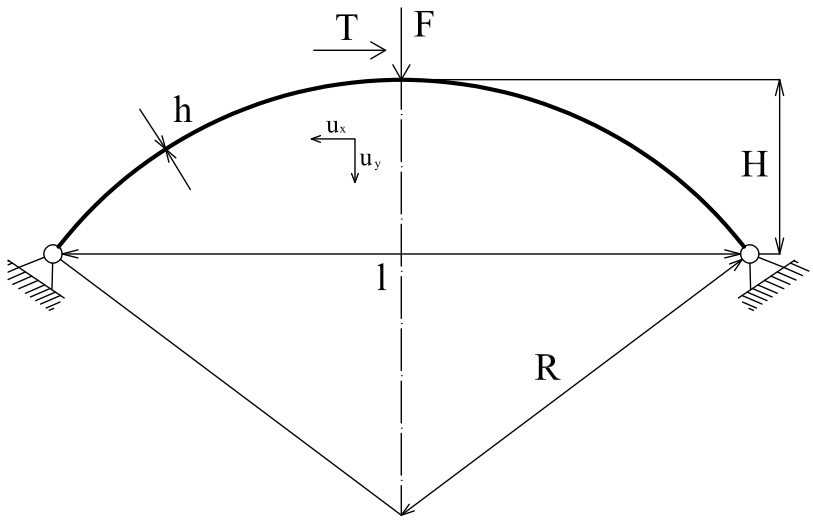

R	l	H	E	ν	A	h
100	160	40	10^6	0.5	1	1

Figure 5.12: A two-hinged arch. Problem definition.

The problem of a shallow two-hinged arch has been extensively treated by Huddleston (19) and by Da Deppo and Schmit (17). Huddleston's analytical solution is more precise as it makes no restrictions on axial deformations;

besides, he considers that plane sections remain plane, that geometric properties of each cross section are constant during the deflection, and neglects shear deformation.

This structural configuration allows us to make also some considerations on the bifurcation phenomenon. In fact both Huddleston in (19) and Da Deppo and Schmit in (17) show that the lowest buckling load occurs in an asymmetric mode which is characterized by a bifurcation in the load deflection curve at a load level $\alpha = 13$, being $\alpha = PR^2/EJ$. Moreover, in (19) a complete plot of dimensionless load α versus dimensionless displacement, i.e. u_x/R, u_y/R and amplified rotation, 10β, shows the evolution of the equilibrium path during the bifurcation mode.

The structure under investigation is shown in figure 5.12 and is solved by means of two node large-displacement small-strain element, as described in appendix B. All the following figures are obtained with such the finite element formulation. Good agreement between analytical and numerical solution are also shown.

We start performing analysis aiming at catching the primary path of the structure. Moreover, the compared observation of two test functions, such as the *Current Stiffness Parameter* (CSP) and the determinant of matrix $\mathbf{K}_t$ (properly scaled), is performed. The determinant test function, following 4.2, is firstly given by an eigenvalue scaling, i.e.

$$\mathrm{sdet}(\mathbf{K}_t) = 1/N^{\gamma} \prod_{i}^{N} d_{ii},$$

where $N = 10$ and $\gamma = 5$, and then by calculation of the *determinant-based singularity test function* (dbstf), i.e.

$$\mathrm{dbstf} = \frac{\mathrm{sdet}(\mathbf{K}_t)_n}{\mathrm{sdet}(\mathbf{K}_t)_1},$$

with $\mathrm{sdet}(\mathbf{K}_t)_1$ calculated at first step. The CSP, instead, is simply normalized with respect to the one calculated at first step.

As it is possible to observe from figure 5.13 and 5.14, the present shallow arch fails in a symmetric mode, whose basic characteristic is the shortening of the centre line of the arch. This kind of buckling is called *snap-through* which is contrast with the behaviour of non-shallow arches, for which the center line shortening is negligible. For the authors previously cited, snapping occurs at $\alpha = 15.2$; thus good agreement with analytical results is shown in figure 5.14.

The progressive monitoring of the two test function shown in figure 5.15 allows us to conclude that a bifurcation point is passed during the analysis. In fact firstly dbstf becomes zero but CSP remains nonzero (bifurcation point) and then both quantities cross the zero condition (limit point).

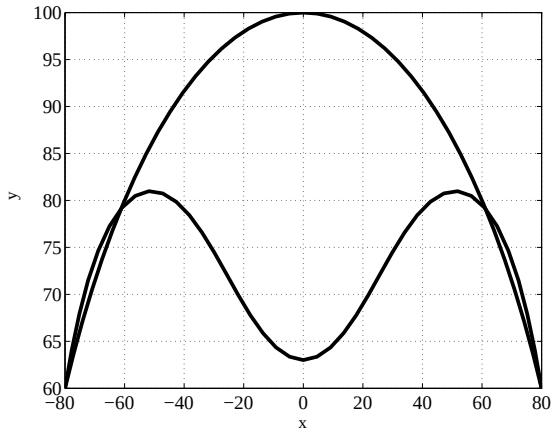

Figure 5.13: A two-hinged arch. Arch symmetric position.

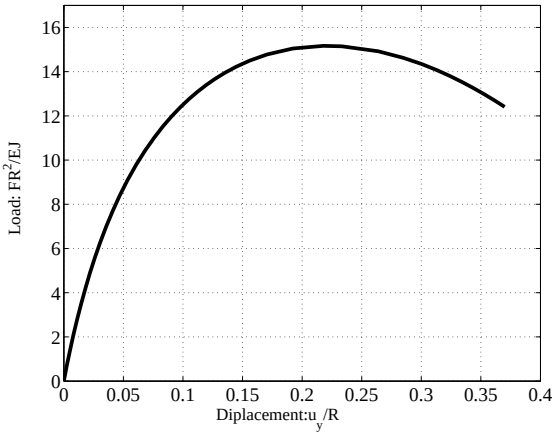

Figure 5.14: A two-hinged arch. Dimensionless load, $\alpha = PR^2/EJ$, versus dimensionless vertical displacement, u_y/R, during *symmetric buckling* (snap-through).

Further considerations can be done by detecting the eigenvalues of the matrix $\mathbf{K}_t$. We expect, in fact, a null eigenvalue both when bifurcation (figure 5.16) and limit point (figure 5.17) points are reached; in particular,

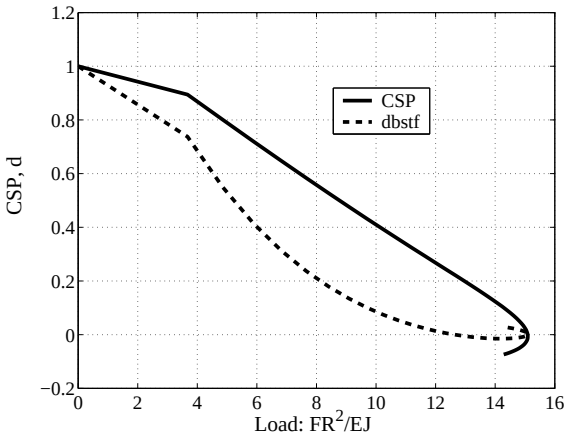

Figure 5.15: A two-hinged arch. *Current Stiffness Parameter* (CSP) versus *determinant-based singularity test function* (dbstf). Observe bifurcation point (dbstf=0) and then limit point (CSP=dbstf=0) detection.

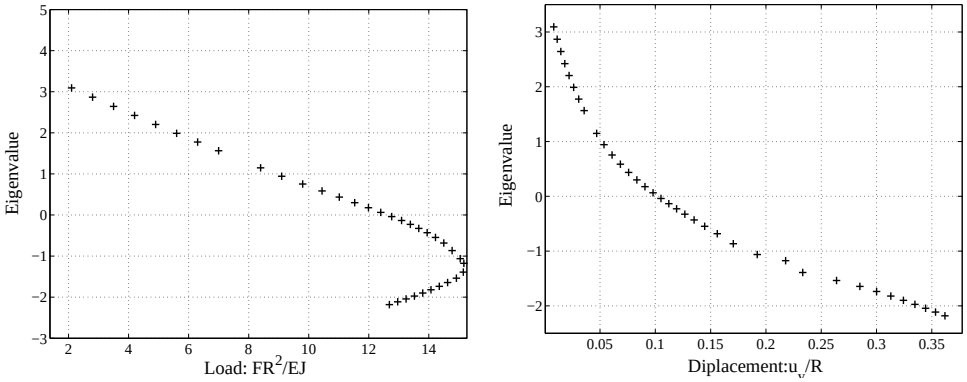

Figure 5.16: A two-hinged arch. Eigenvalue *responsible of the bifurcation point* versus dimensionless load $\alpha = PR^2/EJ$ and dimensionless vertical displacement, u_y/R, during *symmetric buckling*. Note the passage through zero at $\alpha \approx 13$ as we expect from (19).

the negative values after bifurcation point is reached, shown in figure 5.16, lead us to conclude that the followed path is an instable equilibrium branch.

After the identification of the bifurcation point, a tracing procedure for the secondary branch is carried out by a *branching predictor* strategy, leading to the detection of the asymmetric buckling mode (cfr. figures 5.18-5.20).

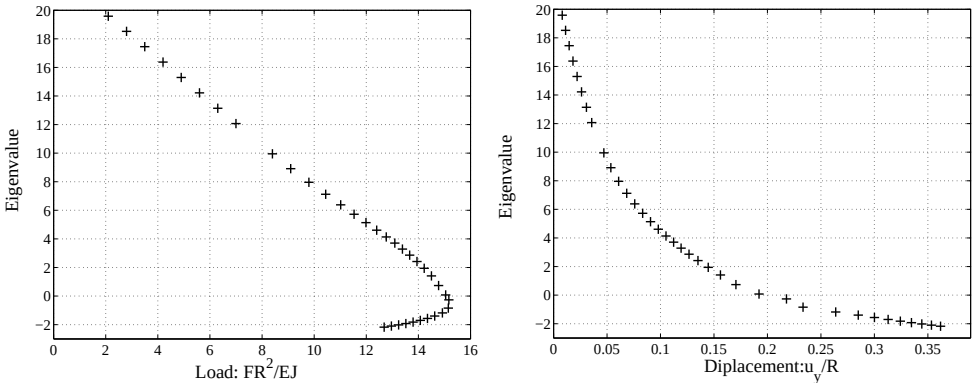

Figure 5.17: A two-hinged arch. Eigenvalue *responsible of the limit point* versus respectively dimensionless load $\alpha = PR^2/EJ$ and dimensionless vertical displacement, u_y/R, during *symmetric buckling*. Note the passage through zero at $\alpha \approx 15.2$ as we expect from (19).

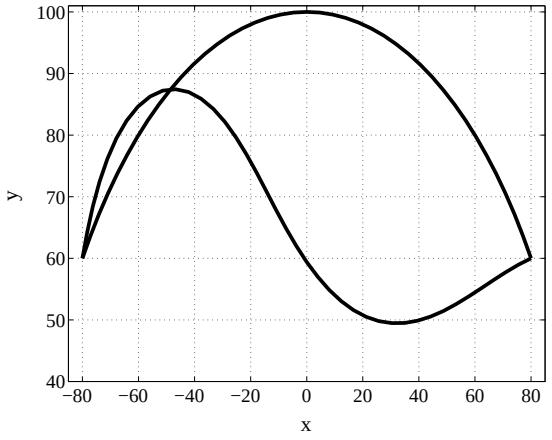

Figure 5.18: A two-hinged arch. Arch asymmetric position.

In particular, a plot of dimensionless load α versus dimensionless vertical displacement u_y/R (figure 5.19) shows good agreement with the results proposed in reference (19). The asymmetric buckling load of $\alpha \approx 13$ also agrees with the one from the numerical results presented by Da Deppo (17), as does the finite central deflection of $0.106R$ compared with Da deppo's value of $0.108R$. Considering once more the eigenvalue respectively re-

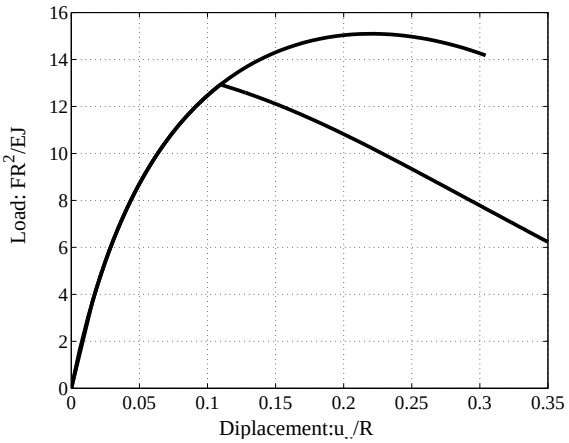

Figure 5.19: A two-hinged arch. Dimensionless load, $\alpha = PR^2/EJ$, versus dimensionless vertical displacement, u_y/R, during *symmetric* and *asymmetric buckling*.

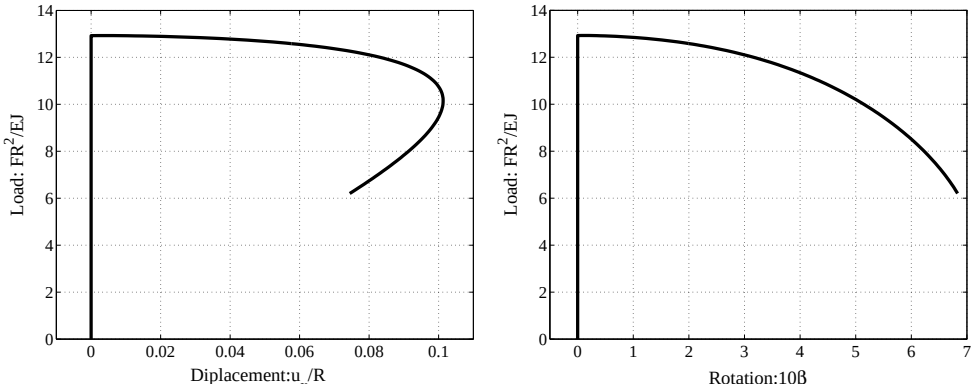

Figure 5.20: A two-hinged arch. Dimensionless load, $\alpha = PR^2/EJ$, versus respectively dimensionless horizontal displacement, u_y/R, and scaled rotation, 10β, during *asymmetric buckling*.

sponsible of limit and bifurcation points, we now observe an inversion of sign when we switch to the second branch (figure 5.21). In particular, bifurcation point eigenvalue firstly becomes negative and then switches positive. Instead limit point eigenvalue behaves in the opposite way. Finally positive

values of bifurcation point eigenvalue marks a stable branch of solution.

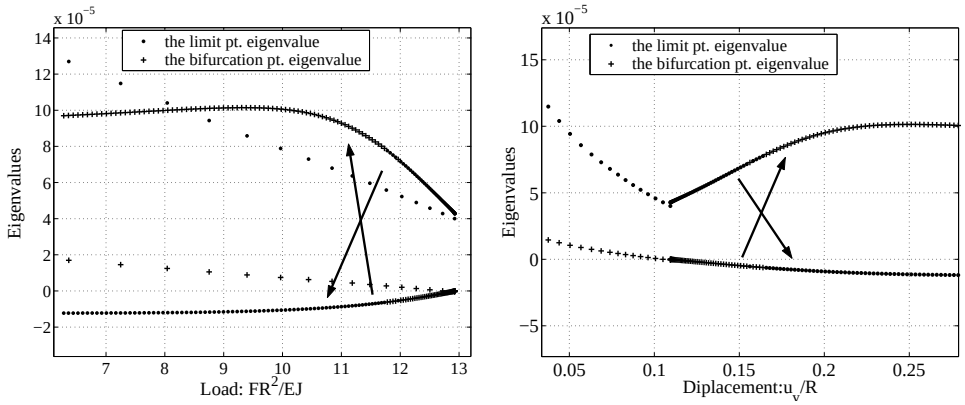

Figure 5.21: A two-hinged arch. Limit and bifurcation point eigenvalues versus dimensionless load (left), $\alpha = PR^2/EJ$, and dimensionless horizontal displacement (right), u_y/R, during *asymmetric buckling*. Note the sign inversion.

In order to test the stability of the two branches, it is also possible to perform an *imperfection sensitivity analysis* loading the structure with an horizontal force T at the apex, i.e. by introducing a small imperfection. Again, we find that the secondary branch is the stable one, as shown in figures 5.22 and 5.23.

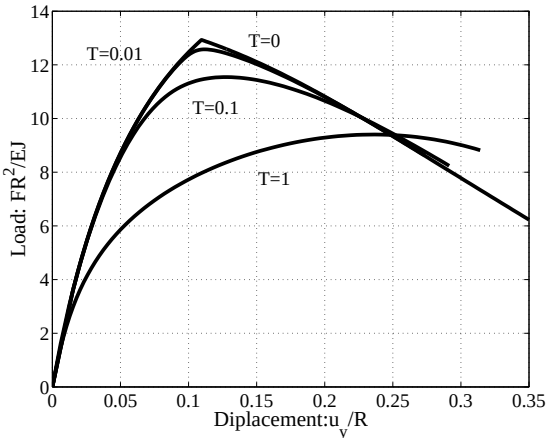

Figure 5.22: A two-hinged arch. Dimensionless load, $\alpha = PR^2/EJ$, versus dimensionless vertical displacement, u_y/R, curves for different levels of imperfection.

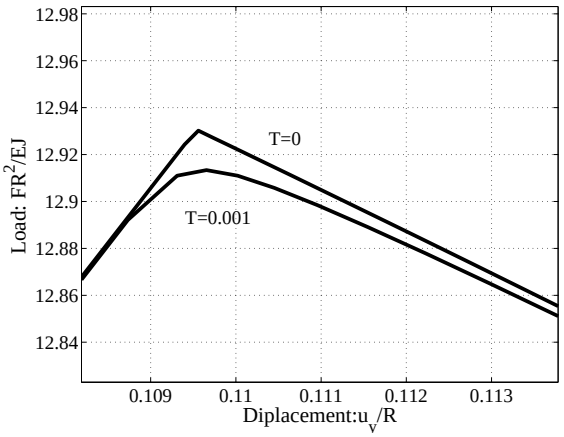

Figure 5.23: A two-hinged arch. Dimensionless load, $\alpha = PR^2/EJ$, versus dimensionless vertical displacement, u_y/R. Detail of the neighborhood of the bifurcation point at a small level of imperfection.

5.4 Williams toggle frame

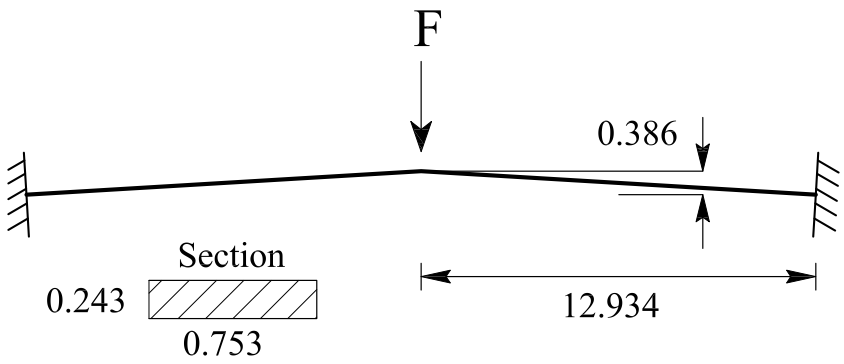

Figure 5.24: Williams toggle frame. Problem definition.

The last test consist of the problem of a rigid jointed toggle, figure 5.24, firstly considered by Williams in (34). The author obtained an analytical expression which links the external load F with the vertical displacement u_y by means of a finite deflection and flexural shortening analysis of a member (shear effect is neglected) and by making some approximations, i.e. small-

strain hypothesis and stresses in the members that do not exceed the limit of proportionality of the material. Such analytical expression is also accomplished by experimental results which shows good agreement with the theory assumed and the hypothesis done (see figure 5.25). The analytical expression has the following form

$$\boxed{F = 2(W + P\sin\beta).} \tag{5.19}$$

In the above expression β is the angle formed between the members and the horizontal direction, and

$$W = \frac{6EJ}{l^3} d_5 u_y, \quad P = \frac{EA}{l}\left(u_y \sin\beta - 0.6\frac{u_y^2}{l}\right),$$

with

$$P_E = \pi^2 \frac{EJ}{l^2}, \quad \rho = \frac{P}{P_E}, \quad w(\rho) = \frac{\pi}{2}\sqrt{\rho}\cot\frac{\pi}{2}\sqrt{\rho}, \quad d_5 = \frac{\pi^2\rho}{6(1-w(\rho))} w(\rho);$$

being E the Young's modulus, assumed equal to $10.3 \cdot 10^6$.

The finite element results, using 20 beam elements within the theory given in appendix B, are shown in figure 5.25 along with experimental and analytical results. A good agreement among the different curves can be observed.

As for shallow arches, we obtain in this case a symmetrical mode, figure 5.26, which exhibits a *snap-through* behaviour. Moreover, no bifurcation phenomena are observed.

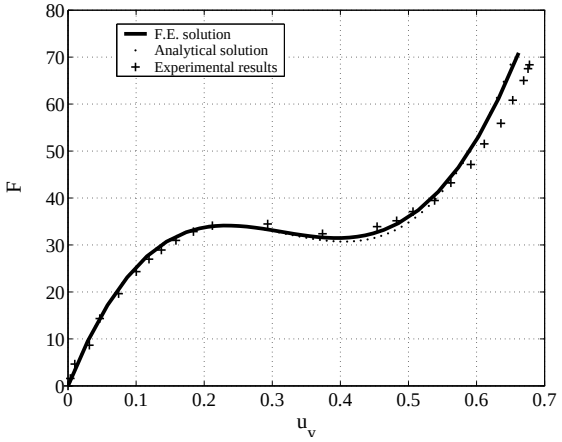

Figure 5.25: Williams toggle frame: load-deflection curve which exhibits a *snap-through* behaviour.

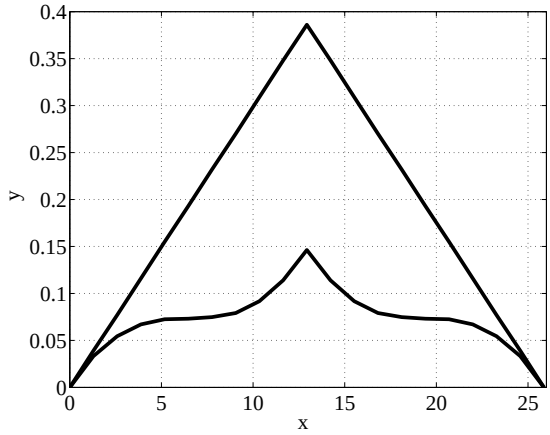

Figure 5.26: Williams toggle frame: arc deformed configuration at $F = 34.12$ and $u_y = 0.2397$.

Conclusions

The goal of the present work was the development of a robust arc-length method and its subsequent use in the stability analysis of structures which exhibit a high degree of nonlinearity.

Usually failures in tracing a nonlinear structural response are connected with equilibrium problems that can be encountered in the neighborhood of critical points, such as limit and bifurcation points. At such points the stiffness matrix that governs the equilibrium behaviour becomes singular, so strategies as arc-length techniques have been designed to overcome such singularity by augmenting the equilibrium equation by means of an efficient constraint equation. In order to prove the good performance of this approach, in chapter 1 a detailed analysis of the critical state for the equilibrium equation has been performed. In particular, we studied how the conditions characterizing the presence of either limit or bifurcation points affect the resolution of such an augmented equilibrium system; in particular a limit point does not compromise the analysis of the structure while simple bifurcation point seems to generate some inconveniences.

Traditional continuation method such as load control have been discussed in chapter 2. They give rise to an inefficient constraint equation which does not overcome stiffness matrix singularity when critical points are reached.

Chapter 3 has been devoted to the review of the existing arc-length strategies. Inserted within a Newton Raphson's iterative scheme, it was proved that such strategies have, when critical conditions appear, an iteration matrix $\mathbf{H}$ which does not become singular, i.e. the iterative solution can be performed without any problem. This consideration can be seen as a direct consequence of what discussed in chapter 1.

As we have at our disposal only one parameter λ to follow the equilibrium path, when bifurcation occurs, we are able to trace only the primary branch of the structural response. This cannot be sufficient to characterize the structural response since critical points can also appear at lower load levels that can be activated by small imperfections (always present in real structures). Thus in chapter 4 we have presented branching techniques allowing us to follow secondary branches when bifurcation occurs. Moreover, also some interesting test functions, useful in critical point detection and distinction, have been shown and discussed in this chapter; they are strictly

connected to limit and bifurcation point properties highlighted in chapter 1.

Having in hand all the information presented in chapters 1,4, an algorithm capable of handling limit and simple bifurcation points can be implemented (section 4.5). As a result of such an implementation, in chapter 5 we have shown many successful numerical example, among which we have reported also the analysis of an elastic-perfectly plastic structure.

However, only simple bifurcations point are treated here; we have chosen to use for them branching predictor technique while the numerical resolution of the extended system has not been performed. This, along with the analysis of multiple bifurcation points, will be the object of future developments. In order to do that, following (33; 12), perturbed branching techniques presented in chapter 4 seem to be the best way to follow all possible branches in case of multiple bifurcation analysis.

Bibliography

[1] Quoc Son Nguyen. *Stability and Nonlinear Solid Mechanics*. Wiley, England (2000).

[2] G. Dahlquist and A. Bjorck. *Numerical Methods*. Prentice-Hall, Englewood Cliffs, N.J. (1974).

[3] E. Riks. A unified method for computation of critical equilibrium states of non-linear elastic system. *Acta tecnica Academiae Scientiarum Hungaricae*, Tomus 87, pp. 121-141 (1978).

[4] E. Riks. An incremental approach to the solution of snapping and buckling problems. *International Journal of Solids and Structures*, Vol. 15, pp. 529-551 (1979).

[5] E. Riks. Some computational aspects of the stability analysis of nonlinear structures. *International Journal of Solids and Structures*, Vol. 47, pp. 219-259 (1984).

[6] E. Riks. The Application of Newton's Method to the Problem of Elastic Stability. *Journal of Applied Mechanics*, Vol. 39, pp. 1060-1066 (1972).

[7] G. Garcea, G.A. Trunfio, R. Casciaro. Mixed formulation and locking in path-following nonlinear analysis. *Computer Methods in Applied Mechanics and Engineering*, Vol. 165, pp. 247-272 (1998).

[8] M.A. Crisfield. *Finite Elements and Solution Procedures for Structural Analysis*. Vol 1: Linear Analysis, Pineridge Press, Swansea, (1986).

[9] E. Ramm. Strategies for tracing the non-linear response near limit-points, in: W.Wunderlinch, E. Stein, K.J. Bathe, eds. *Non-linear Finite element Analysis in structural Mechanics, Proceeding European US Workshop, Ruhr Universitat Bochum, Germany*, Springer, Berlin, pp. 63-89 (1981).

[10] I. Fried. Orthogonal trajectory accession to the nonlinear equilibrium curve. *Computer Methods in Applied Mechanics and Engineering*, Vol. 47, pp. 283-298 (1984).

[11] R. Kouhia, M. Mikkola. Some aspects on efficient path-following. *Computers and Structures*, Vol. 72, pp. 509-524 (1999).

[12] R. Kouhia, M. Mikkola. Tracing the equilibrium path beyond compound critical points. *International Journal for Numerical Methods in Engineering*, Vol. 46, pp. 1049-1074 (1999).

[13] S.R. Kuo, Y.B. Yang. Tracing post-buckling paths of structures containing multi-loops. *International Journal of Solids and Structures*, Vol. 38, pp. 4053-4075 (1995).

[14] P. Nanakorn, L.N. Vu. A 2D field-consistent beam element for large displacement analysis using the total Lagrangian formulation. *Finite Elements Analysis and Design*, Vol. 42, pp. 1240-1247 (2006).

[15] O.C. Zienkiewicz, R.L. Taylor. *The Finite Element Method for Solid and Structural Mechanics*. Butterworth-Heinemann, Oxford, 6th edition (2005).

[16] D.A. DaDeppo, R. Schmidt. Instability of clamped-hinged circular arches subjected to a point load. *Transactions of the ASME*, pp. 894-896 (1975).

[17] D.A. DaDeppo, R. Schmidt. Side sway buckling of deep circular arches under a concentrated load. *Journal of Applied Mechanics*, Vol. 36, pp. 325-327 (1969).

[18] D.A. DaDeppo, R. Schmidt. Large Deflection and Stability of Hingeless Circular Arches Under Interacting Loads. *Journal of Applied Mechanics*, Vol. 41, No.4, *Transactions of the ASME*, Vol. 96, Series E, pp. 989-994 (1974).

[19] J.V. Huddleston. Finite deflection and snap through of high circular arches. *Journal of Applied Mechanics*, Vol. 35, pp. 763-769 (1968).

[20] D.W. Decker, H.B. Keller. Multiple Limit Point Bifurcation. *Journal of Mathematical Analysis and Applications*, Vol. 75, pp. 417-430 (1980).

[21] F. Brezzi, J. Rappaz, P.A. Raviart. Finite Dimensional Approximation of Nonlinear Problems. Part II: Limit Points. *Numerische Mathematik*, Vol. 37, pp. 1-28 (1981).

[22] F. Brezzi, J. Rappaz, P.A. Raviart. Finite Dimensional Approximation of Nonlinear Problems. Part III: Simple Bifurcation Points. *Numerische Mathematik*, Vol. 38, pp. 1-30 (1981).

[31] A. Spence, B. Werner. Non-simple Turning Points and Cusps. *IMA Journal of Numerical Analysis*, Vol. 2, pp. 413-427 (1982).

[24] J.W. Hutchinson, W.T. Koiter. Postbuckling theory. *Applied Mechanics Reviews*, Vol. 23, pp. 1353-1366 (1970).

[25] A. Magnusson. Treatment of bifurcation points with asymptotic expansion. *Computers and Structures*, Vol. 77, pp. 475-484 (2000).

[26] B.Z. Huang, S.N. Atluri. A simple method to follow post-buckling paths in finite element analysis. *Computers and Structures*, Vol. 57, pp. 477-489 (1995).

[27] W. Wagner, P. Wriggers. A simple method for the calculation of postcritical branches. *Engineering Computation*, Vol. 5, pp. 103-109 (1988)

[28] P. Wriggers, W. Wagner, C. Miehe. A quadratically convergent procedure for the calculation of stability points in finite element analysis. *Computer Methods in Applied Mechanics and Engineering*, Vol. 70, pp. 329-347 (1988)

[29] P. Wriggers, J.C. Simo. A general procedure for the direct computation of turning and bifurcation points. *International Journal for Numerical Methods in Engineering*, Vol. 30, pp. 155-176 (1990).

[30] R. Seydel. Numerical computation of branch points in nonlinear equation. *Numerische Mathematik*, Vol. 33, pp. 339-352 (1979).

[31] B. Werner, A. Spence. The computation of symmetry-breaking bifurcation points. *SIAM Journal of Numerical Analysis*, Vol. 21, pp. 388-399 (1984).

[32] B. Werner, A. Spence. Numerical methods for a class of finite dimensional bifurcation problems. *SIAM Journal of Numerical Analysis*, Vol. 15, pp. 1-11 (1978).

[33] J. Huitfeldt. Nonlinear eigenvalue problems - prediction of bifurcation points and branch switching. *Technical Report 17*, Department of Computer Sciences, Chalmers University of technology (1991).

[34] F. W. Williams. An approach to the nonlinear behaviour of the members of a rigid jointed plane framework with finite deflection.. *Quarter Journal of Mechanics and Applied Mathematics* , Vol. 17, pp. 451-469 (1964).

Appendix A

Complementarity proof

The equivalence of bifurcation condition (1.47) and (1.64) follows from the connection between the properties of the matrices $\mathbf{K}_t$ and $\mathbf{C}$. The characteristic values and vectors $[\omega_k, \mathbf{a}_k]$ of the symmetric matrix $\mathbf{K}_t$ are defined by

$$[\mathbf{K}_t - \omega_k \mathbf{I}]\mathbf{a}_k = \mathbf{0}. \tag{A.1}$$

At the critical state

$$0 = \omega(1) < \omega(2) \leq \omega(3) \leq \ldots \leq \omega(N). \tag{A.2}$$

according to the definition given in (1.10) and with $K = 1$ for simplicity reasons. The symmetric matrix $\mathbf{C}$ is defined by (1.57)

$$C_{ij} = \left[\frac{\partial D}{\partial K_{tij}}\right]. \tag{A.3}$$

It satisfy the property

$$\mathbf{K}_t\mathbf{C} = D\mathbf{I}, \tag{A.4}$$

being $\mathbf{I}$ the identity matrix. The characteristic values and vectors $[\phi_k, \mathbf{b}_k]$ are defined by

$$[\mathbf{C} - \phi_k \mathbf{I}]\mathbf{b}_k = \mathbf{0}. \tag{A.5}$$

They can be expressed in terms of ω_k and $\mathbf{a}_k$ by rewriting (A.1) as

$$\mathbf{C}[\mathbf{K}_t - \omega_k \mathbf{I}]\mathbf{a}_k = \mathbf{0}. \tag{A.6}$$

which for equation (A.4) and dividing by ω_k becomes

$$\left[\mathbf{C} - \frac{D}{\omega_k}\mathbf{I}\right]\mathbf{a}_k = \mathbf{0}. \tag{A.7}$$

If we consider

$$\mathbf{a}_k = \mathbf{b}_k \tag{A.8}$$

we get

$$\left[\mathbf{C} - \frac{D}{\omega_k}\mathbf{I}\right]\mathbf{b}_k = \mathbf{0}, \tag{A.9}$$

that compared with (A.5) gives

$$\phi_k = \frac{D}{\omega_k}, \quad k = 1, 2, 3, \ldots, N. \tag{A.10}$$

If we express D as the product of its eigenvalues (1.13), eigenvalues ϕ_k become

$$\phi(1) = \prod_{i=2}^{N} \omega(i), \tag{A.11}$$

and at the critical state, $\omega(1) = 0$, they are expressed as

$$\phi(i) = 0, \quad i = 2, 3, \ldots, N. \tag{A.12}$$

Statement (A.12) together with (A.8) implies that a basis of the null space of $\mathbf{C}$, Ker($\mathbf{C}$), is equal to the basis of the range of $\mathbf{K}_t$, Im($\mathbf{K}_t$). Thus complementarity between $\mathbf{C}$ and $\mathbf{K}_t$ at the critical points has been proved.

Appendix B

2-d beam element for large displacement and small strain analysis

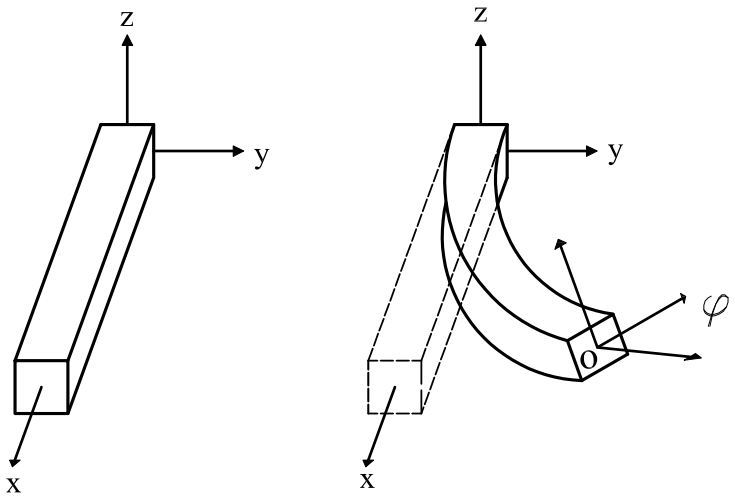

Figure B.1: Finite motion of three-dimensional beams.

A two-dimensional theory of beams is here developed considering an initially straight beam for which the orthogonal triad of the beam cross-section is denoted by the vector $\mathbf{a}_i$ (figure B.1). The motion for the beam can then be written as

$$\varphi_i \equiv x_i = x_i^0 + \Lambda_{iI} Z_I \tag{B.1}$$

where the orthogonal matrix is related to the $\mathbf{a}_i$ vectors as

$$\boldsymbol{\varphi} = [\mathbf{a}_1 \quad \mathbf{a}_2 \quad \mathbf{a}_3]. \tag{B.2}$$

If we assume that the reference coordinate $X_1(X)$ is the beam axis and X_2,

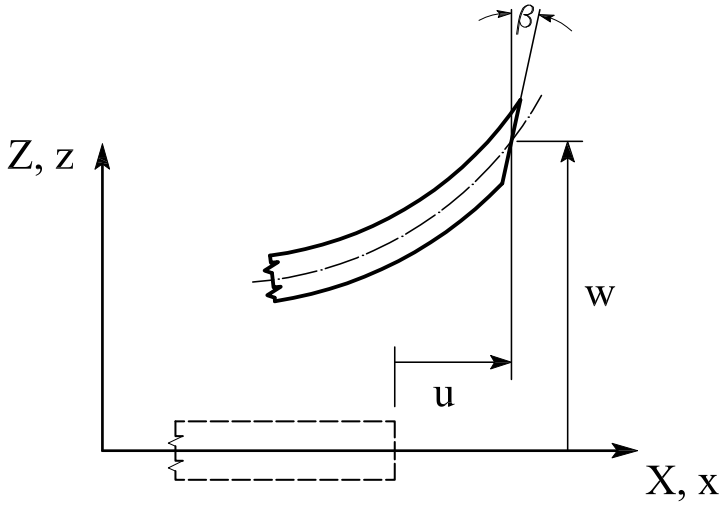

Figure B.2: Deformed 2D beam configuration.

X_3 (X,Y) are the axes of the cross-section the above motion may be written in matrix form as

$$\begin{Bmatrix} x_1 \\ x_2 \\ x_3 \end{Bmatrix} = \begin{Bmatrix} x \\ y \\ z \end{Bmatrix} = \begin{Bmatrix} X \\ 0 \\ 0 \end{Bmatrix} + \begin{Bmatrix} u \\ v \\ w \end{Bmatrix} + \begin{bmatrix} \Lambda_{11} & \Lambda_{12} & \Lambda_{13} \\ \Lambda_{21} & \Lambda_{22} & \Lambda_{23} \\ \Lambda_{31} & \Lambda_{32} & \Lambda_{33} \end{bmatrix} \begin{Bmatrix} 0 \\ Y \\ Z \end{Bmatrix}. \tag{B.3}$$

The expression of the orthogonal matrix $\boldsymbol{\Lambda}$, considering the two-dimensional case where the motion is restricted to the X-Z plane, is

$$\boldsymbol{\Lambda} = \begin{bmatrix} \cos\beta & 0 & \sin\beta \\ 0 & 1 & 0 \\ -\sin\beta & 0 & \cos\beta \end{bmatrix}. \tag{B.4}$$

Inserting this in (B.3) and expanded, the deformed position then is described compactly by

$$\begin{aligned} x &= X + u(X) + Z\sin\beta(X) \\ y &= Y \\ z &= w(X) + Z\cos\beta(X) \end{aligned} \tag{B.5}$$

This results in the deformed configuration for a beam shown in figure B.2. The deformation gradient for this displacement field is given by

$$F_{iI} = \frac{\partial x_i}{\partial X_I}, \tag{B.6}$$

or especially

$$F_{iI} = \begin{bmatrix} [1 + u_{,X} + Z\beta_{,X}\cos\beta] & 0 & \sin\beta \\ 0 & 1 & 0 \\ [w_{,X} - Z\beta_{,X}\sin\beta] & 0 & \cos\beta \end{bmatrix}. \tag{B.7}$$

Equation (B.6) is used to compute the Green strain defined as

$$\mathbf{E} = \frac{1}{2}(\mathbf{F}^{\mathrm{T}}\,\mathbf{F} - \mathbf{I}). \tag{B.8}$$

Since $\mathbf{\Lambda}$ is orthogonal, the Green strain $\mathbf{E}$ can also be written (14) as

$$\mathbf{E} = \frac{1}{2}(\overline{\mathbf{F}}^{\mathrm{T}}\,\overline{\mathbf{F}} - \mathbf{I}) = \frac{1}{2}(\mathbf{L} + \mathbf{L}^{\mathrm{T}} + \mathbf{L}^{\mathrm{T}}\,\mathbf{L}), \tag{B.9}$$

where

$$\overline{\mathbf{F}} = \mathbf{\Lambda}^{\mathrm{T}}\mathbf{F} = \begin{bmatrix} \Lambda + Z\beta_{,X} & 0 & 0 \\ 0 & 1 & 0 \\ (1 + u_{,X})\sin\beta + w_{,X}\cos\beta & 0 & 1 \end{bmatrix}, \tag{B.10}$$

and

$$\mathbf{L} = \overline{\mathbf{F}} - \mathbf{I} = \begin{bmatrix} \Lambda + Z\beta_{,X} - 1 & 0 & 0 \\ 0 & 0 & 0 \\ (1 + u_{,X})\sin\beta + w_{,X}\cos\beta & 0 & 0 \end{bmatrix}, \tag{B.11}$$

so

$$\frac{1}{2}(\mathbf{L} + \mathbf{L}^{\mathrm{T}}) = \begin{bmatrix} \Lambda + Z\beta_{,X} - 1 & 0 & \frac{1}{2}[(1 + u_{,X})\sin\beta + w_{,X}\cos\beta] \\ 0 & 0 & 0 \\ \frac{1}{2}[(1 + u_{,X})\sin\beta + w_{,X}\cos\beta] & 0 & 0 \end{bmatrix}$$

$$\frac{1}{2}(\mathbf{L}^{\mathrm{T}}\,\mathbf{L}) = \begin{bmatrix} -\{\Lambda + Z\beta_{,X} - 1\} + u_{,X} + \frac{1}{2}(u_{,X}^2 + w_{,X}^2 + Z^2\beta_{,X}^2) + Z\Lambda\beta_{,X} & \mathbf{0} \\ \mathbf{0} & \mathbf{0} \end{bmatrix}.$$

Only three non-zero component of $\mathbf{E}$ are obtained, which, ignoring a quadratic term in Z because we suppose a slender beam with respect to its length, are expressed by

$$E_{XX} = u_{,X} + \frac{1}{2}(u_{,X}^2 + w_{,X}^2) + Z\Lambda\beta_{,X}, \tag{B.12}$$

$$2E_{ZX} = 2E_{XZ} = (1 + u_{,X})\sin\beta + w_{,X}\cos\beta = \Gamma, \tag{B.13}$$

where

$$\Lambda = (1 + u_{,X}) \cos\beta - w_{,X} \sin\beta, \tag{B.14}$$

so

$$\mathbf{E} = \begin{bmatrix} E_{XX} & 0 & E_{XZ} \\ 0 & 0 & 0 \\ E_{ZX} & 0 & 0 \end{bmatrix}.$$

If we assume the hypothesis of small strains, the term $\mathbf{L}^{\mathrm{T}}\,\mathbf{L}$ in equation (B.9) can be neglected, so $\mathbf{E}$ con be written as

$$\mathbf{E} \approx \frac{1}{2}(\mathbf{L} + \mathbf{L}^{\mathrm{T}}) = \mathbf{L}^{\mathrm{s}}, \tag{B.15}$$

in which

$$L^{\mathrm{s}}_{XX} = \Lambda - 1 + Z\beta_{,X} = E^{\mathbf{0}} + ZK^{\mathrm{b}}, \tag{B.16}$$

$$2L^{\mathrm{s}}_{ZX} = 2L^{\mathrm{s}}_{XZ} = 2E_{XZ} = \Gamma, \tag{B.17}$$

where $E^{\mathbf{0}}$ and Γ are strains which are constant on the cross-section and K^{b} measures change in rotation (curvature) of the cross sections.

A variational equation for the beam cam be written now by introducing second Piola-Kirchhoff stresses to obtain

$$\delta\Pi = \int_{\Omega} (\delta L^{\mathrm{s}}_{XX} S_{XX} + 2\,\delta L^{\mathrm{s}}_{ZX} S_{ZX}) \mathrm{d}V - \delta\Pi_{\mathrm{ext}}, \tag{B.18}$$

where $\delta\Pi_{\mathrm{ext}}$ denotes the terms from end force and loading along the length. If we separate the volume integral into one along the length times and one over the beam cross-sectional area A and define force resultants as

$$T^{\mathrm{p}} = \int_A S_{XX} \mathrm{d}A, \quad S^{\mathrm{p}} = \int_A S_{ZX} \mathrm{d}A \quad \text{and} \quad M^{\mathrm{b}} = \int_A S_{XX} Z\,\mathrm{d}A \tag{B.19}$$

the equation (B.18) may be written compactly by

$$\delta\Pi = \int_{\Omega} (\delta E^{\mathbf{0}}\, T^{\mathrm{p}} + \delta\Gamma\, S^{\mathrm{p}} + \delta K^{\mathrm{b}}\, M^{\mathrm{b}}) \mathrm{d}X - \delta\Pi_{\mathrm{ext}}, \tag{B.20}$$

where virtual strains for the beam are given by

$$\delta E^{\mathbf{0}} = \delta u_{,X} \cos\beta - \delta w_{,X} \sin\beta - \Gamma\,\delta\beta, \tag{B.21}$$

$$\delta\Gamma = \delta u_{,X} \sin\beta + \delta w_{,X} \cos\beta + \Lambda\,\delta\beta, \tag{B.22}$$

$$\delta K^{\mathrm{b}} = \delta\beta_{,X}. \tag{B.23}$$

A finite element approximation for the displacements is here introduced

$$\begin{Bmatrix} u \\ w \\ \beta \end{Bmatrix} = N_a(X) \begin{Bmatrix} \tilde{u}_a \\ \tilde{w}_a \\ \tilde{\beta}_a \end{Bmatrix}, \tag{B.24}$$

where the shape function for each variable are the same and linear. Using this approximation the virtual work is computed as

$$\delta\Pi = [\delta\tilde{u}_a \quad \delta\tilde{w}_a \quad \delta\tilde{\beta}_a] \int_L \mathbf{B}_a^{\mathrm{T}} \left\{ \begin{array}{c} T^{\mathrm{p}} \\ S^{\mathrm{p}} \\ M^{\mathrm{b}} \end{array} \right\} \mathrm{d}X - \delta\Pi_{\mathrm{ext}}, \tag{B.25}$$

where

$$\mathbf{B}_a^{\mathrm{T}} = \left[\begin{array}{ccc} N_{a\,,X} \cos\beta & N_{a\,,X} \sin\beta & 0 \\ -N_{a\,,X} \sin\beta & N_{a\,,X} \cos\beta & 0 \\ -N_a\Gamma & N_a\Lambda & N_{a\,,X} \end{array} \right]. \tag{B.26}$$

The non-linear equilibrium equation for quasi-static problem that is solved at each load level (or time) is given by

$$\mathbf{\Psi} = \mathbf{f}_{n+1} - \int_L \mathbf{B}_a^{\mathrm{T}} \left\{ \begin{array}{c} T^{\mathrm{p}}_{n+1} \\ S^{\mathrm{p}}_{n+1} \\ M^{\mathrm{b}}_{n+1} \end{array} \right\} \mathrm{d}X = \mathbf{0}. \tag{B.27}$$

For a Newton-type solution the tangent stiffness matrix is deduced by linearization of equation (B.27). To give a specific relation for the derivation we assume, for simplicity the strains are small and the constitution may be expressed by a linea elastic relation between the Green-Lagrange strains and the second Piola-Kirchhoff stresses.
Accordingly, we take

$$S_{XX} = E\, E_{XX} \quad \text{and} \quad S_{ZX} = 2\, G\, E_{ZX} \tag{B.28}$$

where E is a Young's Modulus and G a shear modulus. Integrating (B.19) the elastic behaviour of the beam resultants becomes

$$T^{\mathrm{p}} = E\, A\, E^{\mathbf{0}}, \quad S^{\mathrm{p}} = \kappa\, G\, A\, \Gamma \quad \text{and} \quad M^{\mathrm{b}} = E\, I\, K^{\mathrm{b}} \tag{B.29}$$

in which A is the cross-sectional area, I is the moment of inertia about the centroid, and κ is a shear correction factor to account for the fact that S_{ZX} is not constant on the cross-section. Using these relations the linearization of equation (B.27) gives the tangent stiffness

$$(\mathbf{K}_T)_{ab} = \int_L \mathbf{B}_a^{\mathrm{T}} \mathbf{D}_T \mathbf{B}_b \mathrm{d}X + (\mathbf{K}_{\mathrm{G}})_{ab}, \tag{B.30}$$

where for the simple elastic relation equation (B.30)

$$\mathbf{D}_T = \left[\begin{array}{ccc} EA & & \\ & \kappa GA & \\ & & EI \end{array} \right] \tag{B.31}$$

and $\mathbf{K}_{\mathrm{G}}$ is the geometric stiffness resulting from the linearization of the non-linear expression for $\mathbf{B}$ given by

$$(\mathbf{K}_{\mathrm{G}})_{ab} = \int_L \left(N_{a\,,X} \begin{bmatrix} 0 & 0 & G_1 \\ 0 & 0 & G_2 \\ 0 & 0 & 0 \end{bmatrix} N_b + N_a \begin{bmatrix} 0 & 0 & 0 \\ 0 & 0 & 0 \\ G_1 & G_2 & 0 \end{bmatrix} N_{b\,,X} + \right.$$
$$\left. + N_a \begin{bmatrix} 0 & 0 & 0 \\ 0 & 0 & 0 \\ 0 & 0 & G_3 \end{bmatrix} N_b \right) \mathrm{d}X, \tag{B.32}$$

where

$$G_1 = -T^{\mathrm{p}} \sin\beta + S^{\mathrm{p}} \cos\beta,$$
$$G_2 = -T^{\mathrm{p}} \cos\beta - S^{\mathrm{p}} \sin\beta,$$
$$G_3 = -T^{\mathrm{p}} \Lambda - S^{\mathrm{p}} \Gamma.$$